GKSS
FORSCHUNGSZENTRUM
in der HELMHOLTZ-GEMEINSCHAFT

Assessment of water flow and the impact on sediment motion in a tidal channel of North Sylt basing on radar observation

(Vom Coastal Research Laboratory, Forschungs- und Technologie-zentrum Westküste BÜSUM, der Christian-Albrechts-Universität zu Kiel als Diplomarbeit angenommen)

Author:

M. Z. R. Chowdhury

ISSN 0344-9629

HELMHOLTZ
| GEMEINSCHAFT

wissen
schafft
nutzen

GKSS 2007/10

GKSS 2007/10

Assessment of water flow and the impact on sediment motion in a tidal channel of North Sylt basing on radar observation

(Vom Coastal Research Laboratory, Forschungs- und Technologie-zentrum Westküste BÜSUM, der Christian-Albrechts-Universität zu Kiel als Diplomarbeit angenommen)

Author:

M. Z. R. Chowdhury

(Institute for Coastal Research)

GKSS-Forschungszentrum Geesthacht GmbH • Geesthacht • 2007

Die Berichte der GKSS werden kostenlos abgegeben.
The delivery of the GKSS reports is free of charge.

Anforderungen/Requests:

GKSS-Forschungszentrum Geesthacht GmbH
Bibliothek/Library
Postfach 11 60
D-21494 Geesthacht
Germany
Fax.: (49) 04152/871717

Als Manuskript vervielfältigt.

ISSN 0344-9629

GKSS-Forschungszentrum Geesthacht GmbH · Telefon (04152)87-0
Max-Planck-Straße 1 · D-21502 Geesthacht / Postfach 11 60 · D-21494 Geesthacht

GKSS 2007/10

Assessment of water flow and the impact on sediment motion in a tidal channel of North Sylt basing on radar observation

(Vom Coastal Research Laboratory, Forschungs- und Technologiezentrum Westküste BÜSUM, der Christian-Albrechts-Universität zu Kiel als Diplomarbeit angenommen)

Mohammad Zahedur Rahman Chowdhury

137 pages with 45 figures and 7 tables

Abstract

Remote sensing techniques are being used for monitoring essential environmental parameters. The ground based X-Band nautical radar system in the List West of Sylt, is deployed by the Department of Radar Hydrography of GKSS Research Center. In this thesis, the acquired image sequences by the system were analyzed by the Dispersive Surface Classificator (DiSC). The method was used to determine two most important coastal parameters, water depth and surface current. DiSC is based on the linear dispersion relation of the sea-surface wave and deformation of dispersion relation in coastal water due to the impact of seabed and surface current are taken in account to calculate bathymetry and current map. Though the theoretical limitation is known, a strong wind condition event was chosen for determining depths and mainly current features. The sensitivity of the different parameters in the method was discussed analytically. During the chosen period the wind condition was not strong enough to produce reliable bathymetric map, but suitable to derive current information. The current maps showed dominating inflow during flood phase. Same feature was observed in flow sequence over the tidal channel of List Landtief. Sediment motion in the area was also evaluated. The current information revealed by the method seems promising and reliable. As it is the first time that the method was used for flow calculation, the result shows significant symmetry with known environmental condition, which implies its feasibility for such interpretation. Extensions of the method DiSC, subjected to further modeling of nonlinear theories for coastal waters, which can overcome the limitation of the approach.

Abschätzung des Durchflusses und dessen Einfluss auf die Sedimentbewegungen in einem Tidekanal vor Sylt – mittels Radarfernerkundung

Zusammenfassung

Um wesentliche Umweltgrößen erfassen zu können bedient sich die Wissenschaft der Mittel der Fernerkundung. Auf der Insel Sylt, in der Nähe des Leuchtturms List West, wird von der Abteilung Radarhydrographie des GKSS-Forschungszentrums Geesthacht eine festinstallierte Radarstation mit einem nautischen X-Band-Radar betrieben. In dieser Arbeit wurden die von dem Radarsystem gesammelten Daten mit Hilfe des Dispersive Surface Classificator (DiSC) ausgewertet. Das Ziel der Analyse war es, die wichtigen

Parameter Wassertiefe und Oberflächenströmung zu berechnen. DiSC basiert auf der Linearen Dispersionsrelation von Oberflächenwellen und der modifizierten Dispersionsrelation aufgrund des Einflusses des Meeresbodens und der Oberflächenströmung um daraus die lokale Bathymetrie und Gesamtströmung zu berechnen. Für die Bestimmung der Wassertiefen und der bedeutenden Strömungseigenschaften wurden Profile ausgewählt, bei denen hohe Windgeschwindigkeiten vorherrschten, ohne die Beschränkung der Dispersionstheorie zu vernachlässigen. Im Zuge der vorliegenden Arbeit wurde der Einfluss der Steuerparameter auf die Qualität der Ergebnisse systematisch analysiert. Es wurde eine Periode ausgewählt zu der das Wellenfeld nicht zur bathymetrischen Berechnung geeignet war, weil die langen Wellen fehlten, aber genügend Seegang vorhanden war, um die Strömungsfelder zu berechnen. Auf den erzeugten Strömungskarten ist zu erkennen, dass während der Flutphase der Einstrom in den Haupttidekanal, das Lister Tief, dominierend ist. Der Tidekanal des Lister Landtiefs wies gleiche Strömungseigenschaften auf. Mit Bezug auf die Strömung wurde auch der Sedimenttransport in dem beobachteten Gebiet abgeschätzt. Nach Betrachtung der Strömungsdaten erscheint die verwendete Methode glaubwürdig und zuverlässig. In dieser Arbeit wurde zum ersten Mal die DiSC-Software für Strömungsberechnungen verwendet, aber die Ergebnisse stimmen maßgeblich mit den bekannten Strömungsbedingungen in der betreffenden Region überein, so dass ihre Nutzbarkeit für diese Art der Datenauswertung bestätigt werden kann.

Für die Zukunft ist eine Erweiterung der DiSC-Software in Arbeit, um die Beschränkungen auf lineare Fälle aufzuheben und nicht-lineare Theorien mit einzubeziehen.

Manuscript received / Manuskripteingang in TKP : 11th May 2007

Table of Contents

Tables and Figures III
Acknowledgements VII
Summary (in English) VIII
Summary (in German) IX
Notations X

1. Introduction 1
   1.1 *In-Situ* Point Measurements vs. Remote Sensing 1
   1.2 Objectives 3
   1.3 Background 3
   1.4 The Study Area 5
2. Theoretical Background 7
   2.1 Sea surface Waves 7
      2.1.1 The simple linear wave 8
      2.1.2 Stationarity of Waves fields 11
      2.1.3 Homogeneity of Wave fields 11
      2.1.4 Dispersion relation 13
      2.1.5 Water Depth and Near-Surface Current 15
   2.2 Radar Imaging 17
      2.2.1 Microwave Radar Remote Sensing 18
      2.2.2 Radar Equation 19
      2.2.3 Return Intensity 20
      2.2.4 Sea Clutter 21
         2.2.4.1 Backscatter Mechanisms 23
         2.2.4.2 Bragg Backscattering 24
      2.2.5 Modulation mechanisms 26
         2.2.5.1 Tilt 26
         2.2.5.2 Hydrodynamics 27
         2.2.5.3 Shadowing 27
         2.2.5.4 Aliasing 27

3. Methodology 29
3.1 Pre-DiSC 29
3.1.1 Experimental Setup 29
3.1.2 Wind Data 30
3.1.3 Radar Data 31
3.2 DiSC 33
3.2.1 Assumptions of DiSC 33
3.2.2 The Algorithm of DiSC 34
3.2.3 Basic Steps of the DiSC 36
3.2.4 Implication of DiSC 37
3.3 Post-DiSC 38
3.3.1 Export of Data 40
3.3.2 Identification of the Tidal Signal 40
3.3.3 Averaging the Depths 40
3.3.4 Calculation of Current features 41
3.3.5 Defining a Cross-section 41
3.3.6 Calculation of water transport 41
3.4 Relative Error in Flow Calculation 41
3.5 Velocity Profiling and Sediment Dynamics 42
4 Sensitivity Analysis 45
4.1 Calculation of MapDF 45
4.2 Calculation of Local Wavenumbers 50
4.3 Defining Water Levels 53
5 Results 55
6 Discussion 63
7 Conclusions 67

References 69
Appendices I

Tables and Figures

Figure 2.1: Classification of ocean waves and their relative energy. 8

Figure 2.2: A simple sinusoidal wave. 9

Figure 2.3: Sea-surface obtained from the sum of many sinusoidal waves. 10

Figure 2.4: Spectral instatinarity and inhomogeneity illustrated in a 2D k-ω section. 12

Figure 2.5: Positive and negative dispersion relation of linear deep-water surface-gravity waves in 3D Ω domain. 14

Table 2.1: Validity of the Dispersion Relation 15

Figure 2.6: Dispersion relation of linear surface-gravity waves in 3D Ω domain. 16

Figure 2.7: Dispersion relation of linear waves. 17

Table 2.2: Properties of the X Band Faruno 1201 nautical radar 19

Figure 2.8: Model of surface roughness and return intensity for X-band radar. 20

Figure 2.9: Radar Imaging Geometry and radar resolution 21

Figure 2.10: Scheme to visualize the relation between the scattering wave with the length λ_s and the electromagnetic wave with the length λ_r. 25

Figure 3.1 Location map of the installation site. 30

Figure 3.2: Radar Image sequence 32

Table 3.1 Specification of the Cartesian grid of the nautical radar image sequences. 33

Figure 3.3: Spectral decomposition by filtering. 35

Figure 3.4 Frequency ranges in DiSC to calculate Depth. 37

Figure 3.5: Flow chart of DiSC processing. 39

Figure 4.1: Locations of power in dispersion shell and the bandwidth of frequencies applicable for DiSC algorithm. 46

Figure 4.2: Influence of frequencies in current magnitudes. 47

Figure 4.3: Influence of Power in the number of regression coordinates and results. 48

Figure 4.4: Influence of Power in mean current velocity. 49

Figure 4.5: Frequency Slices of wavenumber planes: with red crosses distributed inside and outside of the wave power area. 50

Figure 4.6: Influence of Power in mean aerial current velocity during wavenumber calculation. 51

Figure 4.7: Influence of Power in the number of regression coordinates and results (current vector) during wavenumber calculation. 52

Figure 4.8: Influence of confidence in mean aerial current velocity during wavenumber calculation. 52

Figure 4.9: Influence of Block Power in mean current velocity during wavenumber calculation. 53

Figure 4.10: Influence of water level to mean current velocity. 54

Figure 5.1 Averaged bathymetry of common area during strong wind condition, black line marks cross section over the tidal channel (12.07.2001). 55

Figure 5.2 Graph representing the tidal cycle. 56

Figure 5.3: Scatter diagram produced by the comparison between radar-deduced water depths and echo sounding depths. 56

Figure 5.4: Tidal cycle of the current velocity. 57

Figure 5.5 Current vector map during the flood phase of the tidal cycle. 57

Figure 5.6: Current vector map during peak flood slug period. 58

Figure 5.7: Current vector map during ebb period. 58

Figure 5.8: Depth profiles over the cross-section in the tidal channel. 59

Figure 5.9: Velocity distribution over the cross section during peak flooding. 59

Figure 5.10: Velocity distribution over the cross section during peak ebbing. 60

Figure 5.11: Flow sequence over the cross-section in the tidal cycle using DiSC deduced bathymetry. 60

Figure 5.12: Flow sequence over the cross-section in the tidal cycle using sounding bathymetry. 61

Figure 6.1: The island of Sylt in 1240 and 1650. 66

Figure I-1: Beach Nourishment by sand at Sylt. I

Figure II-1: Wind speed record of Landstation_List1. II

Table III-1: Input file to DiSC. III

Table IV-1: List of efforts of Processing data for Bathymetric Parameters during the tidal cycle of July 12, 2001. IV

Table V-1: List of efforts of processing data for Current feature during the tidal cycle of July 12, 2001, using DiSC Bathymetry. VII

Table V-2: List of efforts of processing data for Current feature during the tidal cycle of July 12, 2001, using sounding Bathymetry. IX

Figure VI-1: The echo-sounding bathymetry of the investigation area. X

Figure X-1: Grain Size Distribution along the North of Sylt. Black line indicates the cross-section on the List Landtief XXXVIII

Figure XI-1: Visualization of hourly bathymetries of the whole tidal cycle. XLIV

Figure XII-1: Visualization of current maps of the tidal cycle. L

Figure XIII-1: ADCP measurements of the study area during a survey campaign. LI

Acknowledgements

I would like to express my sincere gratitude to Dr. F. Ziemer for giving me the opportunity to work at the Department of Radar Hydrography (KOR) of GKSS Research Center. His continuous support and patience throughout the work make me comfortable and confident to continue my research. I am also truly and deeply thankful to Professor R. Mayerle, Director of the Master Course “Coastal Geosciences and Engineering” for permitting me to pursue my thesis in GKSS and contributes as supervisor.

I extent my thankfulness to Mr. S. Flampouris, PhD student at KOR, for his continuous cooperation. His caring attitude and ability to explain scientific facts always impressed me. I would like to thank Dr. J. Seemann and Dr. C. M. Senet of Vision 2 Technology GmbH, GITZ, for the honour to share their ideas about the method, the Dispersive Surface Classificator (DiSC).

I also want to thank Mr. M. Cycewski, for tutoring me in PV-Wave programming and his instant helps solved most of the pitfalls in working environment. I cannot forget the others in the Radar Hydrography Department, M/S G. Schymura, L. C. Wu and S. Sedlacek, who provide their help to solve practical problems and make the life easier. I also want to acknowledge Dr. R. Riethmuller and Ms. M. Heineke of Coastal Oceanographic Measurement System (KOK), GKSS for providing measurement data for the thesis.

Finally I send my loving thanks to family and friends for remembering me. Shoma and Rasina, my wife and daughter, for their love, which gave me the wings to be here.

Notations

A_e	effective aperture area
C_g	group velocity of sea surface waves (ms^{-1}, ms^{-1})
C_p	phase velocity of sea surface waves (ms^{-1}, ms^{-1})
d_{50}	median grain diameter
∂	partial derivation operator
f	frequency (s^{-1})
g	gravitational acceleration (ms^{-2})
G_t	gain
k	wavenumber (rad m^{-1}), magnitude
$\vec{k}$	2D wavenumber vector of sea surface waves (rad m^{-1}, rad m^{-1})
k_s	Nikuradse equivalent sand grain roughness
κ	von Karman's constant
k_x, k_y, k_z	Cartesian wavenumber components (rad m^{-1})
λ	wavelength (m)
λ_S	scattering wavelength
λ_r	wavelength of electromagnetic wave
Ω	3D wavenumber-frequency domain (rad m^{-1} , rad m^{-1} rad s^{-1})
Θ	3D spatio-temporal domain (m, m, s)
P_r	receiving signal power
P_t	power
ζ	sea-surface elevation (m)
ς	intrinsic dispersion of sea-surface waves (rad s^{-1})
ς^+, ς^-	positive and negative solution of dispersion (rad s^{-1})
t	time (s)
τ	waveperiod
θ	incidence angle
$\vec{r}$	spatial vector (m, m)
$\vec{u}_c$	2D near surface current vector (ms^{-1}, ms^{-1})
U_{cr}	threshold current speed (ms^{-1})
x, y, z	spatial coordinates (m)

1 Introduction

Coastlines are environmentally sensitive interfaces between the ocean and land, and respond to changes brought by economic development and changing land-use patterns. As the coastal communities grow, there is an increasing pressure on the coastal region to provide habitat or livelihood for the humans. Those different land-use patterns need more new coastal infrastructure. Coastal engineering applications such as designing a breakwater or preventing the erosion along a beach require ocean wave information. Ocean wave observation can provide different properties such as wave period, wave direction and significant wave height etc. that can be used for coastal engineering applications, environmental protection, port operations, disaster prevention and rescue. Phenomena such as climate change also increase the necessity of continuous monitoring along the coastline. Additionally, there is an increasing need to establish the sustainability of our coasts as we increase our infrastructure. The rise in sea level and the shift in sediment transport due to coastal construction are constantly redefining our coastlines. These and other coastal phenomena occur on time scales of weeks to decades. Thus long term monitoring using a variety of coastal monitoring systems is needed to better understand coastal phenomena and to assess the sustainability of the coasts.

The near shore current dynamic is of fundamental importance in coastal research for the sake of coastal protection. Especially in shallow water regions with sandy grounds the ongoing change by erosion, transport and deposition of sand is permanently steered by an invariant current regime overlaid by episodic events with enforced current as well as by eddies and with breaking waves acting locally fortifying bottom erosion.

1.1 *In-Situ* Point Measurements vs. Remote Sensing

Diverse ways of wave measurement have been investigated since last few decades. They may be categorized as in-situ measurements and Remote Sensing Techniques. At present, various in-situ measurements have significantly developed and improve to better quality (DOONG et al. 2002). In-situ point sensors, such as buoys or bottom mounted pressure sensors are established ocean wave property retrieval systems and provide excellent temporal resolution because of their high sampling rate capability. However, in-situ point sensors provide no spatial information and in

addition have to be deployed into and survive within the harsh ocean environment. They must withstand wave forces, ocean currents, marine growth, and salt water immersion. Equipments are often damaged in rough sea deployments and must be constantly monitored.

Not exposed to the hampering wave forms are nearshore remote sensing methods, which include: Space-borne (satellite) radar, Synthetic Aperture Radar (SAR), X-Band radar, High Frequency (HF) radar and Video. The space borne sensors have properties of global measurements, large size footprint, and lower resolution of the order of a few ten meters to a few kilometers. But they are limited by their ability to provide long-term correlated, temporal information due to their lack of time on scene.

Shore-based remote sensing systems, such as video and radar remote sensing systems, can be set up at coastal sites and offer much longer times on scene. Video remote sensing systems are limited to daylight hours and cannot be used during environmental conditions that affect visibility (night, storms, hurricanes, rain, fog, etc). High Frequency radar measures with a scale of 1 kilometer and can provide spatial coverage of typical span 20-200 kilometers. But HF radar measurements can only provide one component of the wave field and cannot be used to calculate local water depth.

For the data requirements of coastal engineering, coastal area protection, coastal management and oceanic recreation, the interesting area is always within several kilometers to the land, which need high measurement resolution. Ground based X-band radar is suitable for monitoring the waves in near offshore or shallower zones, with the wave field ranging from a few meters to a few hundred meters. The ground based X-band radar is therefore the adopted wave and current measurement tool. Deployment of nautical X-band radar systems can typically be made in harsh weather without worry of damage to equipment. X-Band radar is not hampered by most weather or light conditions. The only exception is heavy rainfall that increases the background noise in a way that no “signal” is detectable.

1.2 Objectives

The scientific objectives of this study are:

1. Interpretation of X-band radar sequences to extract local water depths and current parameters by using the **Di**spersive **S**urface **C**lassificator (DiSC) (SENET et al. 2000, SEEMANN et al. 2000).
2. Calculation of local current and total water transport over a tidal cycle over a cross-section of a tidal channel in the near shore coastal zone of List West at the north Sylt island.
3. Estimate net water flow during the tidal cycle and its consequences in the morph-dynamics processes of the area.

The long-term goal may be defined as "to improve capability to use X-band marine radar sequences to routinely monitor waves, currents and bathymetry in coastal regions".

1.3 Background

The pioneers of remote sensing of the ocean surface were certainly COX & MUNK (1954a, b) and PIERSON (1962). In their celebrated study of glitter patterns, Cox & Munk provided the first systematic measurements of the roughness of the sea surface; the components of mean square slope, their probability distributions, and their variations with wind speed. Pierson's stereophotographic measurements from two aircraft [the Stereo Wave Observation Project (SWOP)] sampled the sea-surface configuration at several instants in time, which allowed the first direct measurements of the two-dimensional wave spectrum. Afterwards the field got different dimensions.

The radar remote sensing of the ocean surface flourished during the last three decades. The first civil system was the CODAR of NOAA (BARRICK 1977) and it concerns mainly the measurement of ocean waves and surface currents. Since then there were several projects around the world based on spatial and temporal structure analysis of radar images of the sea surface. In the past 20 years, algorithms have been developed to measure the wave directional spectra within

a 1 km^2 patch of the sea using a nautical radar; which enable to provide sea state parameters such as significant wave height and peak period. At least two companies commercialized this radar system, the **Wa**ve **Mo**nitoring **S**ystem (WaMoS), developed by GKSS research center in Germany (ZIEMER 1991 & 1995, ZIEMER & DITTMER 1994 and NIETO BORGE 1999) and the Marine Radar **Wav**e **Ex**tractor (WAVEX), developed by the MIROS AS Company in Norway (GRONLIE 1995 and GANGESKAR & GRONLIE 2000).

X-Band radar research was significantly advanced in the 1980s when technology was developed that allowed researchers to digitally scan photographs taken from radarscopes. This allowed researchers to use computer FFT algorithms to calculate wavelengths and periods providing a more accurate estimation of ocean wave properties. A three-dimensional analysis (YOUNG et al. 1985) of x-band radar images was presented to retrieve spectral information, such as ocean wave directionality and surface currents. From the acquired image sequences, hydrographic parameters, such as the water depth (OUTZEN 1998, WOLFF et al. 1999), the near-surface current-velocity vectors (SEEMANN et al. 1997 and SENET et al. 2001) and the calibrated full-directional wave spectra (SEEMANN et al. 1997) are determined. The method used in those studies is called 'Global method', which is based on the analysis of radar backscatter signal variance spectra calculated by the modulus of a 3D Fast-Fourier Transformation (FFT) performed on the image sequences. The 3D FFT in terms of image processing is a global operator. Therefore stationarity and homogeneity of wave field must be fulfilled.

The recently develop software DiSC, consists an algorithm, that analyses image sequences for the determination of the physical parameters on a local spatial grid. The local analytical method allows the analysis of image sequences of an inhomogeneous, dynamic and dispersive surface (SENET 2004, SENET et al. 2003, SENET et al. 2001, and SEEMANN et al. 2000a, b, c). DiSC was first used to calculate bathymetric change during a storm in the area of "Salzsand" (FLAMPOURIS 2006). Present study aims to investigate current parameters derived from the algorithm and evaluates the transport pattern in the designated area (List West at the north Sylt island).

1.4 The Study Area

Sylt is Germany's northernmost outpost, located in the German Wadden Sea in the federal state of Schleswig-Holstein. The island Sylt provides many recreational opportunities. Each year, the 40 km long west coast with its sandy beaches attracts about 600,000 tourists, which tourism the main sourch of income for the island of about 21,000 inhabitants. In 1999, the island was included in National Park project (the Schleswig-Holstein Wadden Sea National Park) in recognition of the high ecological significance, as a place to feed and rest the migratory birds and is an important for many fishes, crustaceans and marine mammals (DOODY et al. 2004). Activities such as hunting, mussel fishery and boating are severely controlled.

As a barrier island, the largest of the Fresian archipelago, Sylt consists of beaches and dune built against a residual core of glacial drift deposits (AHRENDT 2001). Although mainly composed by hard glacial deposit the shape of the island Sylt is dominated by sand that is in permanent motion. The eroding and transporting force of the tidal currents have a continuous impact on the island. This impact is enforced during storm events and in addition the eroding forces of the waves can increase the amount of sand in motion extremely. On the other side the flexible response of the sand to erosion has helped to keep the core of the island and to keep the loss of its core substance comparatively low during the storms of recent decades. But it is impossible to keep the island without supporting measures.

Past erosion mitigation strategies in Sylt used to be based on hard coastal defense works, including groins and concrete seawall. These measures proved to be counterproductive in the long run since they contributed to disrupt longshore sediment transport, thus generating further erosion downdrift and other environmental problems. Moreover, the seawall at Westerland suffered from severe damage during storm surges as a result of foreshore lowering in front of the structure. This led regional and federal authorities in the early 1970s to adopt new measured based on beach nourishment and other flexible solutions (DOODY et al. 2004). Now Sylt is quite illustrative of successful beach nourishment schemes (Appendix I) (SISTERMANS & NIEUWENHUIS 2007). Thus millions of cubic meters of sand of natural and anthropogenic origin are in motion along the island.

Working the nature, in such crucial areas is quite sensitive. If man interferes nature, he cannot do this without monitoring. This means not only tracking the sand, but as well to map the eroding and deposing forces. The word mapping shows that this monitoring must be conducted area covering to detect critical areas with enforced erosion or deposition. An adequate tool to conduct the area-covering mapping is provided by radar that allows an assessment of the spatial distribution of the forcing currents and waves. Within this thesis we introduce a method to assess the water transport through a given cross section of a near shore tidal channel and to evaluate which of the tidal phases is the dominating in respect of transport.

2 Theoretical Background

Radar is a mature technology that has been in use since the early part of the 20th century. The understanding and application of radar significantly advanced during the beginning of World War II due to its military applications. Radar was designed to detect and display the range to a target using electromagnetic waves generated in short pulses. Radar is an acronym for “RAdio Detecting And Ranging."

Radar Remote Sensing of ocean surface waves may in general be defined as measuring characteristics of the sea surface by means of electromagnetic waves so that the sea surface is itself not disturbed. The electromagnetic waves transmitted by the radar antenna are scattered back from the sea surface, modulated in amplitude and phase or frequency by the interaction with the sea surface in motion. This modulation carries information about sea-surface characteristics, surface waves and currents. Oceanographic data is extracted from the backscatter signal by sophisticated signal processing and data analysis (SKOLNIK 1990).

In the upcoming sections of this chapter, theories of sea surface waves and how the radar ‘see’ the waves shall be described for the better understanding of total approach of radar remote sensing technique.

2.1 Sea-Surface Waves

Ocean surface waves are the result of forces acting on the ocean. The predominant natural forces are pressure or stress from the atmosphere (especially through the winds), earthquakes, gravity of the Earth and celestial bodies (the Moon and Sun), the Coriolis force (due to the Earth’s rotation) and surface tension. The characteristics of the waves depend on the controlling forces. Tidal waves are generated by the response to gravity of the Moon and Sun and are rather large-scale waves. Capillary waves, at the other end of the scale, are dominated by surface tension in the water. The gravity of the Earth and the buoyancy of the water are the major determining factors of the gravity waves. Wind-generated gravity waves are almost always present at sea. These waves are generated locally by winds somewhere on the ocean and can propagate as “swell” thousands of kilometers.

This section consists the fundamental principles of the wave theory through the sea-surface waves and its dispersion relation with mathematical solution, widely published in the scientific community. This section is mainly based on SORENSEN 1997, HORIKAWA 2000, SENET 2004, STEWART 2006 and FLAMPOURIS 2006.

The general concept of the mechanism of wind sea-surface wave generation: If wind skims along the water surface, small perturbations of the near-boundary atmospheric pressure field lead to small perturbations of the water surface. The distorted surface allows viscous or turbulent energy transport, leading to the growth of waves. Several theories have developed for detailed explanation of the phenomenon (MILES 1957, HASSELMANN 1962, PHILLIPS 1966) but still it has not totally been clarified. The figure 2.1 compresses all the information about the energy distribution of the waves versus the frequency or the wavelength.

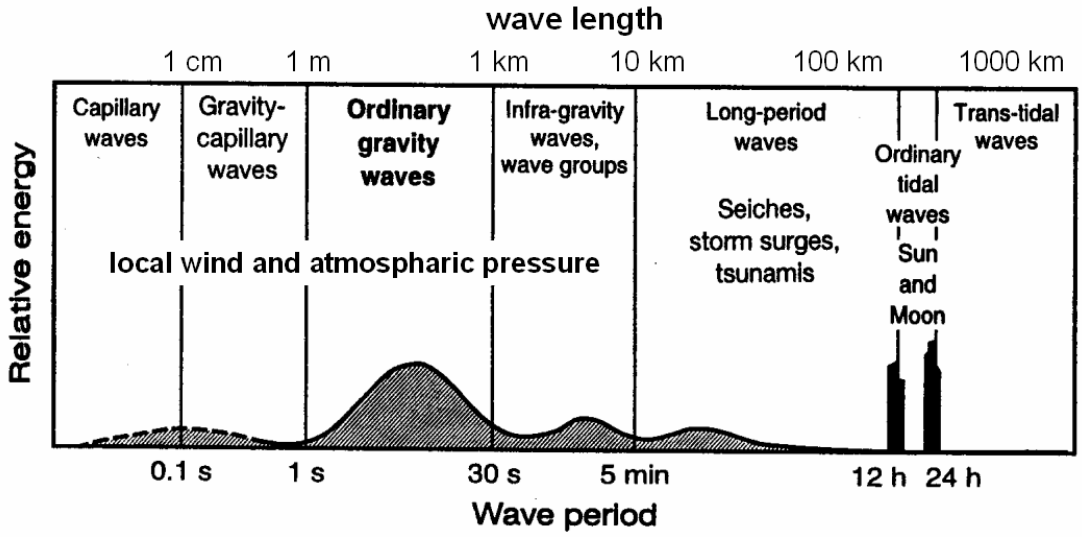

Figure 2.1: Classification of ocean waves and their relative energy.

2.1.1 The simple linear wave

The simplest wave motion may be represented by a sinusoidal, long-crested, progressive wave. The sinusoidal descriptor means that the wave repeats itself and has the smooth form of the sine curve as shown in Figure 2.2. The long-crested descriptor says that the wave is a series of long and parallel wave crests which are all equal in height, and equidistant from each other. The

progressive nature is seen in their moving at a constant phase speed in a direction perpendicular to the crests and without change of form.

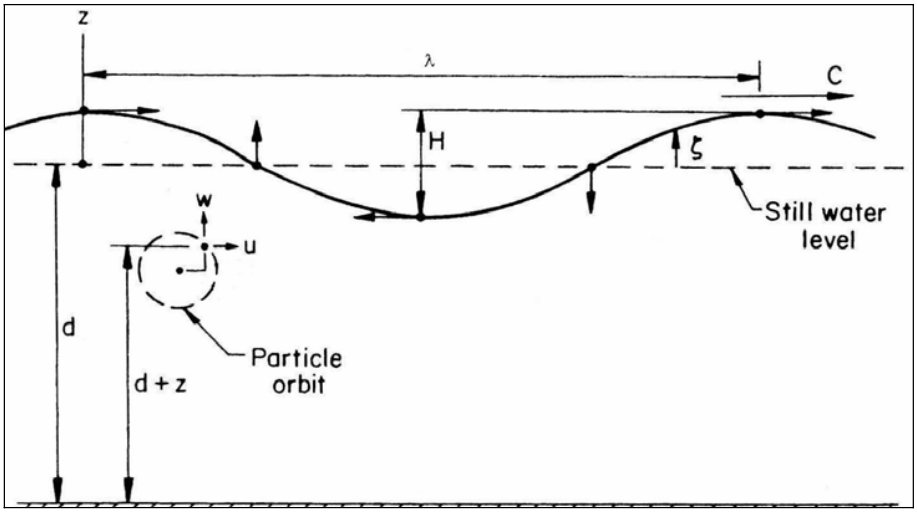

Figure 2.2: A simple sinusoidal wave.

In reality, the simple sinusoidal waves described above are never found at sea; only swell, passing through an area with no wind, may come close. The reason for starting with a description of simple waves is that they represent the basic solutions of the physical equations, which govern waves on the sea surface.

The more common and easy understandable approach of the sea-waves is the concept of a wave as a harmonic oscillation. It is characterized by the wavelength λ or the wavenumber $k=2\pi\lambda^{-1}$, the period τ or the angular frequency $\omega = 2\pi\tau^{-1}$, the amplitude ζ and the direction of propagation θ.

A sea-surface wave is a plane wave and therefore k and θ can be expressed in Cartesian coordinates as a two-component wavenumber vector, $k = (k_x, k_y)$. A linear sea-surface wave is sinusoidal shape. Deviations from this shape are expressed as nonlinearities. A single sinusoidal wave has the form

$$\zeta(\Theta) = \sum S e^{i(\vec{k}\vec{r}-\omega t)} + \sum S_* e^{-i(\vec{k}\vec{r}-\omega t)} \qquad (2.1)$$

where, ζ is the sea-surface elevation in the spatio-temporal domain $\Theta = (x, y, t)$, $S = \zeta_0 e^{i\phi_0}$ is the spectral Fourier coefficient, where ϕ_0 is the initial phase, S_* is the complex conjugated of S and $\vec{k}$ is the wavenumber vector and $\vec{r} = (x, y)$ is the spatial vector. The expression: $\phi = \phi_0 + \vec{k} \cdot \vec{r} - \omega t$ describes the phase, ϕ.

By generalizing the above concept, a wave field is defined as the superposition of single waves and its shape is the sum of n single waves (Figure 2.3).

$$\zeta(\Theta) = \sum S e^{-i(k_n r - \omega_n t)} \qquad (2.2)$$

where k_n is the nth wavenumber vector, ω_n is the nth frequency and $S_n = \zeta_n e^{i\phi_0}$, n is the nth Fourier coefficient for the nth wave.

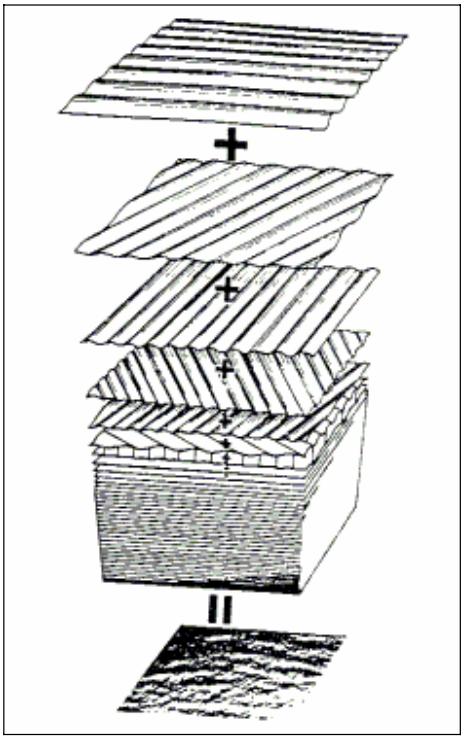

Figure 2.3: Sea-surface obtained from the sum of many sinusoidal waves (derived from PIERSON et al. 1955)

2.1.2 Stationarity of Waves fields

A stationary process is a stochastic process in which the probability density function of one random variable X does not change over time or position. As a result, parameters such as the mean and variance also do not change over time or position, experimental proved for at least short periods (PRINS 1996).

Therefore, the general definition of the stationarity makes clear that for a wave field two conditions must hold to fulfill the criterion of stationarity: the local temporal phase gradient, $\frac{\partial \phi_i}{\partial t}$, have to be invariant in time for a considered time period:

$$\frac{\partial \phi_i}{\partial t} = \omega_i \text{ and } \frac{\partial \zeta_{0,i}}{\partial t} = 0 \qquad (2.3)$$

where ϕ_i is the temporally local phase, $\zeta_{0,i}$ is the temporally local amplitude and ω_i is the temporally local frequency, which is constant. If one of the above criteria does not hold for at least one wave of the wave field for the period of the observation, the wave field is instationary.

2.1.3 Homogeneity of Wave fields

A stochastic process is defined homogeneous in space if the transition probability between any two state values at two given locations depends only on the difference between those state values (PRINS 1996).

For a wave field in an oceanic box two conditions must hold to fulfill the criterion of homogeneity: the spatially local phase gradients, $\frac{\partial \phi_i}{\partial x}, \frac{\partial \phi_i}{\partial y}$ and the local amplitude, y, have to be invariant in space. Defined for the Cartesian coordinates (x,y), the criteria of homogeneity are

$$\frac{\partial \phi_i}{\partial x} = k_{x,i} \text{ and } \frac{\partial \zeta_{0,i}}{\partial x} = 0 \qquad (2.4) \quad \text{and}$$

$$\frac{\partial \phi_i}{\partial y} = k_{y,i} \text{ and } \frac{\partial \zeta_{0,i}}{\partial y} = 0 \qquad (2.5)$$

where ϕ_i is the spatially local phase, $\zeta_{0,i}$ is the spatially local amplitude and ki are the spatially local wavenumber vectors, which are constant. If one of the above criteria does not hold in the considered oceanic box for at least one wave of the wave field, the wave field is inhomogeneous. The above-mentioned processes are inhomogeneous processes. The spectral effects due to inhomogeneous and instationary processes are illustrated in figure 2.4. If a wave field is instationary, the global spectral signal is smeared vertically to other frequencies (green dot); if a wave field is inhomogeneous, the global spectral signal is smeared to other wavenumbers horizontally (red dot).

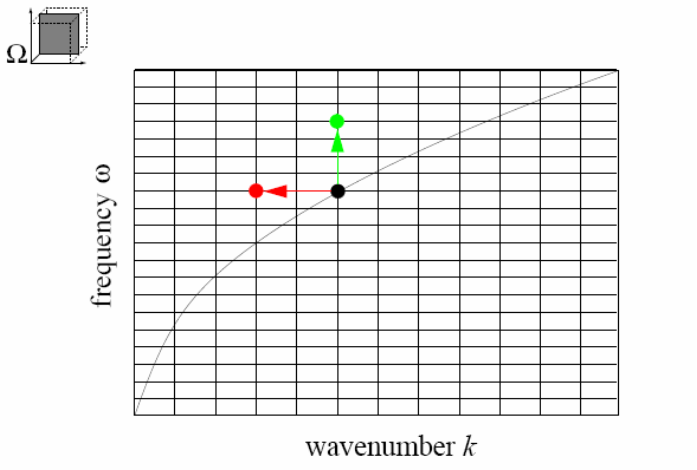

Figure 2.4: Spectral instatinarity and inhomogeneity illustrated in a 2D *k*-*ω* section. (SENET 2004)

2.1.4 Dispersion relation

The dispersion relation of sea surface waves is derived from the Eulerian equation of motion, the continuity equation and the dynamic and kinematic boundary conditions of the dispersion relation is given in (WINKEL 1994).

The phase speed C_p and the group speed C_g are given by

$$C_p = \frac{\omega}{k} \text{ or } C_p = \frac{\lambda}{\tau} \qquad (2.6)$$

and

$$C_g = \frac{d\lambda}{d\tau} \text{ or } C_g = \frac{d\omega}{dk} \qquad (2.7)$$

The phase speed C_p determines the speed of propagation of a single wave component, and the group speed determines the propagation of the wave field's energy. In extremely shallow water (wavelength λ>0.1.d) $C_g = C_p$; in deep water (λ<d/2) the condition $C_g = \frac{C_p}{2}$ holds.

The dispersion relation describes the dynamic relation between wavenumber k and angular frequency ω and determines the phase speed, speed of propagation of a wave. The dispersion relation generates a shell in the 3DΩ domain. The intrinsic dispersion shell is symmetric about the rotational axis, figure-2.5. The dispersion relation has two solutions, ς^+ and ς^-. Those two solutions are redundant, a consequence of the symmetrical attributes $\varsigma^+ = -\varsigma^-$ of the Fourrier transformation.

Because of the redundancy of the dispersion shells $\varsigma^+(\Omega)$ and $\varsigma^-(-\Omega)$ are double conjugate complex and only one of the shells is needed to describe the energy of wave fields in the Ω domain.

Linear surface gravity waves are sinusoidal waves of infinitesimally small amplitude. For a plane wave, the wave number and the angular frequency, connected by the dispersion relation:

$$\omega_0^{\,2}(k) = gk \tanh kd \qquad (2.8)$$

where ω_0 is the intrinsic frequency, g is the gravitational acceleration and d the water depth (STOKER 1957). This function has the shape of a shell within the 3-D wave-number frequency space as shown in Figure 2.6.

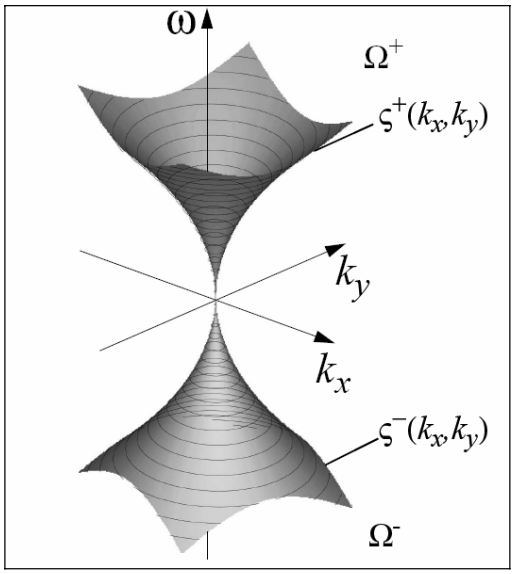

Figure 2.5: Positive and negative dispersion relation of linear deep-water surface-gravity waves in 3D Ω domain, (SENET 2004)

Dispersion relation of sea-surface gravity waves to the wavenumber components k_x and k_y, and angular coordinates ω is not universal. The relation is only dispersive in transient water (Table 2.1) condition. This relation distorted in both deep water ($d > \frac{1}{2}\lambda$) and shallow water ($d < \frac{1}{20}\lambda$) conditions.

Table 2.1: Validity of the Dispersion Relation

Deep Water	$\omega = \sqrt{gh}$	Non-Dispersive
Transient Water	$\omega = \pm\sqrt{gk\tanh(kd)}$	Dispersive
Shallow Water	$\omega = k\sqrt{gd}$	Non-Dispersive

2.1.5 Water Depth and Near-Surface Current

The dispersion relation (2.8) is valid when the velocity of encounter (vector sum of sensor velocity and the near surface current velocity) is zero. The so-called dispersion shell is illustrated in Figure 2.6 (a). The dispersion shell is deformed by the Doppler-frequency shift, which is induced by the near-surface current down to the penetration depth of the waves. The penetration depth for a single wave is approximately half of its wavelength.

Water Depth: For deep-water waves, defined by the condition $d > \frac{1}{2}\lambda$, the approximation $\tanh(kd) \approx 1$ holds and can be substituted into 2.8. By assuming $\vec{u}_c$=0, the deep-water wave solution is as follows:

$$\varsigma^{+}(k) = \sqrt{gk} \qquad (2.9)$$

In shallow waters, where d is small compared to λ, the shallow-water dispersion relation is:

$$\varsigma^{+}(k) = k\sqrt{gk} \qquad (2.10)$$

is obtained when the approximations $tanh(kd) \approx kd$ and $\vec{u}_c$=0 are substituted into (2.8). The deformation of the dispersion relation due to variation of waterdepth is illustrated in Figure 2.6 (b) and 2.7 (a).

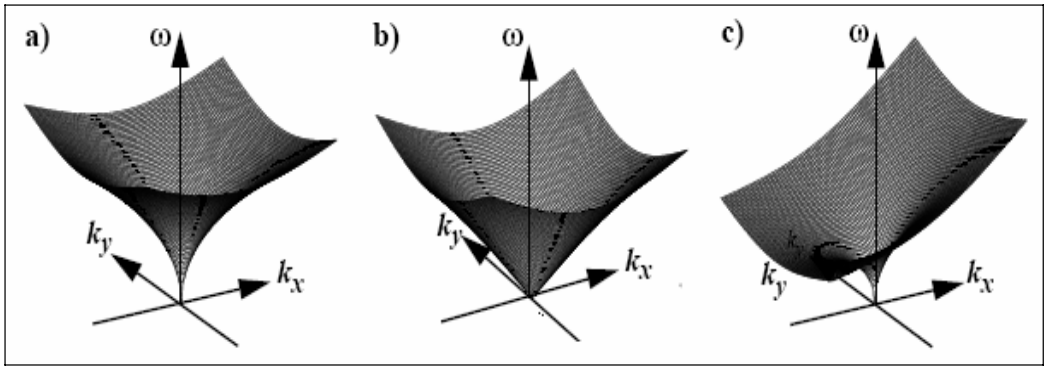

Figure 2.6: Dispersion relation of linear surface-gravity waves in 3D Ω domain: a) intrinsic deepwater dispersion shell, b) intrinsic shallow water dispersion shell and c) Doppler shifted deep-water dispersion shell influenced by near-surface current, (SENET 2004).

Near-surface current: Deformation of the dispersion shell starts with relative movement between the sensor and the ocean surface due to the Doppler effect. The relative movement is a superposition of the near-surface current velocity and the sensor's velocity relative to the ground. Both velocities summarized give the velocity of encounter $\vec{u}_e$. YOUNG et al. (1985) have extended the dispersion relation by this term:

$$\omega = \omega_0(kd) + \vec{k} \cdot \vec{u}_e \qquad (2.11)$$

where, ω is the angular frequency of encounter, and $\vec{k}$ the wave-number vector. Figure 2.6 shows the dispersion shell without and with Doppler shift. If water depth d and velocity of encounter $\vec{u}_e$ are known, the dispersion relation is used to select the signal of the linear surface gravity waves in the wave-number frequency spectrum. Therefore, it can be used as a filter to separate this spectral part from the background noise.

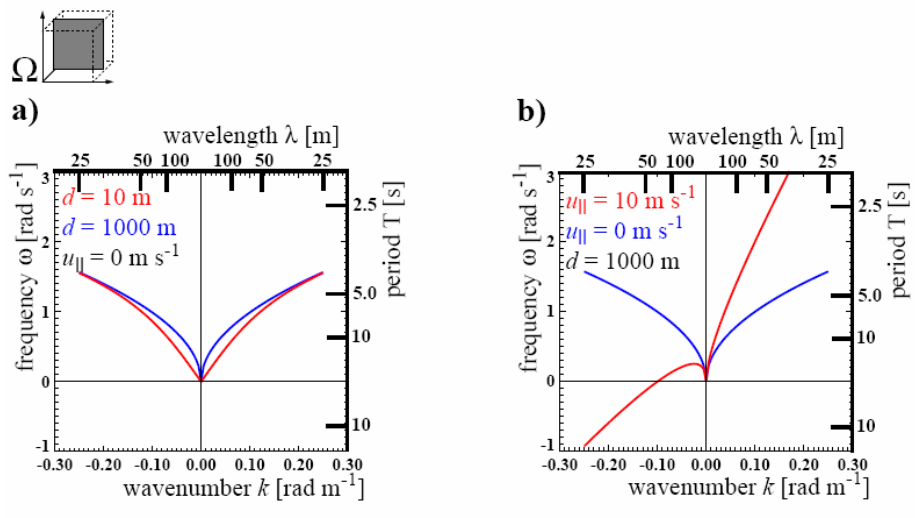

Figure 2.7: Dispersion relation of linear waves a) variation of the dispersion shell due to waterdepth and b) variation of the dispersion shell due to parallel component of the near surface current (SENET 2004).

If a near-surface current, $\vec{u}_c$, is present, waves are Doppler shifted. The Doppler shift, ω_D, leads to frequency shift of ω. If a current is directed in a direction opposite to that a wave, the wave's absolute (in the inertial coordinate system of the observer), frequency is decreased and vice versa. The deformation of the dispersion relation due to the Doppler effect is illustrated in figure 2.6 (c) and 2.7 (b).

2.2 Radar Imaging

Radar signals of electromagnetic waves scattering from the sea surface are used to measure information such as wind speed and direction, currents, currents shear zones and the directional ocean wave spectrum. Application of Radar techniques to oceanography offers a promise and a challenge. The promise is the potential of providing all-weather global measurements of waves, surface winds, current and temperature. The challenge is to gain needed insight to validate their use in solving important oceanographic problems (HASSELMANN et al. 1978).

Recently, considerable interest has been shown and high-level remote sensing technologies originally developed for military purposes have been converted for scientific and civil applications. A number of earth observation missions have been successfully undertaken providing some useful information. Oceanography, geology, hydrology, forestry and agriculture have been targeted for such applications as hazardous events prevention and territory management. Ocean wave remote sensing techniques can be performed from coastal ground, ship, aircraft or satellite. The sensor types include infrared sensor, optical sensor and radar. In this case, the used sensor is radar.

2.2.1 Microwave Radar Remote Sensing

The radar used for transmitting an electromagnetic energy via a rotating antenna and receives the signal by the same antenna. As radar is an active instrument it can be operated day and night. It is called all weather observation instruments as it is influenced only by heavy precipitation (rain and snow).

A pulse modulated radar system tracks the time that it takes for a radiated pulse of electromagnetic energy to travel to and from the target. The distance to the target is calculated from the relationship of speed (c), range (R) and time (T). The time for the range calculation must be divided by two since the electromagnetic pulse travels to and from the target. Therefore the range is $R = \frac{T}{2 \cdot c_{light}}$. The speed of the radiated electromagnetic energy, c, is the speed of light.

The free space velocity of light is 3.0 x 10^8 m/s. The azimuth (azimuth is the angle of horizontal deviation, measured clockwise, of a bearing from a standard direction) of the target can also be recorded if the radar is equipped with a rotating antenna.

Now a days, two bandwidths of electromagnetic waves are in use in ground based radar techniques. The first is High Frequency (HF) band (3 to 30 MHz) and the second is microwave band (frequency greater than 1 GHz). With HF system a wide coverage is possible as the HF signal produce a ground wave that allows to look behind the horizon. Thus a range up to 70 km may be observed. The microwave radars need the line of sight condition for the contact to the

ocean surface. Thus ground based microwave radar covers a range up to some nautical miles only. For the given task an X-band and 9 GHz radar was chosen, as backscatter of this frequency has proven to image wind waves and swell.

Although the observation range of coastal radars is not as extensive as satellites, the superiority of wave measurement by land-based radar lies in its capability to observe 3D images of the sea state by routine operation, as opposed to 2D observation made from satellite or aircraft. In addition, the wave monitoring systems by coastal radars are relatively easy to install and to operate. Thus it would appear that coastal radars are the potential instruments for the remote sensing activities of waves in the future.

For the present study we used ground based X-band, microwave radar (Furuno FR 1201). Details of the radar system are tabulated in Table 2.2.

Table 2.2: Properties of the X Band Faruno 1201 nautical radar

Properties	**Value**
Frequency	9410 MHz ± 30 MHz
Pulse repetition frequency	3 KHz
Antenna Type	Slotted Wave Guide
Antenna beam width	0.95°
Polarization	HH
Rotation speed	35-40 cir/min
Output power	5 KW nominal
Pulse length	0.05 μ sec

The antenna rotation time allows to image successively the ocean surface without the loss of correlation of the imaged wave fields. This allows to acquire image time series of the ocean wave fields, which have the quality to extract wave describing parameters by inverse modeling.

2.2.2 Radar Equation

The easiest way to describe the radars is the physical formation, as the single most useful description of the factors influencing radar performance is the radar equation that gives the range

of radar in terms of the radar characteristics. One form of this equation gives the received signal power P_r as:

$$P_r = \left(\frac{P_t G_t}{4\pi R^2}\right)\left(\frac{\sigma}{4\pi R^2}\right) A_e \qquad (2.12)$$

The right side has been written as the product of three factors to represent the physical processes taking place. The first factor is the power density at a distance R meters from radar that radiates a power of P_t watts from an antenna of gain G_t. The numerator of the second is the target cross section σ is square meters. The denominator accounts for the divergence on the return path of the electromagnetic radiation with range and is the same as the denominator of the first factor, which accounts for the divergence on the outward path. The product of the first two terms represents the power per square meter returned to the radar. The antenna of effective aperture area A_e intercepts a portion of this power in an amount given by the product of the three factors.

2.2.3 Return Intensity

The ocean surface scatters electromagnetic radiation, which is modulated by the properties of the surface. A smooth surface produces no return, intermediate surface roughness responses with moderate return and rough surface results strong return.

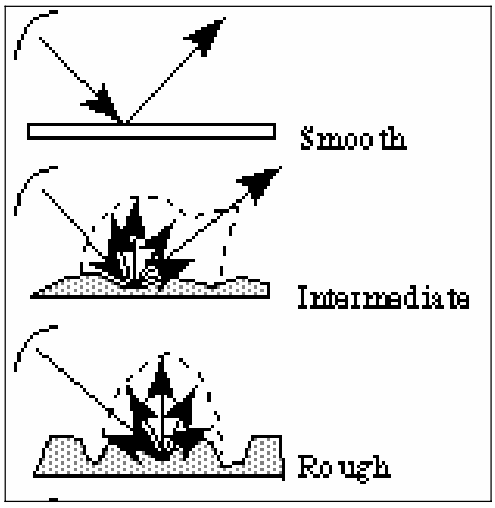

Figure 2.8: Model of surface roughness and return intensity for X-band radar (SABINS 1987)

2.2.4 Sea Clutter

The measurement of sea states using nautical radar is based on the backscatter of the electromagnetic fields by the ripples and roughness of the free sea surface due to the local wind. So, to obtain wave information from radar images, the presence of wind blowing over the sea is necessary (NIETO BORGE & SOARES 2000).

The interaction of electromagnetic waves and wind ripples has been extensively studied and still not fully understood. It appears that electromagnetic energy is mostly backscattered from the ocean surface by two general methods, either by specular reflection or by Bragg-resonant diffraction backscatter (YOUNG et al. 1985). Specular reflection is mirror-like reflection that is most prevalent for small angles of incidence. The incidence angle is the angle that the incident ray makes with the normal to the surface (VALENZUELA 1978). The grazing angle (ψ) is complement of the incidence angle. In specular reflection the electromagnetic energy is reflected directly off the surface of the water. Thus radar altimeters and other radar that look steep down on the sea obtain returns from such mechanism.

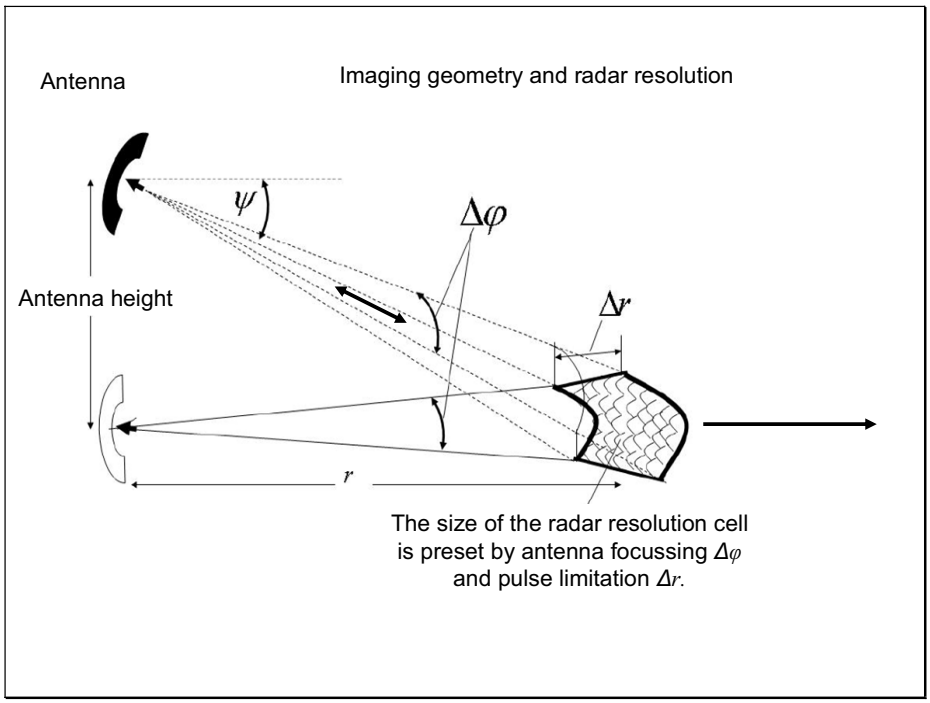

Figure 2.9: Radar Imaging Geometry and radar resolution

Bragg scattering is resonant backscatter that occurs when electromagnetic energy interacts with waves that have a wavelength interacting with the transmitted electromagnetic waves. At larger angels of incidence, Bragg scattering is responsible for the return, at grazing incidence Bragg scattering criterion being fulfilled by those wave having a wavelength equal to one half the electromagnetic wavelength. Small-scale capillary waves on the order of 1 to 3 cm provide the source for Bragg resonant scattering of marine X-band radars. The intensity of the backscattered energy is most affected by the magnitude of the wind velocity, the incidence angle of the emitted electromagnetic energy, and the azimuth angle of the radar relative to the crest of the wave. Bragg scattering is strongest when the radar azimuth angle is aligned with the wave direction.This pattern of returned electromagnetic energy is modulated by the larger structures, such as swell and wind sea waves, which are the aim of the method.

For a navigational radar, backscatter of the transmitted signal by elements of the sea surface often places severe limits on the detectability of returns from ships, aircraft, navigation buoys, and other targets sharing the radar resolution cell with the sea. These interfering signals are commonly referred as ***sea clutter*** or ***sea echo***. Since the sea presents a dynamic, endlessly variable face to the radar, an understanding of interfering signals will depend not only on finding suitable models to describe the surface scattering but also on knowledge of the complex behavior of the sea. Fortunately, a close relationship between radar and oceanography has grown up in the remote-sensing community, leading to the accumulation of a large amount of useful information about scattering from the sea and how this scattering relates to oceanographic variables (SKOLNIK 1990).

It would seem a simple matter to characterize sea clutter empirically by direct measurement of radar returns for a wide variety the radar and environmental parameters that appear to affect it. Parameters relating to the radar or its operating configuration, such as frequency, polarization, cell size, and grazing angle, may be specified by the experimenter, but the environmental parameters are quite another matter for two reasons. First, it has not always been clear which environmental variables are important. Even if the importance of an environmental parameter has been recognized, it is often difficult to measure it with accuracy under real sea condition, and there are practical and budgetary limits to obtain open-ocean measurements in sufficient variety

to develop any really meaningful statistical models of clutter. Little wonder that many aspects of sea clutter remain frustratingly unidentified.

It is commonly noted that the appearance of sea clutter depends strongly on the size of the resolution cell or radar footprint. For large cells it appears distributed in range and may be characterized by a surface-averaged cross section with relatively modest fluctuations about a mean value. As the size of the resolution cell is reduced, clutter takes on the appearance of isolated target like, or discrete, returns that vary in time. At these higher resolutions, the distributed clutter is often seen to consist of a dense sequence of discrete returns. When the discrete returns stand well out of the background, as they are seen to do for any polarization but most clearly with horizontal polarization at small grazing angles, they are called sea spikes and are common clutter contaminant in this radar-operating regime.

In 1956, however it is observed that at high frequency (HF) wavelength (tens of meters) scattering appeared to arise from a resonant interaction with sea waves of one-half of the incident wavelength (CROMBIE 1956), i.e., to be of the Bragg type. Reinforced by the theoretical implications of various small waveheight approximations and wave tank measurements under idealized conditions, the Bragg model was introduced into the microwave regime by many workers. This produced a revolution in thinking about the origins of sea clutter because it involved the sea wave spectrum, thus forging a link between clutter physics and oceanography in what became the field of radio oceanography. However, fundamental conceptual problems in applying the Bragg hypothesis in microwave scattering, along with recent questions about the validity of its predictions and the possibility of alternative scattering hypotheses, have reopened inquiry into the physical origins of sea clutter and how best to model it. This being the case, speculation about models will be kept to a minimum in the sections on the empirical behavior of sea clutter (SKOLNIK 1990).

2.2.4.1 Backscatter Mechanisms

There are various measuring techniques based on the backscatter theories of radar signal. Some are based on the analysis of the backscatter intensity of the return radar signal. Others use both the backscatter intensity and the Doppler spectrum. WRIGHT (1968) developed a composite

surface model to predict the backscatter of the ocean surface. The composite surface theory satisfies backscatter returns for almost all angles of incidence. However, as the angle of incidence approaches 90 degrees (grazing incidence) the situation becomes more complicated and the composite theory does not accurately predict backscatter from the ocean surface. Phenomena, such as wave breaking and wave steepness, complicate the development of a model that accurately predicts backscatter of the ocean surface.

The mechanism that leads to a scattering of the electromagnetic waves from the sea surface is dependent of the incidence angle. At small incidence angles with respect to the vertical (from about 20° to 70°), the main process is the so called “Bragg resonant process”, which is generated by the waves on the surface which are of the same order as the electromagnetic wavelength. At larger incidence angles (grazing angles above 70°), the backscattering is more complex, including shadowing effects and other complex mechanisms. In some case (HF radar) the backscattered signal provides “direct” information on the wavelengths of interest, because the Bragg wavelength is of the same order. In other case, marine radars, airborne or space- borne real or synthetic aperture radars, the backscatter is related to short wavelengths, but its modulations are related to the wavelengths of interest. For systems that use the Doppler information of the backscattered signal, the principle is in the relationship between the Doppler information and the wave orbital velocity that is in turn related to the waveheight.

2.2.4.2 Bragg Backscattering

The Bragg Backscattering consists the main theory broadly used for the backscattering of radars, e.g. ground based or naval radars, ERS SAR.

As the incidence angle of the radar is oblique to the local mean angle of the ocean surface, there is almost no direct specular reflection except at very high sea states. Therefore it is assumed that at first approximation Bragg resonance is the primary mechanism for backscattering radar pulses. The Bragg equation defines the ocean wavelengths for Bragg scattering as a function of radar wavelength and incidence angle:

$$\lambda_S = \frac{\lambda_r}{2\sin\theta} \qquad (2.13)$$

where λ_S is the sea surface wavelength of wind ripple, λ_r is the radar wavelength and θ is the incidence angle.

The short Bragg-scale waves are formed in response to wind stress. If the sea surface is rippled by a light breeze with no long waves present, the radar backscatter is due to the component of the wave spectrum which resonates with the radar wavelength. The Bragg resonant wave has its crest nominally at right angles to the range direction.

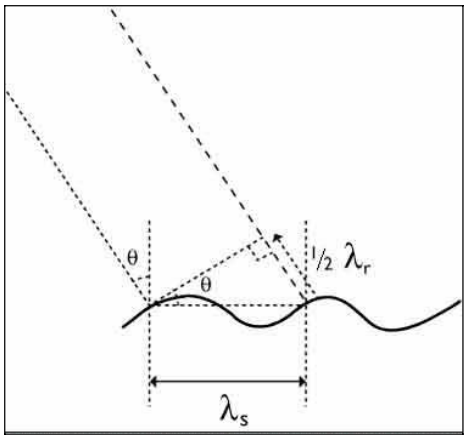

Figure 2.10: Scheme to visualize the relation between the scattering wave with the length λ_s and the electromagnetic wave with the length λ_r. The relation between those two is observed by (CROMBIE 1956) and consist the basic principle of the radar systems.

For surface waves with crests at an angle ϕ to the radar line-of-sight, as shown at the figure 2.9, the Bragg scattering criterion is:

$$\lambda_S^{'} = \frac{\lambda_r \sin\phi}{2\sin\theta} = \lambda_S \sin\phi \qquad (2.14)$$

where $\lambda_S^{'}$ is the wavelength of the surface waves propagating at angle ϕ to the radar line of sight.

The radars directly image the spatial distribution of the Bragg-scale waves. The spatial distribution may be effected by longer gravity waves, through tilt modulation and hydrodynamic modulation and aliasing.

Moreover, variable wind speed, changes in stratification in the atmospheric boundary layer, and variable currents associated with upper ocean circulation features such as fronts, eddies, internal waves and bottom topography effect the Bragg waves.

2.2.5 Modulation mechanisms

There are several modulation mechanisms that effect the measurements by the radar, the integrated effect of the processes are described in the next three paragraphs is that one image of long wave field is impressed to the radar signal that is related to the instantaneous sea surface by a Modulation Transfer Function (MTF). For the study discussed within this thesis, it is only necessary to localize the position of the moving wave crests and not the retrieve the real shape of the surface. The linear scaled imaging of the wave crests within the radar backscatter fields is not affected by the MTF, thus the intense about it is not real strong.

2.2.5.1 Tilt

Tilt angle modulation, hydrodynamic modulation and shadowing modulate the ocean surface backscatter allowing the gravity waves to be imaged on the radar. Tilt modulation is a purely geometrical phenomenon that is created by gravity waves “tilting” the ocean surface towards and away from the radar. Radar backscatter increases as the wave is tilted towards the radar and decreases as the wave is tilted away from the radar. Tilt modulation is most prevalent when the radar beam is perpendicular to the wave front. Tilt modulation provides no contribution to the backscatter if the wave crest is parallel to the radar beam.

2.2.5.2 Hydrodynamics

The sea clutter depends on the hydrodynamic conditions of the area of investigation; the effect of the currents on the signal is the most investigated. Hydrodynamic modulation is caused by the change in shape of the small-scale waves that cause Bragg scattering. Capillary waves increase in

amplitude and decrease in wavelength on the front of gravity waves and decrease in amplitude and increase in wavelength on the back of gravity waves. The modulation of the small-scale capillary waves on the front of the wave leads to a higher amount of backscatter on the front part of the wave.

Shipboard observers have reported bands of roaring breakers passing by on an otherwise smooth surface, presumably produced by powerful surface-current shears associated with large-amplitude internal waves. The general effect of the current is a change in the surface roughness, which can be expected to give rise to a change in sea clutter cross section (LONG 1983).

2.2.5.3 Shadowing

Shadowing occurs when the crest of one wave prevents illumination of the following trough. Thus a "shadow zone" is created between successive crests. Shadowing is the most prevalent modulating mechanism at high angles of incidence (DANKERT & ROSENTHAL 2004).

The shadowing effect at the image sequences of the coastal radar caused by the shape of the waves. The waves are characterized by bright signals from the near slopes and the absence, not illuminated by the radar, of signals from the far slopes. For the sea, it is likely that effects of shadowing become appreciable for angles of incidence closer to horizontal that the crest height and the sea wavelength. The shadowing of troughs by crests cause the reduction in expected scattered power. At near grazing incidence angles, when shadowing is appreciable, it is expected that the top of the crests contribute significantly to create the effective reflective surface.

2.2.5.4 Aliasing

The low rotation time of nautical radar antennas causes temporal undersampling, which leads to aliasing in the frequency domain (SENET et al. 2001). Aliasing occurs if a signal of a certain wavelength or certain wave period is spatially or temporally undersampled. Due to the relatively slow repetition time T_r of a nautical radar antenna, signals that have a shorter period than $2\,T_r$ are temporally undersampled. The repetition time T_r normally is of the order of 2 seconds.

3 Methodology

The complete methodology of the investigation is described analytically in this chapter. FLAMPOURIS (2006) described the methodology for the calculation of the bathymetry using Dispersive Surface Classificator (DiSC) in three basic sections, Pro-DiSC (3.1), DiSC (3.2), and Post DiSC (3.3). Pro-DiSC includes the necessary preparations for the exertion of the DiSC and at the Post-DiSC the post process analysis and the investigation of the results of DiSC.

3.1 Pro-DiSC

Before using DiSC, the choice of the appropriate radar data set is prerequisite. The choice depends upon the aim of the investigation. In this section, experimental setup for the study (radar station of the List West), logical approach to choice radar data and pre-processing of that data set are described in brief.

3.1.1 Experimental Setup at Sylt

The island of Sylt is one of the most prominent and famous tourist sites in Western Europe affected by coastal retreat. Sylt, which is directly influenced by wave attack, is situated on the west cost of Schleswig-Holstein, northern Germany.

The radar was mounted near the lighthouse List West on the island of Sylt (Figure 3.1). The areas covered by the radar images are List West, the Lister Landtief, and parts of the Lister Tief. The motivation for the coastal area at Sylt is its high morphdynamical activity. A sand bar between the Lister Landtief and the Lister Tief is in the process of wave breaking, which would change the flood stream situation dynamically.

In general Sylt is a tourist island with a history of rapid erosion. Within the observation area the tide is semi-diurnal and the tidal range reaches approximately 2m. Tidal currents are dominant where water depth is less than 10m seaward, with resulting sediment transport to the north (AHRENDT 2001).

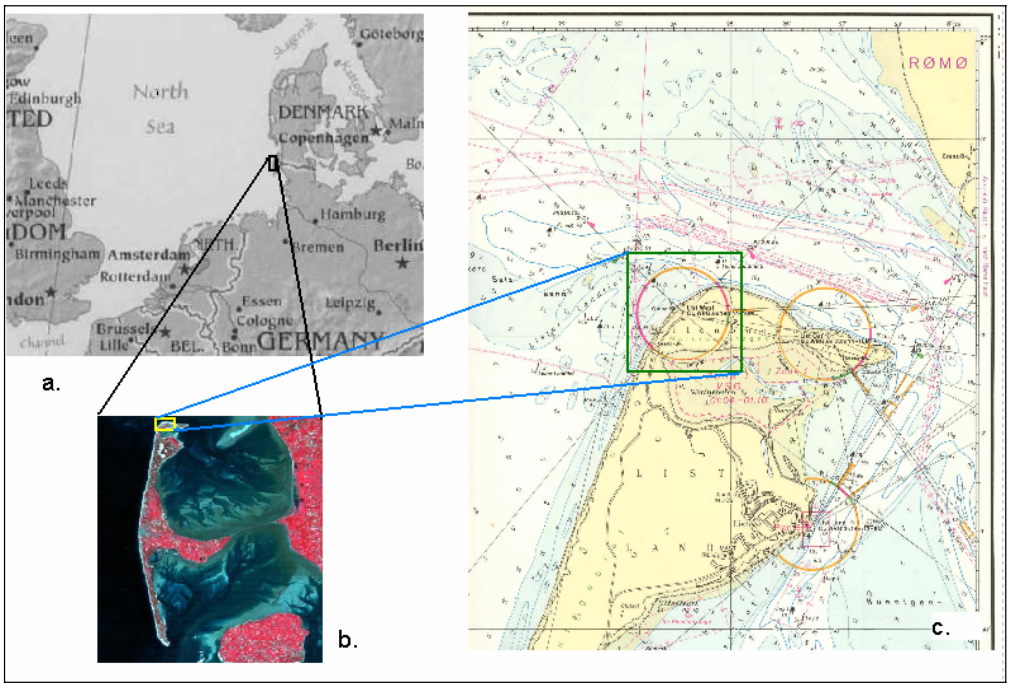

Figure 3.1 Location map of the installation site; a. and b. Locations of the island of Sylt and the Lister Tief in the German Bight of the North Sea; c. Radar Station located in the List West of Sylt, in the center of green frame.

The used instrument for the acquisition of the sea-surface is a software-hardware combination, presented by NIETO BORGE et al. (1999), as a part of the Wave Monitoring System (WaMoS), consisting of a Furuno FR 1201 nautical radar (FURUNO MANUAL 1989), a WaMoS II analog-digital converter and a WaMoS II software package for the acquisition of the radar images. The radar is a ground-based nautical X-band radar with horizontal polarization (HH), mounted 25m above the NN. The range of the radar covered circle of about 1km radius. The radar was mounted in the year 1999. The detailed specification of the radar is tabulated in Table 2.1.

3.1.2 Wind Data

Wind parameters were used as indicator of the appropriate weather condition that matches with the objective of the investigation. It is important to be underlined here that the intensity of the backscattering depends on the wave conditions and wind, as the generating force is determiner. The available raw radar data are about six years, 1999 till 2005, with gaps, so it was essential to define a criterion about to choice of the period. FLAMPOURIS (2006) chose storm condition to estimate bathymetric change during the storm. As long as the aim of the present study is the

calculation of local current over a cross-section of a tidal channel, storm condition is not required. A strong windy condition over a moderate period of time is necessary to get reasonable sea-clutter for interpretation. A threshold level of the wind velocity of 6 Beaufort (22 knots) was defined as strong wind condition for the investigation.

The wind data set used here, is provided by Seewetteramt of Hamburg. The weather station is laying on Sylt, 55°00′48″N and 8°24′47″E, 10m above the ground and over 20m over NN. In the data files, year, month, day, the wind direction in degrees and the 10min means of the wind velocity in nautical miles per hour, were recorded.

There were plenty of events with the criterion of wind speed, (see: Appendix II). But for the selection of the investigation period, the conditions that ultimately resulted storm were avoided. A moderate duration (more than 12 hours) of strong wind condition was also looked for. After considering all above conditions the period was selected randomly by matching with the radar recording time (it has gaps). It is essential to mention the reasons that there are not available radar data during full period of the six years, even though the radar was on function. The reason behind discontinuity of radar data in this case was requirement for huge storage capacity for the raw data. Every sampling needed about 90Mb of memory space. Archiving of this bulk quantity raw data confronts various problem, mainly at the hardware level.

Finally, the period was chosen on 12th August of 2001. It has an additional advantage of getting a eco-sounding data (see: Section 3.2.4).

3.1.3 Radar Data

During the investigation period, radar sequences, which consisted of 256 single images, were acquired with a time interval of approximately 1.8s, which is equal to the antenna rotation time. Thus, the total sampling time was approximately 8 minutes. The polar images cover a radius of approximately 1km, were interpolated to a Cartesian grid with a cell size of approximately 6.82m x 6.82m, corresponding to the spatial resolution of the radar. The number of pixels for one image is 288 x 288. The image sequence, presented here as an example (Figure 3.2), was acquired during the strong wind condition. The exact specifications of the Cartesian grid of the nautical radar image sequences are list at the table 3-2. The antenna rotation time varies from sampling to sampling but lies near the 1.8s; the reason of the variance is the wind impact to the antenna.

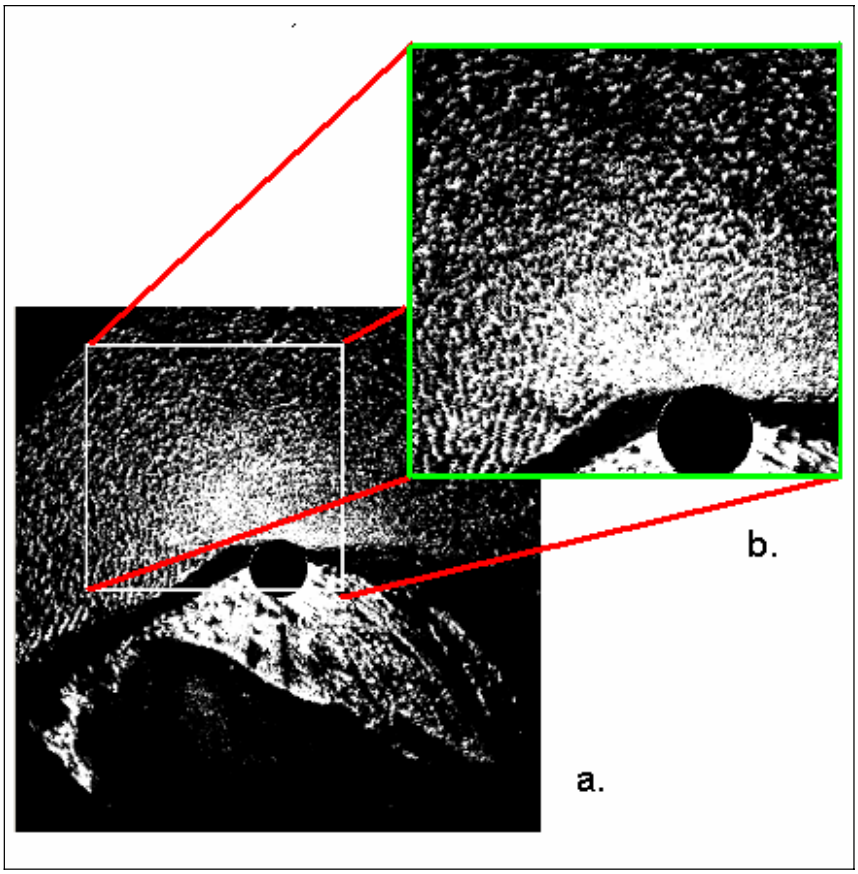

Figure 3.2: Radar Image sequence; a. An image sequence of the whole radar range and b. Sequence of the investigation area. (Source: Radar Hydrography, GKSS Research Center)

The radar data sets for the selected period were downloaded from the archive and those data sets contained polar coordinates. The transformation of the coordinates of the radar data from polar to Cartesian was done by using pre-developed software in PV-Wave (SENET & SEEMANN 1999). The algorithm of the software is the Nearest Neighbor interpolation method. For each cell of the polar coordinates, the distance between the cell and the center of the image and angle between the line which connects each cell with the center and the y-axis are calculated, so for each cell there is a pair of coordinates, (distance, angle). By using the nearest neighbor algorithm all these pairs are matched to the Cartesian grid.

Table 3.1 Specification of the Cartesian grid of the nautical radar image sequences.

Number of pixel in x-direction (west-east) N_x	288
Cartesian-grid pixel resolution in x-direction (west-east) Δ_x	6.82m
Spatial length in x-direction (west-east) X	1964m
Number of pixel in y-direction (south-north) N_y	288
Cartesian-grid pixel resolution in y-direction (south-north) Δ_y	6.82m
Spatial length in y-direction (south-north) Y	1964m
Number of image per image sequence N_t	256
Temporal resolution (antenna-rotation time) Δ_t	1.8s
Temporal length of an image sequence T	460s

3.2 DiSC

The DiSC is a multi step method that has been developed at the Radar Hydrography Department of the GKSS. The product is currently available commercial software of Vision 2 Technology GmbH, partner of the Geesthachter Innovations und Technologie-Zentrum (GITZ).

By using the commercial software DiSC, the radar data were analyzed. The DiSC is a recently developed algorithm (SENET 2004), which analyses image sequences for the determination of physical parameters on a local spatial scale, it consists a local analysis method, which allows the analysis of inhomogeneous image sequences of a dynamic and dispersive surface. The basic idea of the method is that in shallow waters wave fields become inhomogeneous due to spatially variable bathymetries. Local changes of the wave field, containing the local bathymetry information, which are taken into account.

3.2.1 Assumptions of DiSC

The use of DiSC has two basic assumptions, stationarity and validity of the multi-component image model (SENET et al. 2003).

Stationarity: the imaged process analyzed by DiSC has to be stationary. Stationarity implies the temporal invariance of the statistic of the process. Assuming stationarity, DiSC can treat the

spatial Fourier decomposition of the distinct frequency components independently, with complex-valued spatial image at a constant frequency.

Validity of the multi-component image model: for inhomogeneous images the amplitudes or the spatial phase gradients (i.e. the local wavenumber vectors) vary. This information is only implicitly included in the coefficients of the Fourier decomposition. To enable explicit analysis, the spatial Fourier decomposition is transformed to an image representation, composed of a superposition of 2D jointly amplitude-frequency-modulated, locally coherent, analytic signals, multi-component image model.

3.2.2 The Algorithm of DiSC

The method to measure the bathymetric and current maps based on the analysis of radar image sequence was developed (SENET et al. 2001, SENET 2004). A nautical radar measures in space x and y, and time t (see: Chapter 2). This method therefore suitable to measure the spatial and temporal evolution of the sea-surface wave field $\zeta(x, y, t)$.

3D Fast Fourier Transformation: The WaMoS system provides digitized time series of sea-clutter images. The spatial and temporal sea-state information is stored as an image sequence cube of gray values $I(x, y, t)$. A three-dimensional fast Fourier transformation (3-D FFT) is used to transform the spatio-temporal information into the spectral wavenumber-frequency domian Ω

$$\left|FFT(I(x,y,t))\right|^2 = P(k_x, k_y, \omega) \qquad (3.1)$$

where $k_x = 2\pi x^{-1}$ and $k_y = 2\pi y^{-1}$ are the components of the wavenumber vector $\vec{k}$, and $\omega = 2\pi t^{-1}$ is the angular frequency. The result of (3.1) is a 3-D image power spectrum $P(k_x, k_y, \omega)$. The spectral energy (or gray-level variance) of the imaged surface waves is located on a surface in the Ω-domain defined by the dispersive relation of surface gravity waves.

Spectral Decomposition: The aim of the spectral decomposition of the spectral signal of the inhomogeneous wave field is the division of the signal into one-component images containing separated and analyzed parts of the wave field. The spectral decomposition technique DDF-S (Directional Dispersion Frequency-Separation) is based on the combination of

- a frequency separation (taking a $k_x - k_y$ slice of the 3D wavenumber-frequency spectrum, and
- a directional-wavenumber band pass filter in the $k_x - k_y$ centered on the dispersion shell (dispersion filtering),

yielding a spectral DDF bin. The principle of DDF-S is outlined in Figure 3.3.

Dispersion filtering is required because of the non-linearity of radar imaging of the sea surface waves. The nonlinear modulation transfer function (MTF) can be expanded in a Volterra series (CHERRY 1994), creating sum-difference and harmonic signals in addition of the linear fundamental mode in the radar image spectrum. The linear (fundamental mode is selected by dispersion filtering. The remaining spectral smearing is caused by the inhomogeneity of analyzed area.

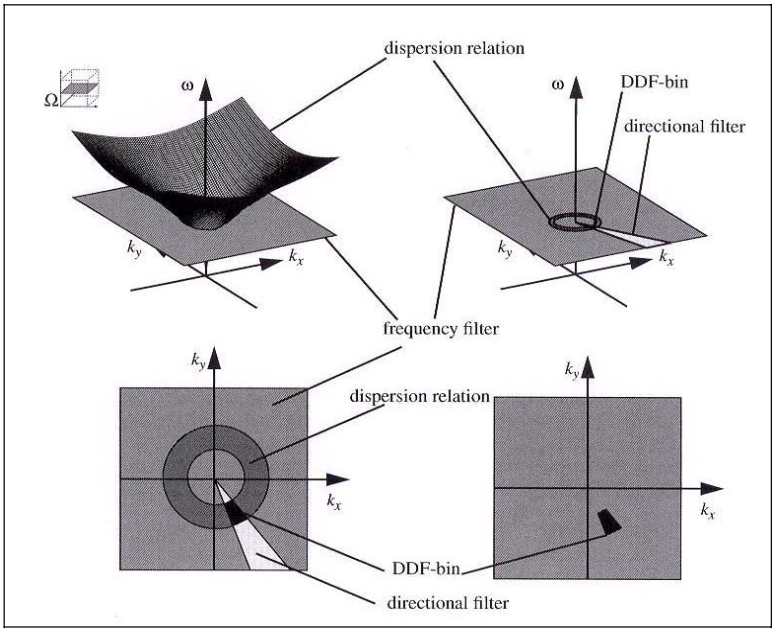

Figure 3.3: Spectral decomposition by filtering [extracted from DiSC (SENET, 2004)]

Inverse 2D FFT: Complex-valued one-component images are calculated by transforming the filtered Frequency Slices of wavenumber planes of the 3D image spectrum into the spatial domain, using a 2D FFT^{-1}. The spectral decomposition and inverse 2D FFT yields complex-valued spatial one-component images. These complex-valued one-component images are illustrated as power phase of a separate part of the wave field.

Calculation of local wavenumber: Determination of spatial maps of local-wavenumber vectors is achieved using the phase of the complex-valued one-component images. Initially an approximate version of the Multiple-Signal Classification algorithm (STOICA & NEHORAI 1989, HAVLICEK et al. 1996) was used to estimate local wavenumber vectors. The method provides complex-valued wavenumber vectors.

Calculation of hydrographic parameters maps: In the gray-level variance spectrum, the linear portion of signal energy of the waves is located on the dispersion shell surface waves $\tilde{\omega}(\vec{k})$. The sum of the sensor's velocity, $\vec{u}_s$ (i.e. ship velocity), and the near-surface current, $\vec{u}_c$, deforms the dispersion shell to the Doppler-frequency shift, ω_D.

The first approach (YOUNG et al. 1985) to determine the near-surface current was based on a least squares fitting technique. The idea behind the least-squares technique is that the theoretical dispersion shell (see: Section 2.1.4) is fitted to the linear portion (fundamental mode) of the spectral signal of the imaged wave.

3.2.3 Basic Steps of the DiSC

- Transformation of the image sequence to the spectral domain by 3D FFT,
- Decomposition of the complex-valued image spectrum for the separation of the wave signal from the noise, by using filtering techniques,
- Directional and dispersion separation of the complex-valued spectrum into spectral bins at 2D wavenumber planes of constant frequency,
- 2D inverse Fast Fourier Transformation (2D FFT-1) of the spectral bins yielding complex-valued, one-component spatial maps in the spatio-frequency domain,
- Calculation of spatial maps of local wavenumbers from the one-component images of constant frequency,
- Composition of one-component local wavenumber maps of constant frequency to local 3D spectra and
- Use of the spatial maps of local wave number vectors and power for the calculation of spatial hydrographic parameter maps.

3.2.4 Implication of DiSC

The imported data set of the DiSC is the 3D image sequence that has to be analyzed, each of the radar image sequence, has three dimensions, the x (easting), the y (northing) and the time t (as number of images), these information are imported at the beginning of the process to the DiSC. In addition to them the number of pixels at x and y-axis, the real size of each pixel and the rotation period of the antenna are imported (Appendix III).

The implication of DiSC involves multiple steps. FLAMPOURIS (2006) described the steps in details with emphasis on Import parameters, the Algorithm and the Exertion of DiSC, 3D Fast Fourier Transformation, Spectral Decomposition and the Inverse 2D FFT, Calculation of Local Wavenumbers and Calculation of Hydrographic Parameter Maps.

For the purpose of the present investigation, DiSC was used at two different levels. First, it was used to calculate depths. Depth calculation considers the longer waves, which are distorted by the bottom. Therefore frequencies in consideration were low (green zone in Figure 3.4). Later, for the calculation of the local current shorter waves with higher frequencies were considered (red zone in Figure 3.4).

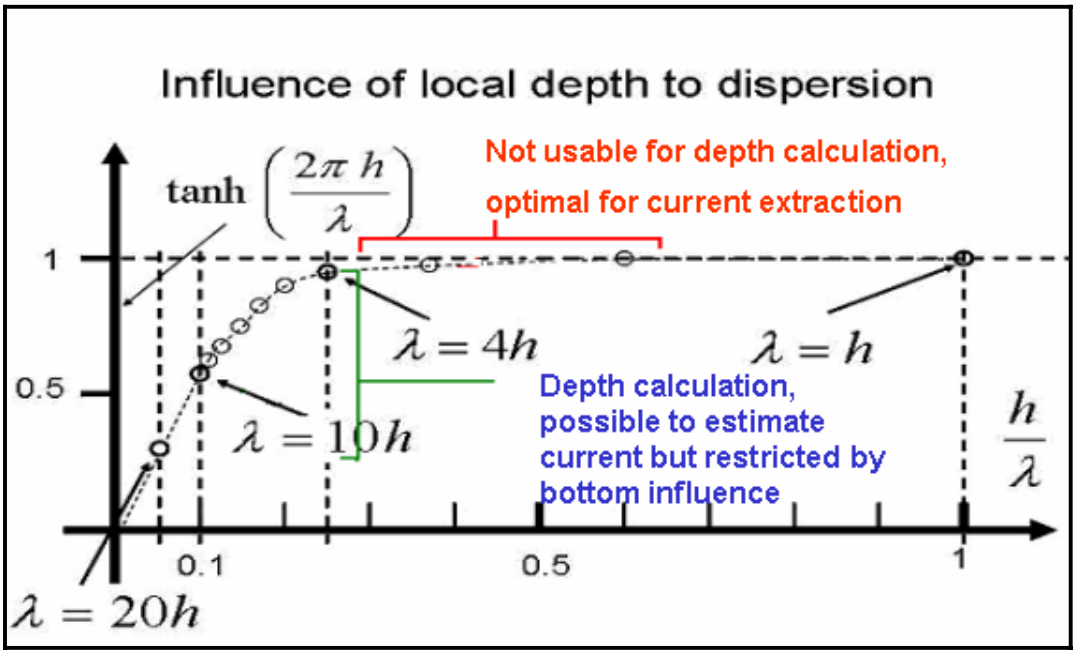

Figure 3.4 Frequency ranges in DiSC to calculate Depth (adopted from ZIEMER et al. 2004).

During the process, the user has to define, from the sequence of the calculated spectrum, the anchor positions for the spectral filter bank in the 3D spectral domain, which is used for the spectral separation. The demanded parameters are the frequency **minimum** and **maximum**, the **power** where these minimum and maximum lies and the **number of the bins**. For the calculation of the wavenumbers, the required spatial parameters are **power**, **block power**, **confidence limits** and also the **size of the cell** (Figure 3.5). All the efforts in calculating depth and current are tabulated in Appendices IV and V respectively.

During the calculation of current, bathymetry gained from the DiSC was imported to calculate current vectors. The parameters defined in the process have variety of influences in the output of DiSC. Those influence were analytically presented in the next chapter.

In the recent version of DiSC an option for defining cross section in the hydrographic map was included. By using the tool, user can select a profile in the map to calculate normal and parallel vectors of the current components. The flow rate is calculated based on the velocity vectors. The tool also provides visualization of the results and saving function of the profile for further implication.

For comparison, echo-sounding bathymetry of the region also used in DiSC to calculate current vectors with same tidal deviation. The soundings were performed on campaign SS02 of Coastal Oceanographic Measurement System (KOK) of GKSS dated 17.09.2001 (Appendix VI). As sounding data were consisting of small grids (2m in each dimension), those data were converted to the same grid size as DiSC grid. For this reason, a program in the PV-Wave has been developed, Appendix VII. The concept of the program was averaging. It took all small grids in account and averaged the depth for the large grid cell.

3.3 Post-DiSC

After the DiSC processing the outputs were evaluated by comparing with recent navigational chart of the area. The first step was the optimization of the reliability of the results according to the number of the regression coordinates. The second step is the identification of the tidal cycle from the calculated sea level; the next step is the averaging the bathymetry from the whole tidal cycle. This mean bathymetry was used as reference depth for calculating surface current. The

fourth step is to define a cross-section in the tidal channel and finally calculating the transport over the cross-section during the period.

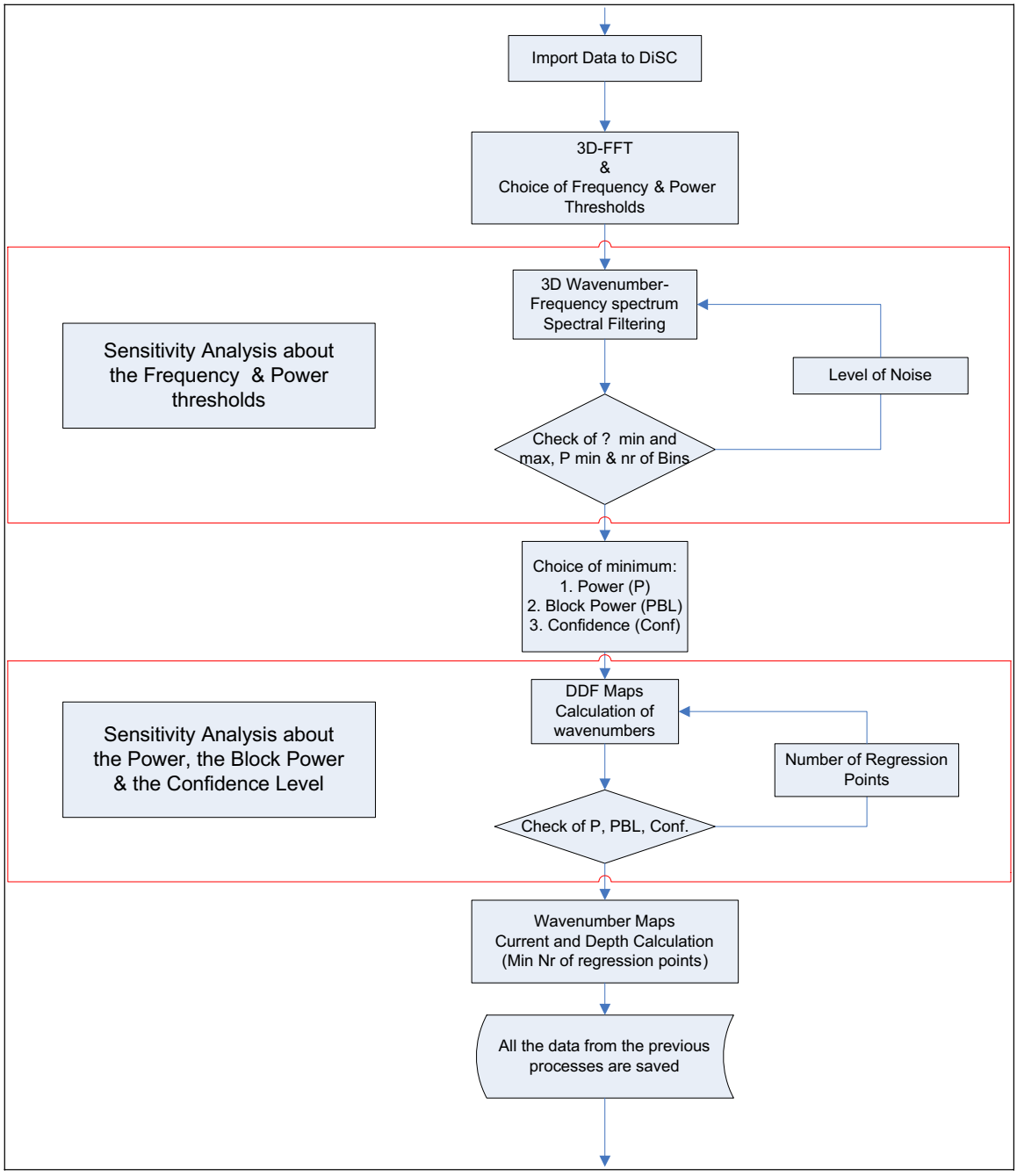

Figure 3.5: Flow chart of DiSC processing. The first step is the import of dataset and calculation of 3D-FFT. The next step is the choice of frequency bins and the inverse 2D FFT, the third step is the choice of the regression for calculation of local wavenumbers and their calculation. The last step is the calculation of hydrographic maps.

3.3.1 Export of Data

The final result of the DiSC software is a text file, in which are stored the coordinates of every cell for which has been calculated the instantaneous water depth, the number of the regression coordinates, the calculated depth and the current vector. For the further processing of the data, it was necessary to export the data and to create a new file, which includes all the results. For this reason, a program in the PV-Wave has been developed, Appendix VIII. The program consists of 6 subroutines, the basic concept is that the complete grid of the area of analysis is created, the coordinates of the grid are compared with the coordinates of each of the results and the output is one file where the results are stored in the whole grid. For the cells that have not been calculated any depth, an extreme value is matched.

The structure of the program permits to the user to define the check of the number of coordinates and to export any of the calculated variables, number of regression coordinates depth or current vectors. The calculation time for a grid of 2256 cells and for 60 files is approximately 4 minutes. The averages of the process are the grouping of the results according to the requirements of the user and the easy manipulation of the results by using any commercial program, for data analysis, e.g. Microsoft Excel, Golden Software Surfer.

3.3.2 Identification of the Tidal Signal

The identification of the tidal cycle consists of common (BELL 1999; ROBINSON et al. 2000) way to control the whole series of the image sequence analysis and the comparison with gauge measurements consist strong evidence about the reliability of the results. In this case, for the estimation of the tidal cycle were averaged the calculated sea levels of 9 neighboring cells around the point (3460639.94, 6101546.477), which cover an area of 14,400 m^2, and they have been plotted for the twelve hours of each period of analysis.

3.3.3 Averaging the Depths

As the water depth fluctuates during a tidal cycle, all hourly water depths were considered to get a reasonable average. The mean bathymetry was calculated by averaging the 12 depths of a tidal cycle. Microsoft Excel was used for the averaging.

3.3.4 Calculation of Current features

From the repeated DiSC implications with imported bathymetry, two components of the horizontal current vector (V_x and V_y) were derived. A program in the PV-Wave has been developed (Appendix IX), to calculate current magnitudes and current directions. In the assumption of the DiSC, the current velocity is depth averaged (average in the vertical column). Current vector maps of the study area for complete tidal cycle were produce by using commercial software (Surfer of Golden Software).

3.3.5 Defining a Cross-section

A cross-section in the tidal channel was defined, avoiding the shallower area in the List Landtief. The process was done by using Digitizing component of Golden Software Surfer. Later a module was added in DiSC to define cross-section. Further calculations for flow estimation were carried out by using DiSC module.

3.3.6 Calculation of water transport

From the DiSC current calculation, the transport of the water masses over the cross-section was calculated according the nearest neighbour values of the line. Based on the DiSC results, normal and parallel components of the current vectors were calculated from the defined cross-section. The water transport over the cross-section was estimated mainly based upon the normal component of the current vectors.

3.4 Relative Error in Flow Calculation

The accuracy of the technique, its limit, and adaptability are described and discussed by several researches (SENET 1996, NIETO BORGE et al. 1998). Validation of the depth results revealed an accuracy of ±0.25 m per cell (SENET & SEEMANN 2000b), whereas the current results were as accurate ±0.10 m per cell. The relative error or fractional uncertainty of the flow estimation was calculated by standard statistical means (LINDBERG 2000). As the errors propagated in two different phases, multiplication (Equation 3.2) was performed for point error.

$$\varepsilon = \varepsilon_{u_n} \cdot \varepsilon_d \qquad (3.2)$$

where, ε is the relative error for the flow estimation, ε_{u_n} is the error in normal current estimation and ε_d is the error of depth calculation. The errors propagate across the line of flow calculation as follows:

$$\frac{\Delta\varepsilon}{\varepsilon} = \frac{\Delta\varepsilon_{u_n}}{\varepsilon_{u_n}} + \frac{\Delta\varepsilon_d}{\varepsilon_d} \qquad (3.3)$$

Simple average errors were used to get the relative error. The total error was calculated by summing up all-relative errors in question:

$$\sum_{1=i}^{n} \varepsilon = \varepsilon_1 + \varepsilon_2 + \varepsilon_3 + \ldots\ldots\ldots + \varepsilon_n \qquad (3.4)$$

3.5 Velocity Profiling and Sediment Dynamics

The depth averaged current velocity from DiSC result was used to produce velocity profile in the cross section using equation 3.5. The simplified assumption for the profiling was "no influence of long wave and tide". The logarithmic velocity profiles at specific point were constructed using log law and interpolation was applied for the whole cross section.

$$U_z = \frac{u_*}{\kappa} \ln\left(\frac{z}{z_0}\right) \qquad (3.5)$$

where, u_* = friction velocity, z_0 = bed roughness length and κ = von Karman's constant (0.40). The friction velocity, u_*, is related to the bed shear stress (τ) through the relationship:

$$u_* = \sqrt{\tau / \rho} \qquad (3.6)$$

The bed roughness length, z_0, depends on the viscosity of water, the current speed and the dimensions of the physical roughness of the bed. A simplified solution (COREBROOK AND WHITE 1937) for z_0, was used.

$$z_0 = \frac{k_s}{30} + \frac{\nu}{9u_*} \qquad (3.7)$$

For *hydrodynamically rough* flow ($u_* k_s / \nu > 70$), $z_0 = k_s / 30$ and for *hydrodynamically smooth* flow ($u_* k_s / \nu < 5$), the relation becomes $z_0 = \nu / (9u_*)$. In transitional flow ($5 \le u_* k_s / \nu \le 70$) the full equation should be used. The Nikuradse roughness k_s, for flat, featureless mixture of gravel, sand and shell in a tidal area was given (SOULSBY & HUMPHERY 1990) in terms of grain size:

$$k_s = 2.5 d_{50} \qquad (3.8)$$

Echo soundings (Appendix VI) data were used to define the bottom slope and grain size information was obtained from different operational campaigns of Coastal Oceanographic Measurement System (KOK) of GKSS Research Center dated September 14-19, 2006 (Appendix X).

Critical velocities for sediment motion were calculated in different points along the cross-section to evaluate stability of bed materials. As the d_{50} values, in the cross section, were higher than 0.002 m, depth averaged critical velocity (U_{cr}) for the sediment movement was calculated by the following relation (VAN RIJN 1984):

$$U_{cr} = 1.5 \sqrt{\Delta g d_{50}} \left(\frac{h}{d_{90}} \right)^{\frac{1}{6}} \qquad (3.9)$$

where, $\Delta = \frac{\rho_s - \rho_w}{\rho_w}$; ρ_w and ρ_s represents the density of seawater and sediment respectively.

4 Sensitivity Analysis

Mapping bathymetry and current maps by means of X-band radar sequences and DiSC algorithm is an operational oceanographic tool. Researchers (SENET & SEEMANN 2002, SENET et at. 2001) identified the basic source of errors associated with the method. Further optimization in the interface of DiSC (FLAMPOURIS 2006) was also justified for the calculation of bathymetry. The present study deals with the local current features in the observation area. Therefore focus on the sensitivity of parameters for current estimation is the prime importance.

In this chapter further evaluation of the method regarding sensitivity of the input parameters of DiSC associated with current features are discussed.

4.1 Calculation of MapDF

For the calculation of the MapDF, the spectral decomposition and the inverse 2D FFT, the user has to define, the power and the minimum and maximum of the frequency bins that this power laid. These parameters are the anchors of the filtering process in the algorithm.

After the 3D FFT, DiSC provides visualization the spectral wavenumber-frequency domain in separate bins, which are vertical intersections of the k_x, k_y plane with the frequency axis. At the low frequencies (where $d > \frac{1}{2}\lambda$), the real signal cannot be distinguished from the noise and also has nonlinear effects as produced by wave grouping (SMITH et al. 1996). As a result, the dispersion relation does not model the waves. At the intermediate frequencies, most of the distinct signals can be obtained for morphodynamic and hydrometric information. For the bathymetric features the bandwidth lies in this intermediate portion of the spectral domain. For calculating the current information high frequencies, mostly produced by capillary waves and caused Doppler shift in the dispersion shell, are taken in account. But at very high frequencies (where $d < \frac{1}{20}\lambda$), the power tends to zero.

Therefore, the user has to define interactively the power level and the minimum and maximum of the bins, which is also depends on the user's interest. For bathymetric information lower frequencies can provide better signals as longer waves have an influence of depth. But for current features, user has to relay on possible high frequency waves.

The proper selection of the ω_{min} and ω_{max}, mainly depends upon the user and is the main sensitive step in the process along with power. DiSC interface provides slices of wavenumber plane at various frequencies. In each slice wavenumber planes, white points show the locations of power that could be detected within the 'global' spectrum.

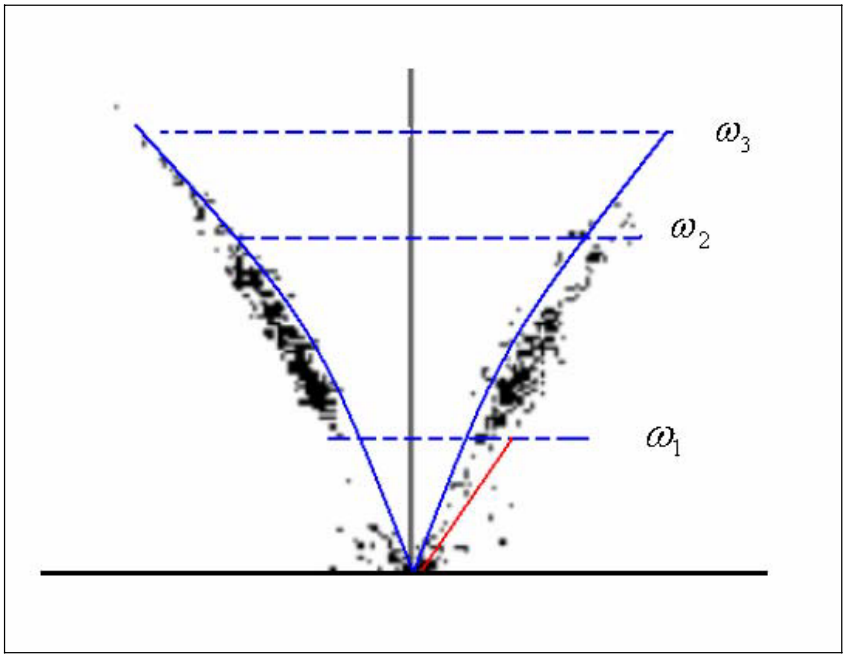

Figure 4.1: Locations of power in dispersion shell and the bandwidth of frequencies applicable for DiSC algorithm; ω_1 to ω_2 be suitable for depth calculation, ω_2 to ω_3 optimal for current calculation. Frequency slice from dataset: 12th July 2001 on 02:00 UTC.

The influence of minimum frequency with fixed bandwidth range and same input parameter shows that higher frequencies provide more current information (see section 3.2.4) than that of the lower ones (Figure 4.2). But empirical selection of the bandwidth (which was the case in this analysis of Figure 4.2) of frequencies is not the perfect procedure. This selection depends on the individual dataset in question and also the objective of the user, whether to calculate bathymetry or to find current information. By checking the location of power in the spectral wavenumber-frequency domain, user has to determine the power of wave or current which is available, according to his aim.

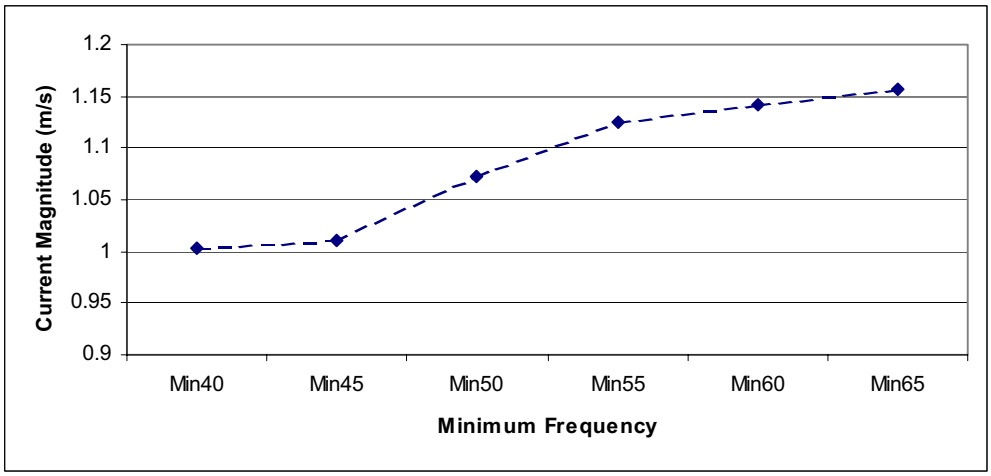

Figure 4.2: Influence of frequencies in current magnitudes. [Dataset: 12th July 2001 on 01:00 UTC; Import parameters: for MapDF calculation Frequency bandwidth 36, Power=210, Number of bins=130; for wavenumber calculation Power=115, Confidence level= 0.985, Blockpower=130, Block size =6x6]

Besides the frequencies, selection of correct 'Power' during the spectral decomposition and the inverse 2D FFT has a great influence to determining the number of regression coordinates and thus the results at the end (Figure 4.3). Lower 'Power' contributes an even distribution of the number of regression coordinates (Figure 4.3, a). An increase in the power leads to concentration of high number of regression coordinates only in the deeper areas (Figure 4.3, c & e). But in contrast lower power with evenly distributed the number of regression coordinates cannot provide good current information (Figure 4.3, b). The current vectors produced with higher power look promising with certain pattern on it (Figure 4.3, d & f).

Considering the number of regression coordinates, intermediate values contribute more acceptable results as observed during the whole investigation. In case of very low the number of regression coordinates the results contains more relative errors in it that results are not reliable. Again, a high number of regression coordinates usually underestimates the results.

The influence of power to current results shows a higher power contributes high values of velocity (Figure 4.4). But indiscriminate increase in the power can also cause loss of real information in shallower areas.

Therefore, the difficult part is to find out a right combination of frequency bandwidth and power, which only can produce results with good accuracy even though, the theoretical limits are known.

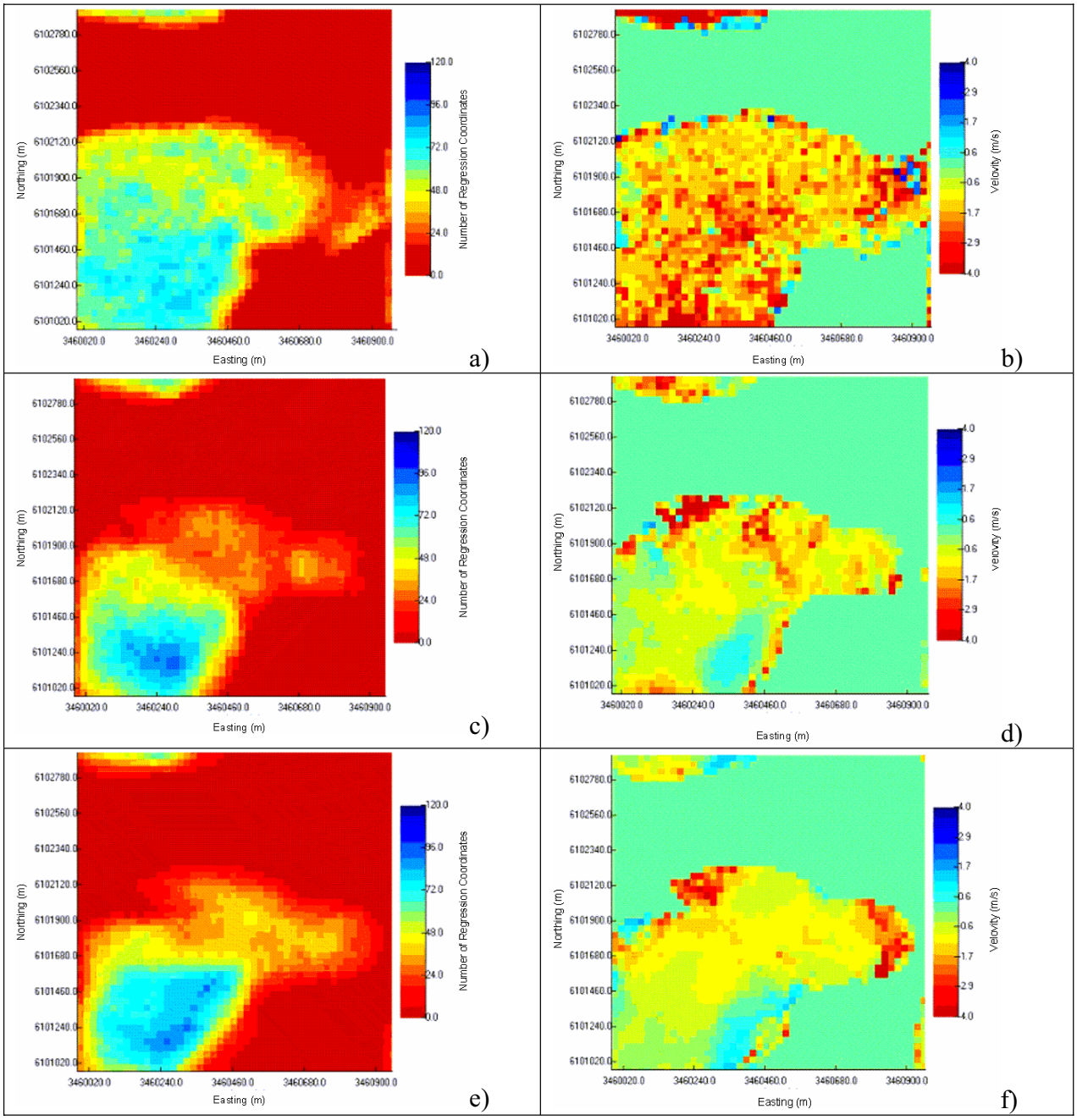

Figure 4.3: Influence of Power in the number of regression coordinates and results (x component of current vectors); a), c), and e) represents distribution of the number of regression coordinates with input power 212, 220 and 228 respectively; b), d) and f) represents normal components of the velocity vectors with input power 212, 220 and 228 respectively, while all other input parameter were same. [Dataset: Dataset: 12th July 2001 on 01:00 UTC]

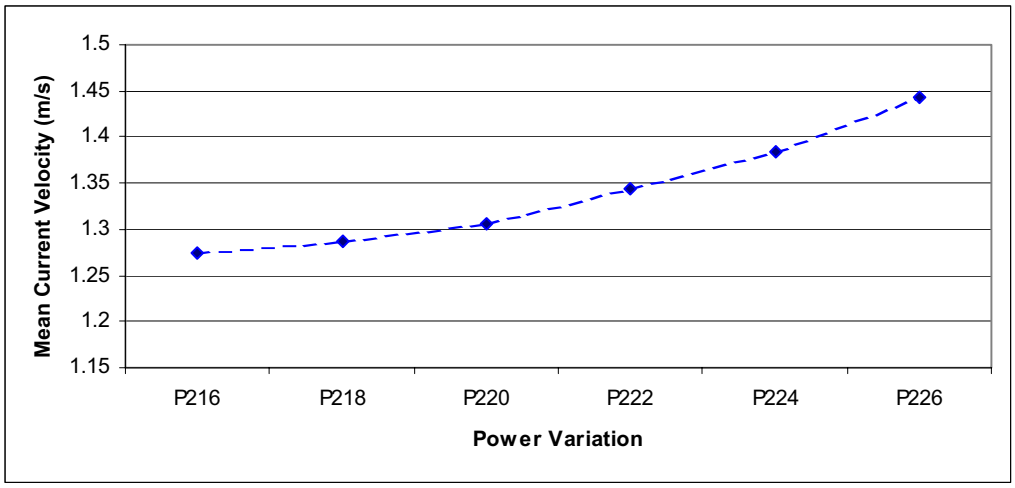

Figure 4.4: Influence of Power in mean current velocity. [Dataset: 12th July 2001 on 01:00 UTC; Import parameters: for MapDF calculation Frequency minimum=58, Frequency maximum= 90, Power=210, Number of bins=130; for wavenumber calculation Power=115, Confidence level= 0.985, Blockpower=130, Block size =6x6]

Facilities from software, such as checking the MapDF results are also a very important option to improve the accuracy of the result and undermine the error. The *Check Results* of the DiSC provides *Check Mapdf* option, which can visualize the centers of the filters and shows the location where the power values are high enough to be taken in account for the inverse 2D-FFT (Figure 4.5). Red crosses in the wavenumber slices provide the position of power for existing grid cell achieved by using wave information from the power spectrum during the spectral decomposition and inverse 2D- FFT. The lower frequencies with little wave-power can produce such crosses outside of the wave power-filtering region.

So any cross outside the wave power area represents error in the result. Isolation of single cross cannot be possible by the DiSC algorithm. But checking the wavenumber planes by the *Check Mapdf*, can reveal presence of erroneous results produced by lower frequencies during the inverting process. These errors can be eliminated either by adjusting the power or by increasing the $\omega_{\min}$.

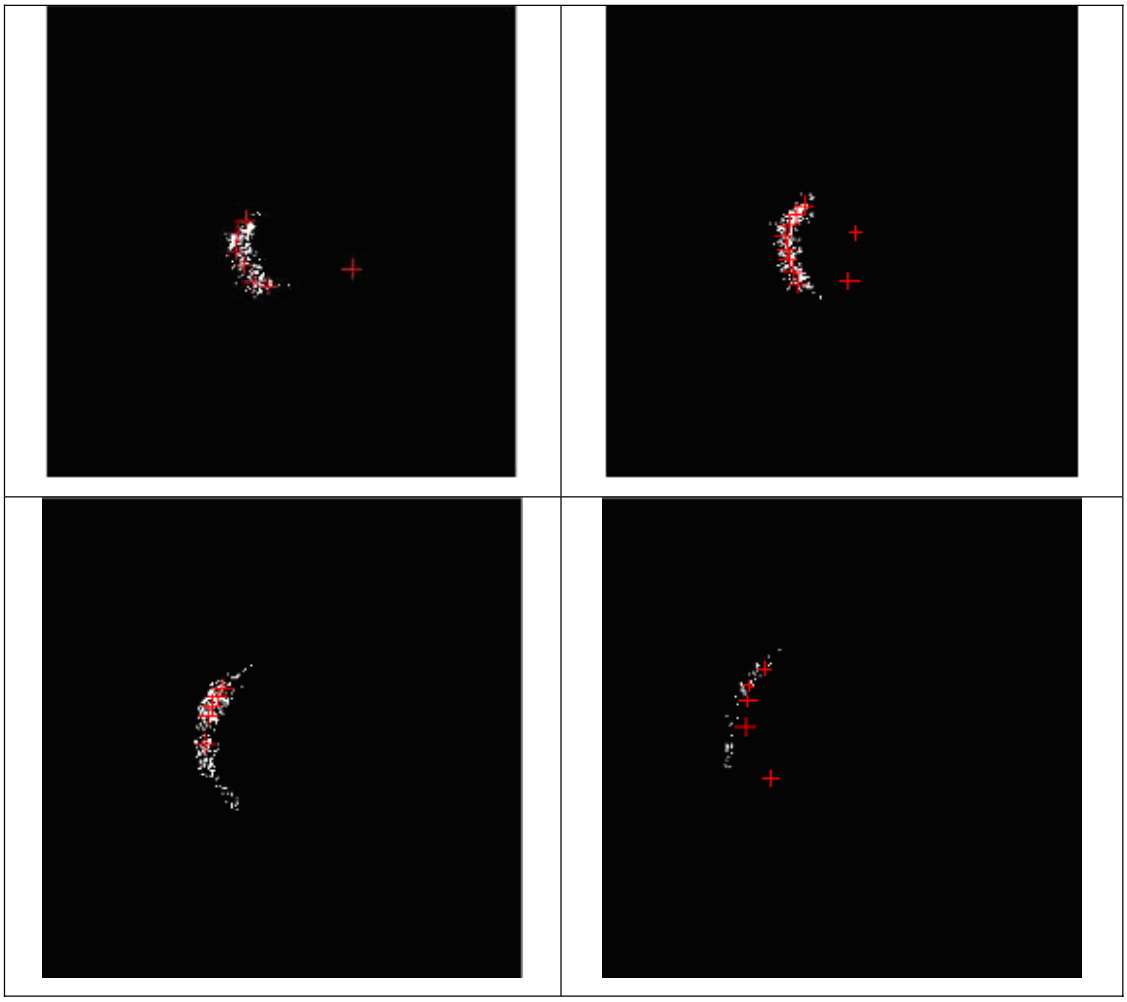

Figure 4.5: Frequency Slices of wavenumber planes: with red crosses distributed inside and outside of the wave power area. [Dataset: 12th July 2001 on 01:00 UTC]

4.2 Calculation of Local Wavenumbers

For the calculation of the local wavenumbers, the required spatial parameters are 'Power', 'confidence limits', 'block power', and also the size of the block cell. During the whole investigation of this thesis the block size is kept constant and has been defined as the highest resolution which produces significant results.

The other parameters, which are the qualifiers to reconstruct the local wavefield, were verified for their influence to the output of current features. The selection of those parameters is an interactive process by visual control of the result of the inverse 2D FFT. The result of the 2D FFT

is spatial visualization of the wave components, magnitude and phase, which has been extracted from the previous steps, for each frequency; the threshold level for the power that has to be chosen by increasing the magnitude in such way that there are no crossings of the local wavelengths in each frequency. The scale of the magnitude has to arrange such a way that there are no forking in the phase visualization.

The fluctuation due to the power input is not uniform (Figure 4.6). The current velocity varies drastically at very low and high 'Power', this is because of vast number of missing values of results in the designated area. At these two extreme regions of power distribution valid current values reduce drastically, contains only 30% to 40% of valid results comparing with the intermediate region. So the appropriate values of 'Power', which can produce significant results over a wider area always lays in the intermediate values.

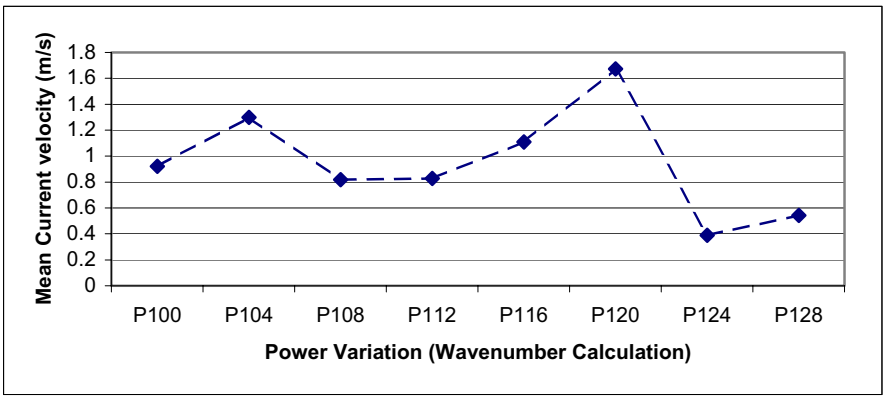

Figure 4.6: Influence of Power in mean aerial current velocity during wavenumber calculation. [Dataset: 12th July 2001 on 01:00 UTC; parameters: for MapDF calculation Frequency min=58, Frequency max= 90, Power=210, Number of bins=130; for wavenumber calculation , Confidence level= 0.985, Blockpower=130, Block size =6x6]

The influence of power is mainly associated with the number of regression coordinates (Figure 4.7). Designated 'Power' qualifies the reconstruction of local wavefield, which essentially limits the calculation of results for each block cell, if it is higher than the 'Power' of the block in question. Thus higher power reduces the number of the regression coordinates. An inappropriate input of power may also cause information loss over a range of areas.

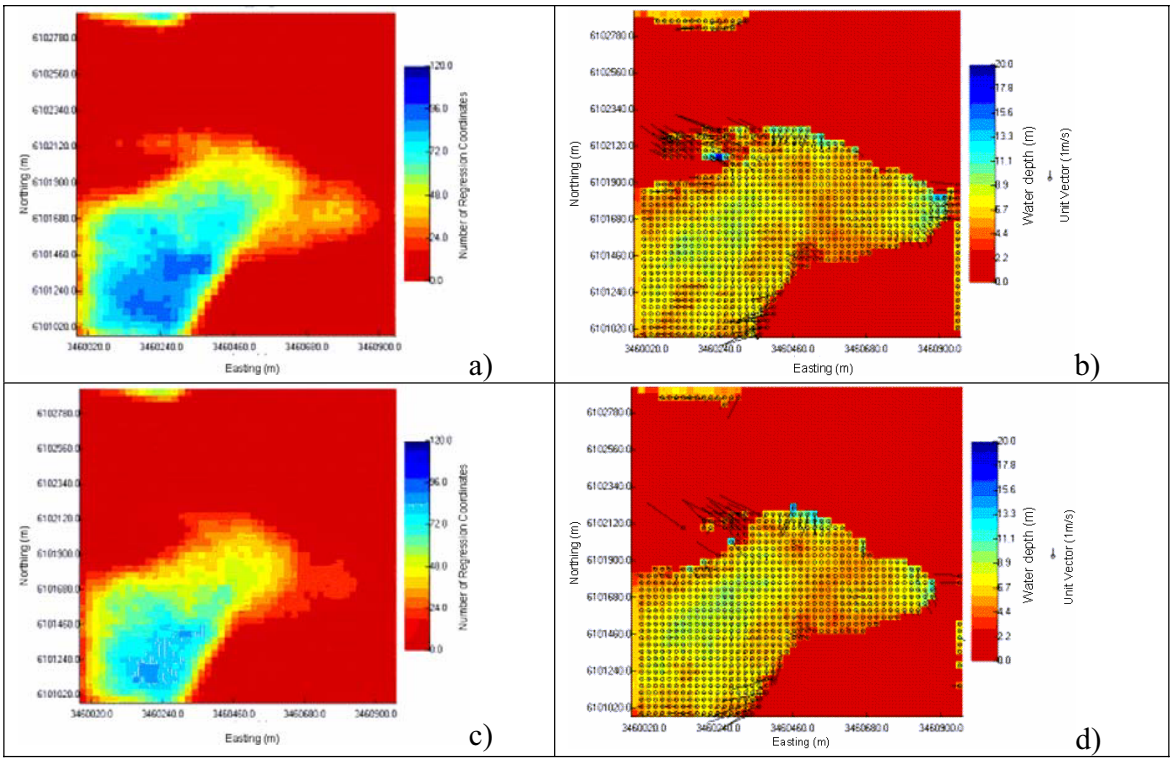

Figure 4.7: Influence of Power in the number of regression coordinates and results (current vector) during wavenumber calculation; a & b) contributed by a power input of 108, whereas c & d) reflected the results with power 112. [Dataset: Dataset: 12th July 2001 on11:00 UTC]

Confidence level has very little influence on current velocity even in the higher percentile of 98.5 (Figure 4.8). But the result becomes unstable after that position. So peaking the higher confidence that produce stable and reliable result is the right choice.

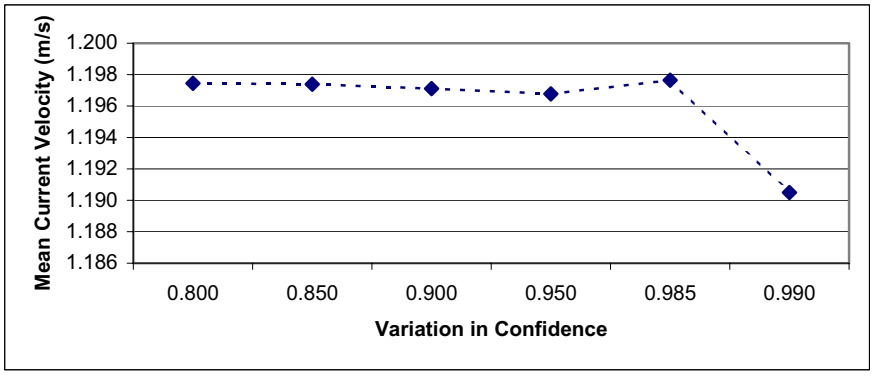

Figure 4.8: Influence of confidence in mean aerial current velocity during wavenumber calculation. [Dataset: 12th July 2001 on 00:00 UTC; parameters: for MapDF calculation Frequency min=58, Frequency max= 90, Power=221, Number of bins=130; for wavenumber calculation, power= 110, Block power=130, Block size =6x6]

Block power or power of each block cell also influence the result as well as regression point. Current features and even bathymetric information are more pronounced at around 130 (Figure 4.9). For this reason, the parameter is sometimes default as 130 during DiSC operation.

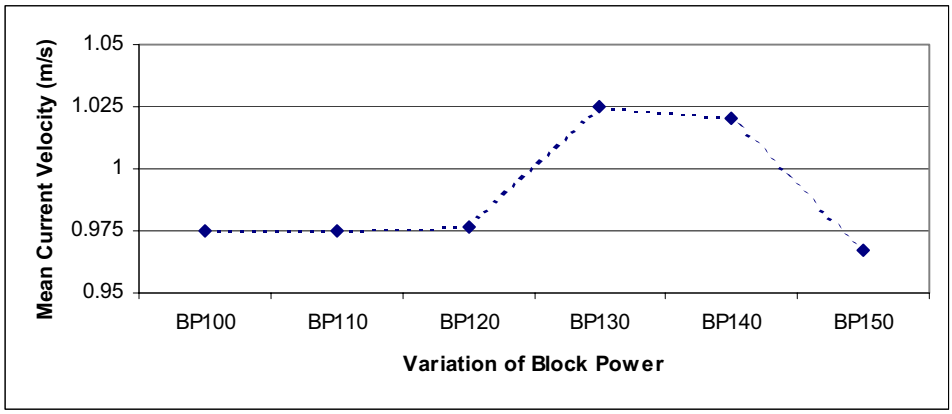

Figure 4.9: Influence of Block Power in mean current velocity during wavenumber calculation. [Dataset: 12th July 2001 on 02:00 UTC; parameters: for MapDF calculation Frequency min=58, Frequency max= 90, Power=221, Number of bins=130; for wavenumber calculation, power= 110, Confidence=0.985, Block size =6x6.]

With the help of all discussed tools of DiSC, user can produce reliable results from radar dataset. The extreme values in both ends of the regression coordinate limits either contaminated by errors or by underestimation of results. For the bathymetric results a minimum threshold point can be obtained by comparing with the nautical chart. For current features, it becomes difficult to evaluate the result. But looking for the current pattern and tidal information can reveal a clue for the answer. Usually number of the regression coordinates under 30 does not qualify for reliable results.

4.3 Defining Water levels

The other main parameter that involves during the calculation of current features is water depth. With the new version of DiSC, user can import a bathymetric grid to define water depth. In such case DiSC uses radar information to calculate only current features (two vectors of the current components). But when we deal with a tidal zone, the water level should be corrected with in-situ tidal situations for the different tidal phases.

In the final Module of DiSC, called *Currentfit*, used have to input tidal gauge information to define water level at specific period. Usually this information is deviation of water level from the Mean water level, it may either positive or negative value.

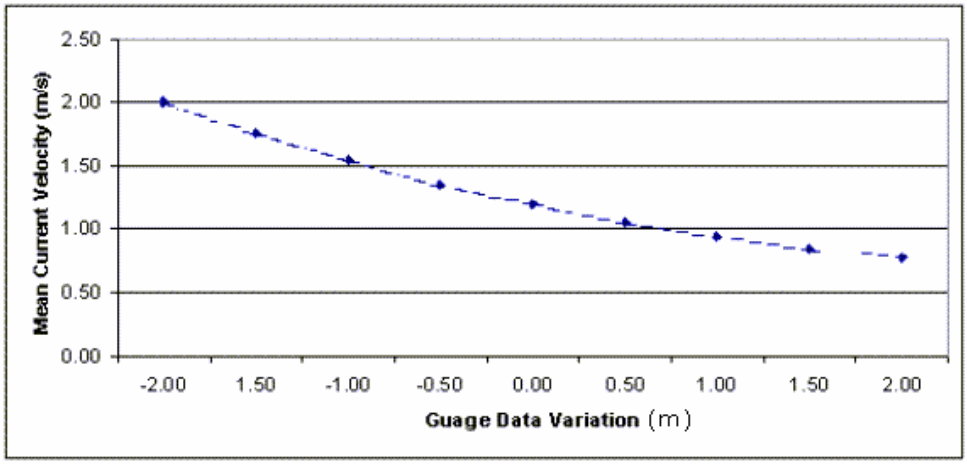

Figure 4.10: Influence of water level to mean current velocity. [Dataset: 12th July 2001 on 00:00 UTC; parameters: for MapDF calculation Frequency min=58, Frequency max= 90, Power=221, Number of bins=130; for wavenumber calculation, power= 110, Block power=130, Confidence=0.985, Block size =6x6]

This input has an important impact in the determination of current features. A lower water level (input of negative gauge data) results higher current velocities as it is expected due to reduction of aerial surface. In this figure a fluctuation of about 0.5 m/s velocity was observed for 1.0m of water level fluctuation (Figure 4.10), though this change mostly depends upon the signal of the specific dataset. The variation of current with the water level is highly sensitive in the shallower region.

5 Results

DiSC was used to produce 12 hourly bathymetries (Appendix XI), during strong wind condition of 12th July 2001. The averaged bathymetry of the common results covers an area of about 136,865 m^2 (Figure 5.1).

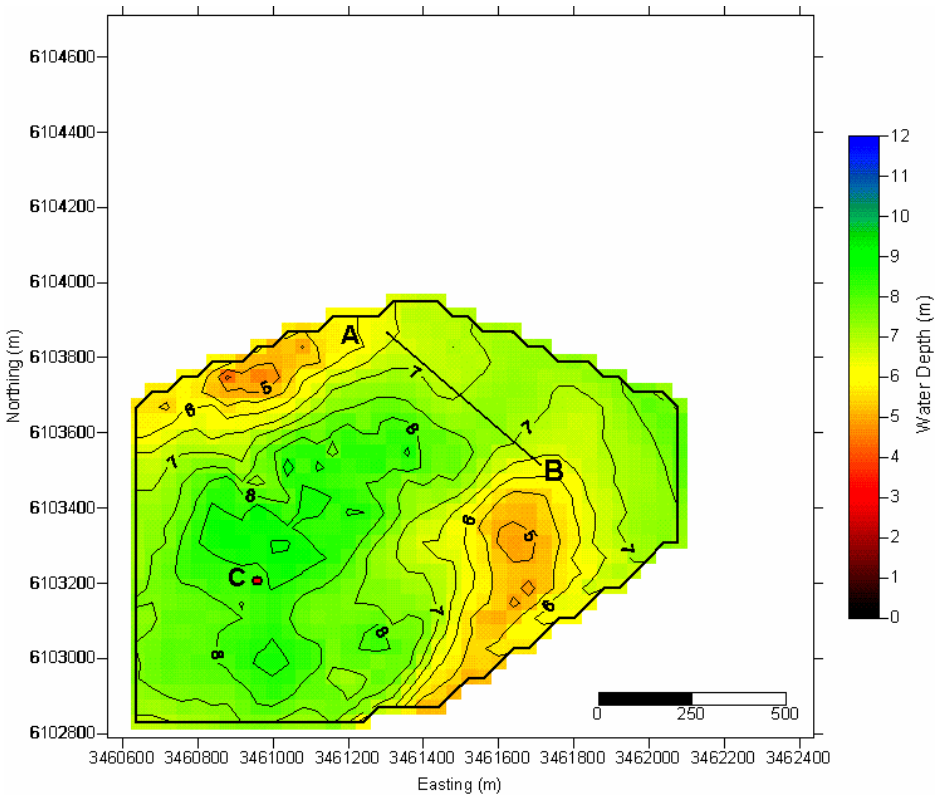

Figure 5.1 Averaged bathymetry of common area during strong wind condition, black line marks cross section over the tidal channel (12.07.2001).

According to the tidal calendar (BUNDESAMT FUR SEECHIFFAHRT UND HYDROGRAPHIE 2001), the high water (HW) period in List West was at 07:28h local time (06:28h UTC) and the low water (NW) at 12:34h local time (11:34h UTC). The nearest gauge measurement facility is in Westerland. It has a 0.5h lag due to distance. In figure 5.2, gauge data (red-line) from the Westerland was used to compare the trend of water level during the same period. Strong tidal signature was observed in the deeper part C (an area of 14,400 m^2 around coordinates 3460966 m and 6103237 m) of the tidal channel. In the figure green line indicates water level derived from the radar sequence. In the shallower part of the study area, tidal signature was not so prominent.

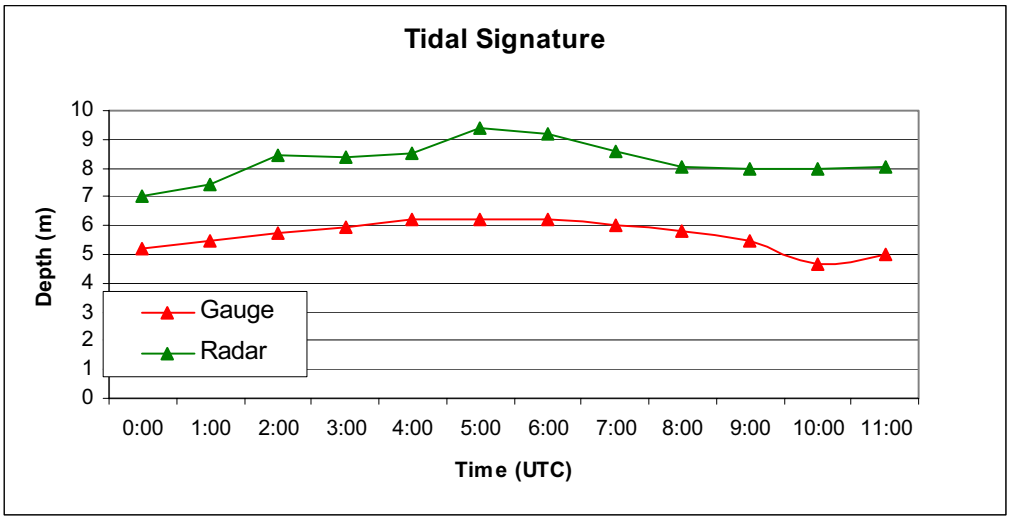

Figure 5.2 Graph representing the tidal cycle. The red line is measured by tidal gauge in Westerland and green line is the estimated tidal cycle from radar sequences.

An echo-sounding bathymetry (Appendix VI) of the area was used to compare the bathymetric results. The sounding bathymetry covers an area of about 883,200 m^2. The comparison shows positive moderate correlation (0.57) between the two depths.

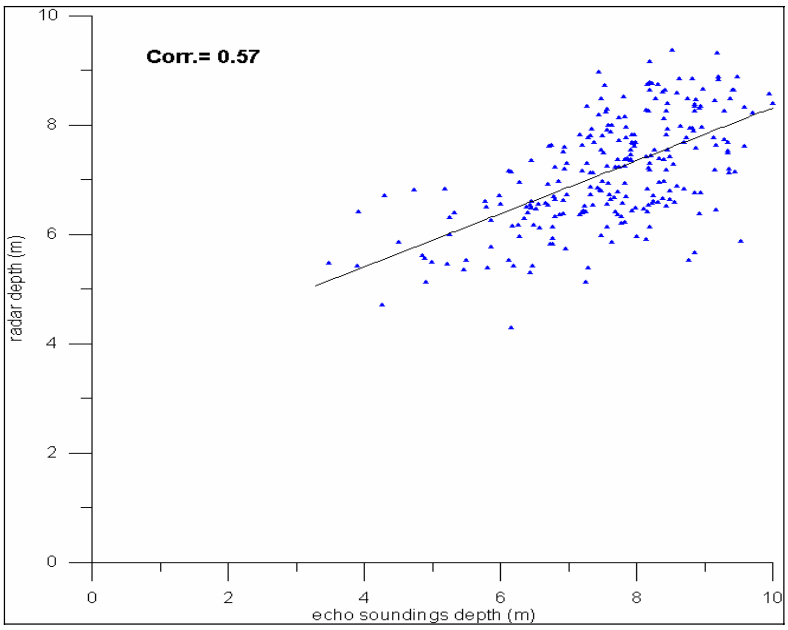

Figure 5.3: Scatter diagram produced by the comparison between radar-deduced and echo sounding water depths.

Current pattern in the same point (c in Figure 5.1) also flowed the tidal sequences (Figure 5.4). The magnitude of the current velocity increases during the flood phase, followed by a decrease toward high water slug. Current velocity also fluctuated during ebb tide with a maximum in the intermediate period. The velocities during the flood phase were stronger than during the ebb period. Directions of the currents also followed the tidal pattern.

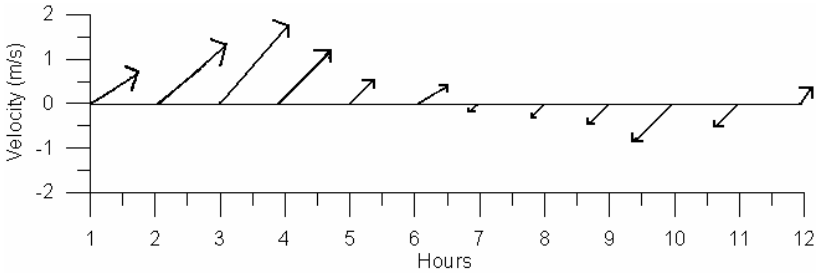

Figure 5.4: Tidal cycle of the current velocity. Arrow directions represents north oriented flow (going to) directions. The radar datasets were acquired on July 12, 2001 (0:00 to 11:00 UTC) from a land based station on the island of Sylt.

The current magnitudes and directions for the investigation area were calculated for the whole tidal cycle (Appendix XII). During the flood phase the magnitude varies from 0.34m/s to 2.36 m/s. The directions varied from 50° to 105° from north (Figure 5.5). During slug period of high water, the magnitudes were low and directions were irregular and varied all around (Figure 5.6).

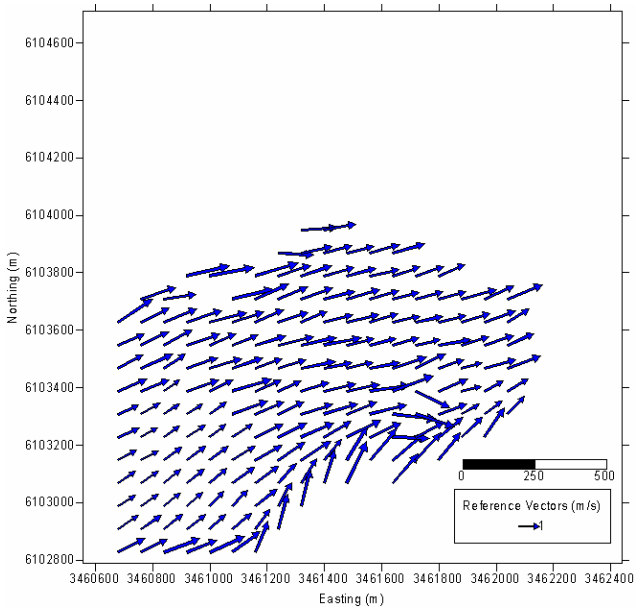

Figure 5.5 Current vector map during the flood phase of the tidal cycle (03.00 UTC).

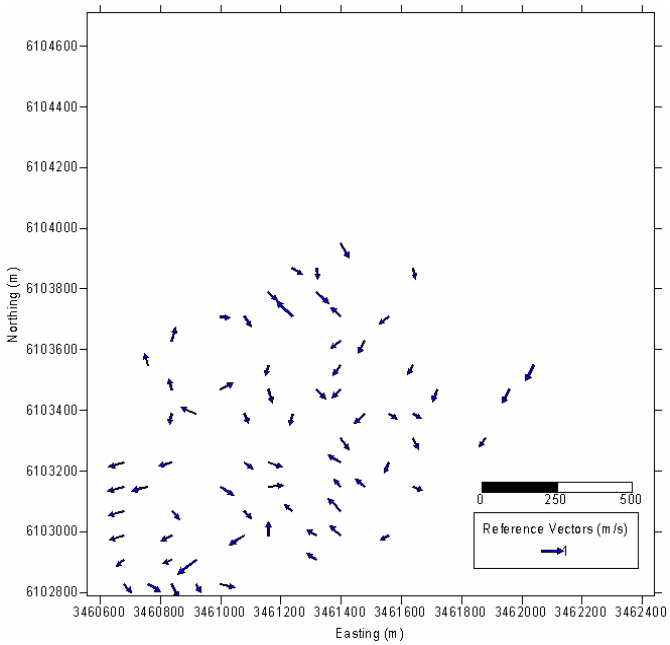

Figure 5.6: Current vector map during peak flood slug period (07:00 UTC).

During the ebb period, the magnitudes were comparatively low (lies between 0.11 to 1.74 m/s) and the directions varied from 191° to 288° (Figure 5.7). Some extreme results in the shallow water zone were not reliable.

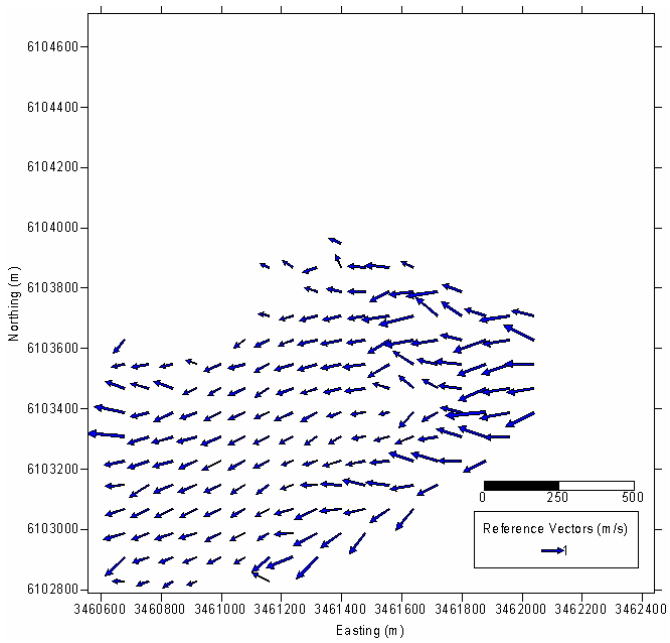

Figure 5.7: Current vector map during ebb period (09:00 UTC).

Velocity distribution over the tidal channel of Lister Landtief was also calculated over a cross section (marked in Figure 5.1). The cross-section was 557.2 meters wide (Figure 5.8), starting at coordinates A (3461360.44, 6103801.23) and end point of B (3461596.04, 6103296.33). The blue and red lines represent respectively the DiSC depth and sounding profile over the cross-section.

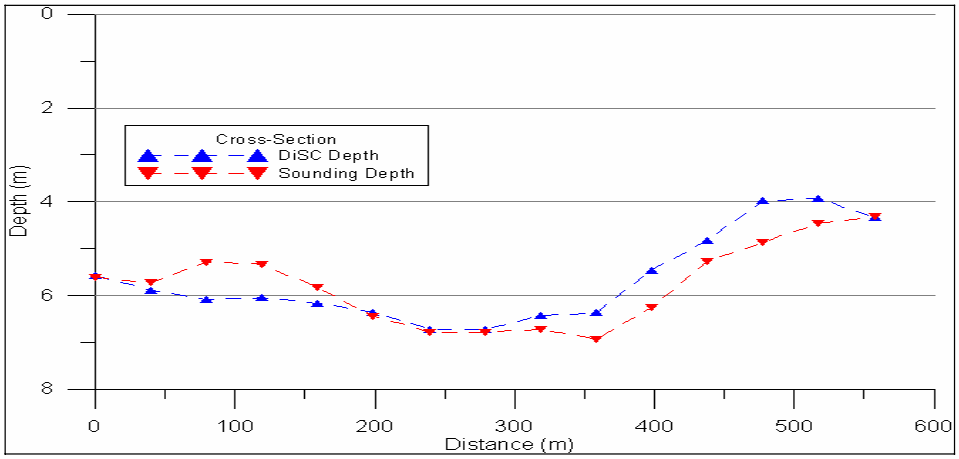

Figure 5.8: Depth profiles over the cross-section in the tidal channel.

Velocity distributions over the cross section during the peak flooding (Figure 5.9) and ebbing (Figure 5.10) were also constructed. The results indicate that higher velocity regime during flood phase. The velocity magnitudes at the shallower area were as high as 2.2 m/s in the near surface region. Movement of bed materials was also observed during the period (critical velocity was 1.92 m/s).

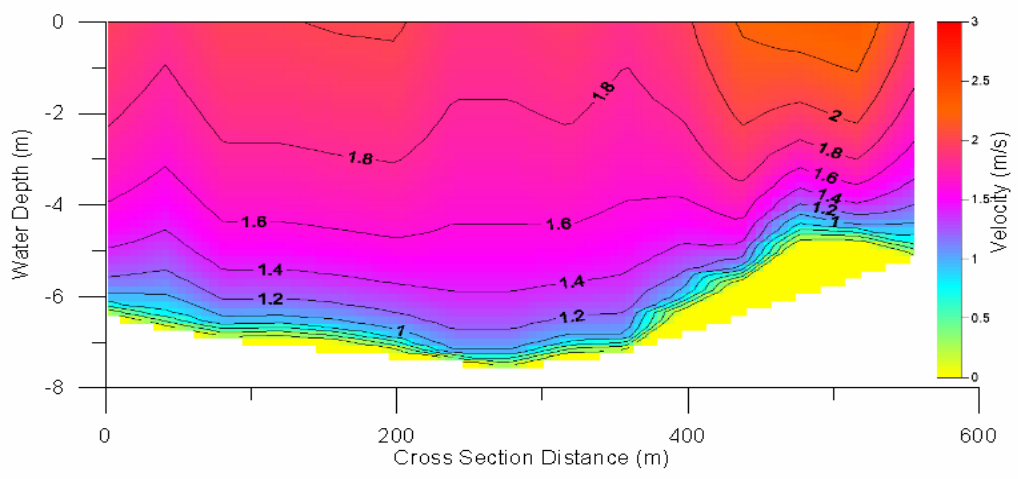

Figure 5.9: Velocity distribution over the cross section during peak flooding (03.00 UTC).

During the ebb phase the velocity did not exceed 1.5 m/s in the cross section and there was no significant movement of bed materials, except in the deeper parts (Appendix X). During flooding an extreme velocity region was observed in the shallower area. This was not observed during the ebb period.

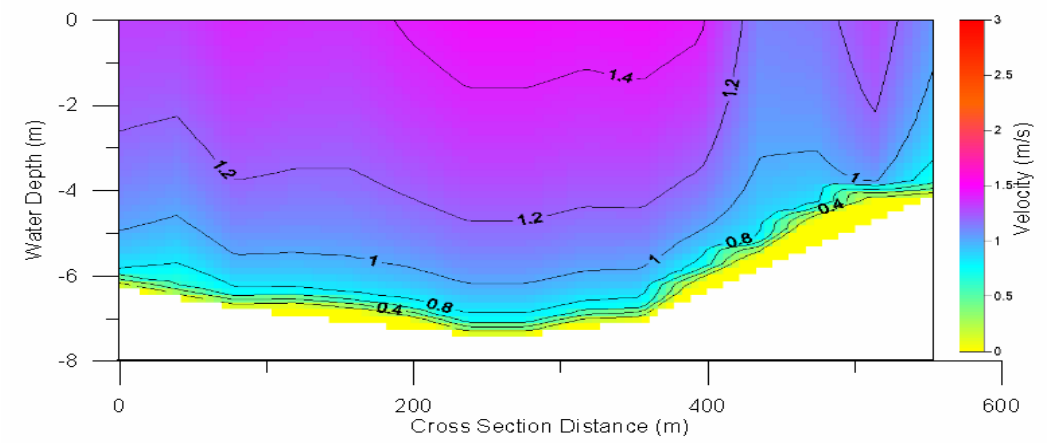

Figure 5.10: Velocity distribution over the cross section during peak ebbing (09.00 UTC).

Total water transport over the tidal channel was also estimated at the same cross section (Figure 5.1) of the tidal channel. In case of DiSC bathymetry, the flow rate varied from 4,398 m^3/s to –2,292 m^3/s during the 12 hours of the tidal cycle (Figure 5.8). Highest positive (flood currents) flow was observed during the third observation hour (02:00 UTC). The negative flows started with very minor magnitude during slug period of high tide at the 7th hour of observation.

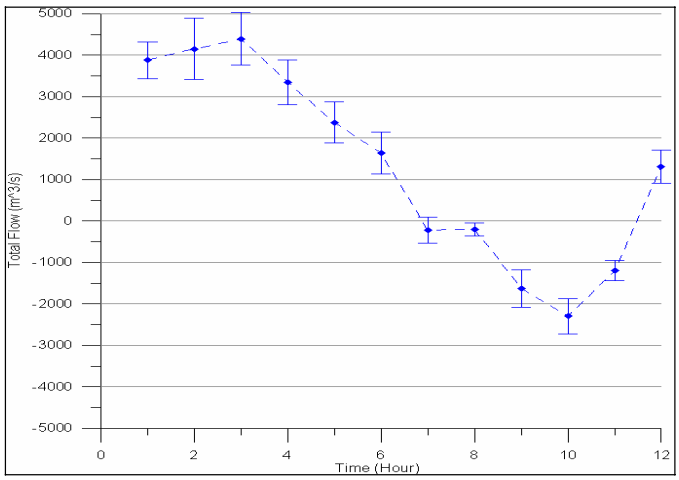

Figure 5.11: Flow sequence over the cross-section in the tidal cycle using DiSC bathymetry.

The strongest ebb currents were observed during the 10th hour. Calculation errors for the flow, was highest (±38%) during the high water slug (7th and 8th hour) phase. Errors varied from ±5.7% to ±15.5% for the rest of the observation hours. The total assessed water transport during the flood phase (inflow) over the cross section was about 75,996,000 (±15%) m^3, whereas the outflow during ebb phase was about 19,908,000 (±15%) m^3 only.

The echo-sounding bathymetry of the area was also used to calculate total flow over the same cross-section. For echo-sounding bathymetry, the flow varied from 4,027 m^3/s to –2,180 m^3/s during 12 hours of the tidal cycle (Figure 5.12). Highest positive (flood currents) flow was observed during the second observation hour (01:00 UTC).

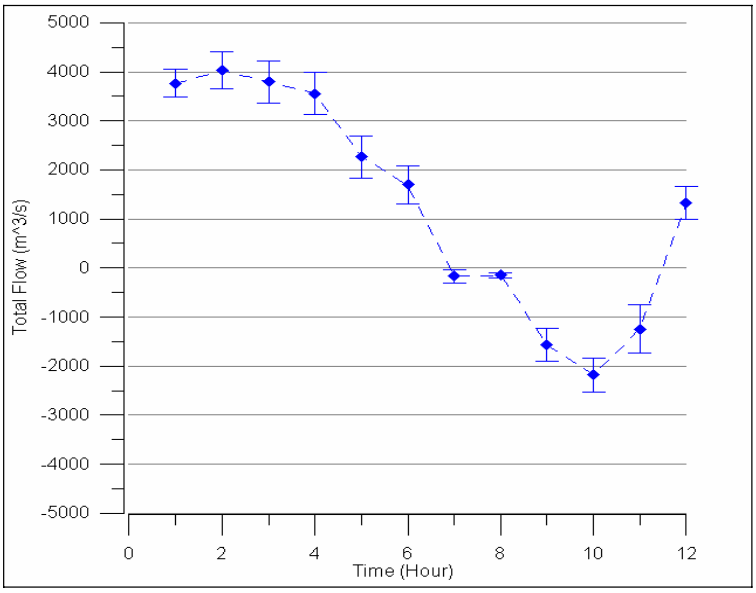

Figure 5.12: Flow sequence over the cross-section in the tidal cycle using sounding bathymetry.

The strongest ebb currents were observed during the 10th hour. Errors for the flow calculations were relatively low and varied between ±3.73% and ±12.8% for the 10 active flood and ebb hours. As of the other observation, errors during slug hours (7th and 8th hour) were also high, ±40.0% to ±36.8% respectively. The total assessed water transport during the flood phase (inflow) over the cross section was about 73,540,000 (±15%) m^3, whereas the outflow during ebb phase was about 19,105,200 (±15%) m^3 only.

6 Discussion

The main objective of this thesis is to estimate the current features and calculate flow sequences over the tidal channel during a tidal cycle on July 12th 2001, using DiSC. As the basic algorithm of the software provides an interactive result of depth and current information, an extensive effort was also made to produce a mean bathymetry (Figure 5.1).

Resulting bathymetry shows three distinctive depth regions. The clearly visible deeper middle portion of the tidal channel of Lister Landtief is the main feature of the area. Water depths reach up to 9 m in some part of the channel. The other two regions are the near shore area in the southeast and the shallower area at the northwest (Salzsand). In both sides of the Lister Landtief, the result is limited to almost 5 m contour lines. Shallower areas are out of reach of the algorithm, due to the shortcoming of nonlinearity of the propagating waves (see: section 2.1.4). Although depths up to 3m (Annexure XI) are detectable in different wave conditions, those results are eliminated during the process of either filtering or averaging. The deeper parts in the north and east are also not visible in the map due to the same limitation. The Admiralty charts, 2002 and previous work (FLAMPOURIS 2006) in the same area revealed the similar morphological structures.

The comparison with echo soundings shows poor quality (Figure 5.3) of the radar deduced bathymetry. This may be contributed by several features. Firstly the wind speed, the strong wind condition chose for the investigation with 6 Beaufort scale (40-50 km/h), was not strong enough to produce waves long enough to detect water depth. Secondly the wind directions during the period were varied between 250° and 280° with northern orientation, where looking angle was almost perpendicular to the radar antenna. In such situation, backscattering from the sea surface can also be reduced (see: section 2.2.3.1). Thirdly measurements by radar (dated 12.07.2001) and echo soundings (dated 17.09.2001) were not synchronized. Such delay can cause significant change in the morphological structure. Furthermore, the spatial orientations of echo soundings and radar results were not accurately same. Averaging (spatial averaging of echo soundings and averaging of temporal radar deduced bathymetries) of both datasets also has an impact in the mean bathymetry. The previous studies (FLAMPOURIS 2006) on bathymetries showed more accuracy with storm wind conditions of 7-8 Beaufort scale (63-75 km/h).

A clear tidal signature was observed in the deeper region of the channel (Figure 5.2). A tidal variation of 2.0 m (±10%) was observed from the radar sequences, whereas the variation recorded by the tidal gauge at Westerland, 17 km south of the area, was 1.54 m. The local effect of barrier accumulation was about 0.2 m. Further increment in the water level in the study area was probably due to strong wind condition resulting longshore current along the island, which was finding its way through the tidal channel.

As the main concern of the thesis is to detect current features, a lower wind condition is justified (see: section 3.1.2). The result shows a normal current regime during a tidal cycle over the investigation area. During flooding, inflow velocity vectors over the shallower area (extreme north and south-eastern part of the result) are significantly higher than in the deeper part and channel (Lister Landtief) area (Figure 5.5). Maximum current velocity reached up to 2.3 m/s during the flooding. During the ebbing, outflow current velocities were comparatively low and tend to increase in the eastern most part of the area, and directions also shifted towards northwest (Figure 5.7). The maximum current velocity during outflow reaches 1.7 m/s in eastern part. This may be contributed by the stronger outflow of the deeper channel, Lister Tief. Currents parameters in the branching area of Lister Tief to Landtief, were influences by its own outflow. A study (LUMBORG & WINDELIN 2003) in the Lister Tief area shows dominancy of ebb outflow in the deep channel.

Later, an ADCP (Acoustic Doppler Current Profiler) measurement campaign by Radar Hydrography Department (KOR) of GKSS in the Lister Landtief also observed higher values of current velocities during flooding (Appendix XIII). During onboard measurement current velocities were found between 0.2 m/s and 1.2 m/s with a moderate breeze condition of wind (Beaufort scale 3-4).

Considering the cross section, stronger velocities were also observed in the shallower part (Figure 5.9) during flooding. This phenomenon also reflected by the larger grain size in that area (Appendix X), which was attributed by erosion of smaller bed materials by higher velocity regime. Considering the morphological pattern, the flow used to bend towards southeast during flood phase as Lister Tief has its own inflow. This observed flow pattern also validate velocity enhancement in the shallower area of the cross section.

Velocity distribution over the cross section during ebbing reflects lower velocity regime during the period. A sharp division between deep and shallower part was observed, which indicates a dichotomy of flow sources (Figure 5.10). Main flow in the deeper area obviously contributed by Lister Tief, the other subsequent flow is probably feed by the inundated intertidal zone.

The inflow during the flooding was much more prominent than the outflow of ebbing (Figure 5.11 & 5.12). Estimated net flow in the direction of flooding (northwest) was the three quarts of the total flow, which summarizes most of the water masses find their ways in the deeper channel (Lister Tief), northwest to the study area (LUMBORG & WINDELIN 2003).

Considering the estimated critical velocity, instability of bed materials was observed during the flood phase over the whole cross section. Whatever only the deeper part of the cross section remains active during the ebbing; shallower parts in both sides remain stable, as water outflow was not strong enough to move larger grains.

The influx of water to the deeper channel contributes a net sediment replacement toward the northwest (Lister Tief). A multibeam survey in the same area also indicated depositional features in the Lister Tief, (CYSEWSKI 2003). Though the outflow has the capacity to initiate sediment movement in the deeper part of the cross section (Lister Landtief), it does not result in a rational retrieve for several reasons. Firstly, outflow is weaker than the inflow. Secondly, the transported sediment use to settle down during slug phase (Figure 5.6) at the bottom of the deeper channel, which may either find its way to seaward direction through the Lister Tief or move to adjacent near shore areas. The available information (AHRENDT 1994, AHRENDT 2001, REISE 2004, SISTERMANS & NIEUWENHUIS 2007) also supports this findings.

Erosion is almost synonymous to the Sylt Island. The entire coast of Sylt has been severely eroding since a long period of time; accumulation of sand is not seen at any part of the coast. After 1950 the erosion rate in Westerland-Kampen (north of Westerland) has been increasing as compared to the southern area (SISTERMANS & NIEUWENHUIS 2007). The same case study also reveals that, the average annual retreat at the western coast from 1870 to 1950 has been 0.9 m/year but increased during the past couples of decades with the increase in the number of winter storms and severity. The expected erosion for now in the northern most part (study area) is about 1.5 m/year. The annual sediment loss at the north part of the Sylt is about 850,000 cubic meters

(AHRENDT 1994). Having a single storm event it is estimated that about 50,000 m^3 (± 20%) of sediment is replaced in the area (FLAMPOURIS 2006).

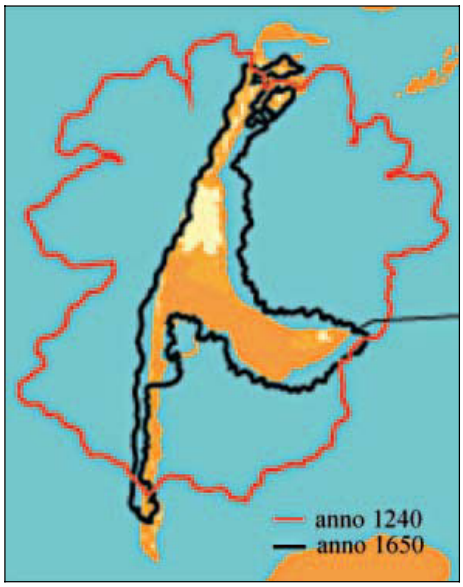

Figure 6.1: The island of Sylt in 1240 and 1650 (AHRENDT 2001).

A shore parallel longshore current system prevails along the whole west coast of the island. In Figure 6.1, erosion pattern of the island is physically illustrated. The complex sediment exchange takes place between the longshore bar and the beach, with resulting sediment loss both along northward and southward direction. This process results in the formation of elongated barrier sandbars in both directions of the island. The radar station is itself situated on such a depositional structure, which was not a part of the main island in recent past.

7 Conclusions

The method, Dispersive Surface Classificator (DiSC), for the interpretation of radar image sequences is proven to be a useful tool for coastal remote sensing. Even knowing the theoretical limitation of the method, comprehensive results on two different important hydrographic parameters, water depth and current features, can be achieved. It could be a very useful technique especially to monitor the consequences of extreme weather events of storm surges, when the other monitoring systems are inaccessible.

Being a commercial product, DiSC is repeatedly developing by accommodating new ideas to interfere and users friendly options. Introduction of different visualization modules work as quality inspection devices. As the basic algorithm based on the combination of image processing with wave theory and three different complicated scientific domains, the use of DiSC requires deep understanding and intense training.

Theoretical selection of basic input parameters, such as, minimum and maximum frequencies and the power of global spectrum seems easy and distinctive. But defining such parameters depends not only on theory but also on the quality of specific dataset for practical reason. The question number of frequency bins for the decomposition of global spectrum entirely depends on the computational capability of the system (usually default at 130). The other qualifiers for the regression parameters (power, block power, confidence limits and the cell size) are also deeply dependent of dataset, which is discussed analytically in Chapter 4. The choices of those parameters are based on the visual interpretation of the power and phase of the decomposed global spectrum and the importance, for the reliability of the regression coordinates is not clear. Moreover error during filtering process is still to be addressed.

The recent inclusion of an advance option for defining flow profile and calculating flow rate with defined profile makes the tool handier to the user. Upgradation can also be made for sedimentary interest to check stability, incipient motion and even to calculate bedload for known bed material. Such development will make the method a complete monitoring package of morphodynamic processes in the coastal area.

The out come of the study proved, lighter wind conditions can effectively be used in the method to reveal current features, though the requirement for depth calculation is known to be stronger. The wave properties, associated with wind condition, vary significantly in coastal

shallow regions. The appropriate threshold level of wind condition for bathymetric calculation also depends upon the morphological structure of the area.

The achievements of the thesis are mainly concentrated on feasibility of the method to calculate current features. Finding a tidal sequence in velocity vectors was the first benchmark. Velocity maps of the area revealed spatial and temporal patterns of the water flow. The flow sequences of the tidal period showed dominant flooding. Profiling flow over the tidal channel showed vertical velocity distributions and its nature in both vertical and horizontal dimensions. The further calculation of net flow also supported by grain size information of the area. Velocity associated sediment motion seems realistic according to the physical condition.

The vulnerability of costal areas to conscious wave action is a known phenomenon. The dynamic nature of wave, tide and current system may cause colossal loss of sediment in the long run. The island of Sylt is one of the prefect examples of such type. Radar image sequences of designated area acquired during the tidal cycle revealed the reality of excessive inflow during flooding. The consequences of such flow on bed materials over the tidal channel of Lister Landtief observed net sediment transport to the northeastern deeper part of the region. The use of echo soundings depths for flow estimation also justified the reality. More validation of the method can also be possible by appling different other in-situ techniques in a synchronize manner. But the required wind condition for getting sufficient radar signals still to high that restricts onboard measurements.

The method DiSC and the implementation software consists a stable base for further development of the method. Extending the method to non-linear theories for modeling wave refraction, wave breaking, current influence and other complex phenomena, theoretical restriction of implementing the method in the shallower region can be eliminated.

The proposed development of DiSC (FLAMPOURIS 2006, SENET 2004), for operationalisation of the method for image sequences captured by video cameras under real condition seems reasonable, as cost minimization is one of the basic logics for remote sensing. Such development can also provide access the developing coastal nations to such sophisticated technology.

References

AHRENDT, K. (1994): Geologie und Küstenschutz am Beispiel Sylt/Deutsche Bucht. Ber For u Techn.zent Westküste 4, Forschungs- und Technologiezentrum Westküste, Büsum (*in German*).

AHRENDT, K. (2001): Expected effect of climate change on Sylt island: results from a multidisciplinary German project. *Clim. Res*., 18: 141-146.

ANONYMOUS (1989): FURUNO – Operators manuals for FR 1201; Nishimomiya, Japan (FURUNO ELECTRIC CO. LIMITED).

BARRICK, D. E. (1977): Ocean surface current mapped by Radar. *Science* 198: 138-144

BELL, P.S. (1999): Shallow water bathymetry derived from an analysis of X-band marine radar images of waves. *Coastal Engineering* 37: 513-527

CHERRY, J.A. (1994): Distortion analysis of weakly nonlinear filters using volterra series. Master's thesis, Ottowa Carleton Institute for Electrical ngineering, Ottawa, Canada.

COLEBROOK, C.F. & WHITE, C.M. (1937): Experiments with fluid friction in roughened pipes. *Proc. Roy. Soc.*, Series A, 161, 367-381.

COX, C. S., & MUNK, W. H. (1954a): Statistics of the sea surface derived from Sun glitter. *J. Mar. Res.* 13:189-227.

COX, C. S., & MUNK, W. H. (1954b): Measurements of the roughness of the sea surface from photographs of the Sun's glitter. *J. Opt. Soc. Am.* 44:838-50

CROMBIE, D. D. (1956): Doppler spectrum of sea echo at 13.56 Mc/s. *Nature,* 175: 681-682

CYSEWSKI, M. (2003): Radarscanning in der Hydrographie (*in German*). Diplomarbeit GKSS 2003/26. GKSS Research Center, Geesthacht.

DANKERT, H. & ROSENTHAL, W. (2004): Ocean surface determination from X-Band radar-image sequences. *Journal of Geophysical Research*, 109, pp C04016.

DODDY, P.; FERRERIA, M.; LOMBARDO, S.; LUICUS, I., MISDORP, R; NIESING, H.; SALMAN, A. & SMALLEGANGE, M. (2004): Living with coastal Erosion in Europe – Sediment and Space for Surtainability, Results from the Eurossion Study, European Commission Publication, Luxembourg, 38p.

DOONG D. J.; WU, L. C. & DANKERT, H. (2002): Dependence of Wave Remote Sensing and In-Situ Observations. First German-Chinese Joint Symposium on Coastal and Ocean Engineering, April 10-12, 2002, Rostock, Germanny.

FLAMPOURIS, S. (2006): Investigation of correlations between radar deduced bathymetries due to the outer impact of a storm in the area "Salzsand". Master thesis, Coastal Geosciences and Engineering, CORELAB, University of Kiel, Germany.

GANGESKAR, R. & GRONLIE, O. (2000): Wave Height Measurement with a Standard Navigation Ship Radar – Result from Field Trials. In: Proceedings of the Sixth International Conference on Remote Sensing for Marine and Coastal Environments, Charleston, South Carolina.

GENERALPLAN KÜSTENSCHUTZ (2001): Integriertes Küstenschutzmanagement in Schleswig-Holstein.

GRONLIE, O. (1995): Microwave Radar Directional Wave Measurements – MIROS Results. *In*: Proceedings of the WMO/IOC Workshop on Operational Ocean Monitoring using Surface Based Radars, WMO Report no. 32, WMO/TD-No. 694, Geneva.

HASSELMANN, K. (1962): On the non-linear energy transfer in a gravity wave spectrum. 1: General theory. *J. Fluid Mech.*, 12, 481–500.

HASSELMANN, K.; ALPERS, W.; BARICK, D.; CROMBIE, D.; FLACHI, C.; FUNG, A; VAN HUTTEN, H.; JONES, W.; DE LOOR, G.P.; LIPA, B.; LONG, R.; ROSS, D.; RUFENACH, C.; SANDHAM, W.; SHEMDIN, O.; TEAGUE, C.; TRIZNA, D.; VALENZUELA, G.; WALSH, E.; WENTZ, F. AND WRIGHT, J. (1978): Radar Measurements of Wind and Waves. *Boundary-Layer Meteorology*, 13, 405-412.

HAVLICEK, J; HARDING, D. AND BOVIK, A. (1996): The multicomponent AM-FM image representation. *IEEE Transactions on Image Processing* 5(6), pages 1094-1100.

HORIKAWA, K. (2000): Nearshore Dynamics and Coastal Processes – Theory, Measurement, and Predictive Models (First Edition). 378pp.; University of Tokyo Press.

LINDBERG, V. (2000): Uncertainties and Error Propagation, in Manual on Uncertainties, Graphing and the Vernier Caliper, Part I. Rochester Institute of Technology, New York, USA. (http://www.rit.edu/~uphysics/uncertinities/Uncertinitiespart2.html#addsub)

LONG, M. W. (1983): Radar Reflectivity of Land and Sea (Second Edition). 385pp.; Dedham (Artech House, Inc).

LUMBORG, U. & WINDELIN, A. (2003): Hydrography and cohesive sediment modeling: application to the Romo Dyb tidal area. *Journal of Marine Systems*, 38, 287-303p.

MILES, J. W. (1957): On the generation of surface waves by shear flows. *J. Fluid Mech.*, 3, 185–204.

NIETO BORGE, J. C.; REICHERT, K.; DITTMER, J. & ROSENTHAL, W. (1998): WaMoS II: A wave and current monitoring system, Presented at the COAST 714 conference, Sept., Paris Proceedings.

NIETO BORGE, J.C. & SOARES, C. G. (2000): Analysis of directional wave fields using X-band navigation radar. *Coastal Engineering*, 40, 375-391.

NIETO BORGE, J.C.; REICHERT, K. & DITTMER, J. (1999): Use of nautical radar as wave monitoring instrument. *Coastal Engineering*, 37, 331-342.

OUTZEN, O. (1998): Bestimmung der Wassertiefe und der oberfl¨achennahen Str¨omung mit einem nautischen Radar. In Diploma Thesis, GKSS Report98/E/60 (*in German*) University of Hamburg, Germany.

PHILLIPS, O.M. (1966): Thy dynamics of the upper ocean (First Edition); Cambridge University Press.

PIERSON, W. J. (1962): The directional spectrum of a wind-generated sea as determined from data obtained by the Stereo Wave Observation Project. *Coll. Eng. NYU Meteorol. Pap*. 2, No. 6.

PIERSON, W. J., NEUMANN, G. & JAMES, R. W. (1955): Practical methods for observing and forecasting ocean waves by means of wave spectra and statistics. US Navy Hydrographic Office Pub., 603.

PRINS, J. (1996): Statistical Methods Group – In: NIST/SEMATECH e-Handbook of Statistical Methods. (http://www.nist.gov/stst.handbook).

REISE, K. (2004): Sea-Level Rise and the Future of Barrier Island in the North Sea; in proceedings of SeaLevel Rise and Coastal Defence in the Southern North Sea, Norfolk on 18 March 2004, 38-43p.

ROBINSON, I.S., WARD, N.P., GOMMENGINER, C.P, & TENORIO-GONZALES M.A (2000): Coastal oceanography applications of digital image data from marine radar. *Journal of Atmospheric and Oceanic Technology*, 17, pp. 721-725.

SABINS, F. F. (1987): Remote Sensing, Principles and Interpretation (Second Edition). W.H. Freeman, New York.

SEEMANN, J., ZIEMER, F. & SENET, C. M. (1997): A method for computing calibrated ocean wave spectra from measurements with a nautical X-band radar. Proc. Oceans '97, Halifax, NS, Canada, MTS/IEEE, 1148–1154.

SEEMANN, J.; SENET, C.M.; WOLFF, U. & ZIEMER, F. (2000a): Nautical X-band radar Image Processing: Monitoring of Morphodynamic Processes in Coastal Waters, Ocean 2000, Conference Proceedings, Rhode Island, USA.

SEEMANN, J.; SENET, C.M.; WOLFF, U.; HATTEN, H. & ZIEMER, F. (2000b): Hydrographic Parameter Maps Retrieved from Nautical Radar Image Sequences of inhomogeneous Water Surfaces. IGARSS"2000, Conference Proceedings, Volume V, pp. 1898-1900, Honolulu, Hawaii.

SEEMANN, J.; SENET, C.M.; & ZIEMER, F. (2000): Verfahren zur Ermittlung von ein in situ Seegangafeld beschreibenden hydrogrephischen Parametern mittels einer Radareinrichtung. German patent office, Munich, Germany, in German, German and international patent application, Ref. No. 100 35 921.3, Ref. No PCT/DE 00/02413 (international patent application).

SEEMANN, J.; SENET, C.M.; ZIEMER, F. (2000c): Local analysis of inhomogeneous Sea surfaces in Coastal waters using Nautical Radar Image Sequences, Mustererkennung 2000, Springer, Berlin, Informatik aktuell, pp. 179-186.

SENET, C., SEEMANN, J. & ZIEMER, F. (2001). The near-surface current velocity determined from image sequences of the sea surface. IEEE Trans. *Geosci. Remote Sens*., 39, 492–505.

SENET, C.M. (1996): Untersuchungen zur Bestimmung der oberflachennahen Stromung-sgeschwindigket mit einem nautischen Radar (*in German*). Master's thesis, University of Hamburg, Institute of Oceanography, GKSS Research Center, Geesthacht, Germany.

SENET, C.M. (2004): Dynamics of Dispersive Boundaries: The determination of Spatial Hydrographic-Parameter Maps from Optical Sea-Surface Image Sequences. PhD thesis, GKSS Research Center, University of Hamburg.

SENET, C.M. & SEEMANN, J. (1999): Old_Pol_2_Cartesian (Computer Program), Internal Resource, Radar Hydrography (KOR), GKSS Research Center GmbH, Geesthacht, Germany.

SENET, C.M. & SEEMANN, J. (2002): Studie II: "Validation". Technical report, GKSS Research Center GmbH, Geesthacht, Germany.

SENET, C.M.; SEEMANN, J. & ZIEMER, F. (2000): Verfahren und Vorrichtung zur Ermittlung von ein Seegangafeld in einem Wellentank beschreibenden hydrogrephischen. German patent office, Munich, Germany, in German, German and international patent application, Ref. No. 100 35 931.0, Ref. No PCT/DE 00/02413 (international patent application).

SENET, C.M.; SEEMANN, J. & ZIEMER, F. (2003): Determination of Bathymetric and Current Maps by the Method DiSC Based on the Analysis of Nautical X-Band Radar-Image Sequences of the Sea Surface, (Elsevier Science).

SISTERMANS, P. & NIEUWENHUIS, O. (2007): Isle of Sylt: Isles Scheslwig-Holstein (Germany)-a Case Study of European Initiative for Sustainable Coastal Erosion Management (Eurosion), Amersfoort, The Netherlands. 21p.

SKOLNIK, M. (1990): Radar Handbook (Second Edition). McGraw-Hill, Inc., New York, St. Louis, London, Lisbon, Madrid, Mexico, Paris, Singapore, Sydney, Tokyo, Toronto.

SORENSEN, R. M. (1997): Basic Coastal Engineering (Second Edition). 301p. Kluwer Academic Publishers, Boston, Dordrecht, London..

SOULSBY, R.L. & HUMPHERY, J.D. (1990): Field observations of wave-current interaction at the sea bed, in Water Wave Kinematics, [eds] A. Torum and O.T. Gudmestad, pp. 413-428. Kluwer Academic Publishers, Dordrecht.

STEWART, R.H. (2006): Introduction to Physical Oceanography. Department of Oceanography, 344p., Texas A & M University Press.

STOICA, R. & NEHORAI, A. (1989): MUSIC, maximum likelihood, and Cramer-Rao bound. *IEEE Transactions on Acoustics, Speech, and Signal Processing* 37, Pages 720-741.

STOKER, J. J. (1957): Water Waves, vol 4. Pure and Applied Mathematics [eds.] R Courant, L Bers and J J Stoker. New York, Interscience.

VALENZUELA, G. R. (1978): Theories for the interaction of electromagnetic and oceanic waves--a review. *Boundary-Layer Meteorol*.13:61-85

VAN RIJN, L.C. (1984): Sediment Pick-Up Functions. *Journal of Hydraulic Engineering*, ASCE, Vol. 110, No. 10.

WINKLE, N. (1994): Modellierung von Seegang in extremen Flachwasser, PhD Thesis, GKSS Research Center, University of Hamburg.

WOLFF, U.; SEEMANN, J.; SENET, C.M. & ZIEMER, F. (1999): Analysis of Morphodynamical Processes with a Nautical X-Band Rader, Mustererkennung ‘99, Springer, Berlin, Ch. Pages 372-380.

WRIGHT, J. W. (1968): A new model for sea clutter. *IEEE Trans. Antennas Propag*., AP-16, 217–223.

YOUNG, I., ROSENTHAL, W., & ZIEMER, F. (1985). A threedimensional analysis of marine radar images for the determination of ocean wave directionality and surface currents. *J. Geophys. Res.,* 90,C1, 1049–1059.

ZIEMER, F. & DITTMER, J. (1994): A System to Monitor Ocean Wave Fields. In: Proceedings of the OCEANS'94, October 13-16: 28-31.

ZIEMER, F. (1991): Directional spectra from shipboard navigation radar during LEWEX. In Directional Ocean Wave Spectra, edited by R.C. Beal, The Johns Hopkins University Press, Baltimore, USA, pp. 80-84.

ZIEMER, F. (1995): An Instrument for the Survey of the Directionality of the Ocean Wave Field. Workshop on Operational Ocean Monitoring using surface based radars, Geneva, WMO/IOC Report No. 32, pp. 81-87.

ZIEMER, F., BROCKMANN, C.; VAUGHAN, A. R.; SEEMANN, J. & SENET, C.M. (2004): Radar Survey of Near Shore Bathymetry within the OROMA project. EARSel eProceedings 3, 2/2004, pp. 282-288.

Appendix I

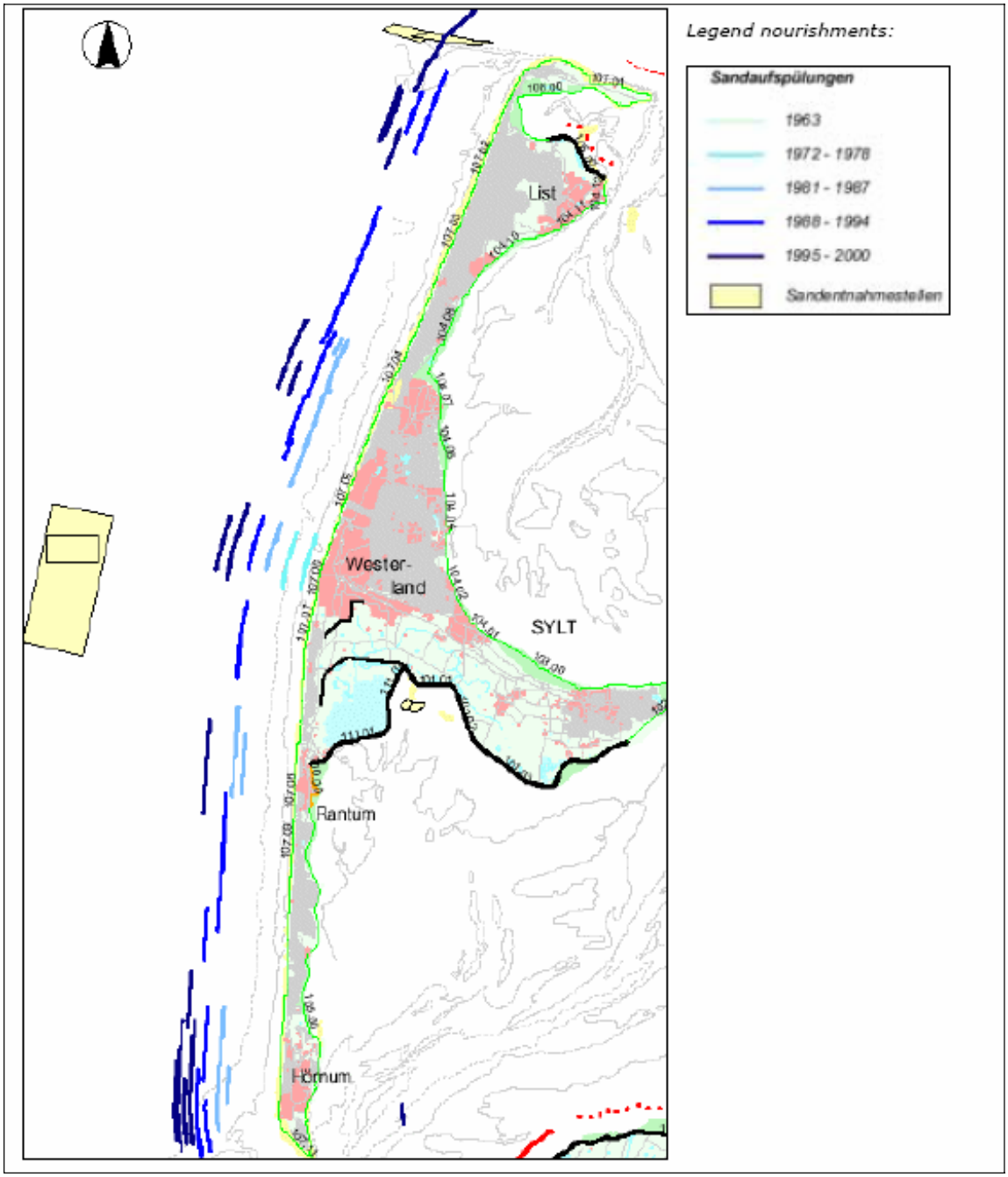

Figure I-1: Beach Nourishment by sand at Sylt (GENENALPLAN KUSTENSCHUTZ 2001).

Appendix II

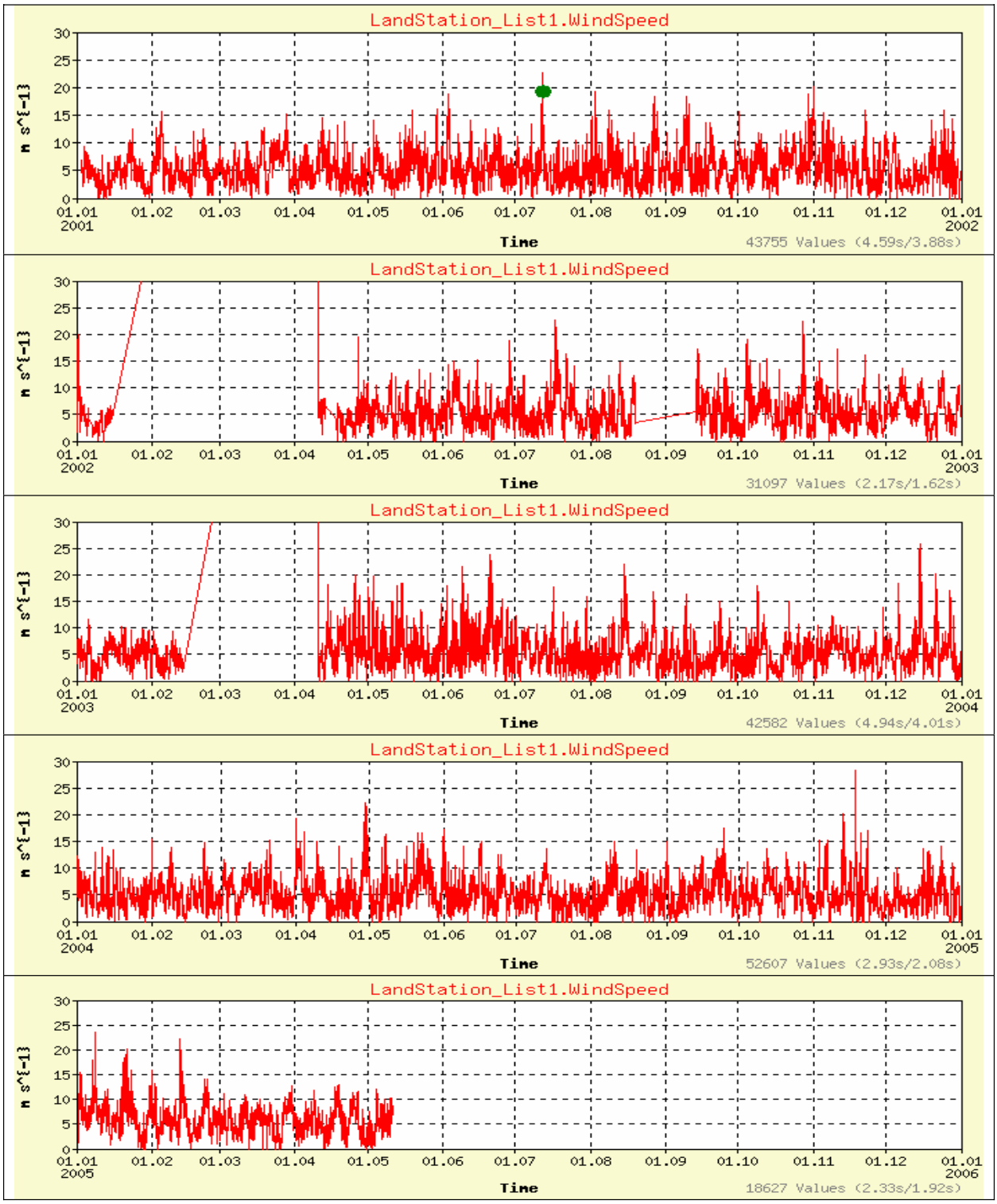

Figure II-1: Wind speed record of Landstation_List1 (from 2001 to 2005), green dot in first graph indicating strong wind condition of the study period.

Appendix III

Table III-1: Input file to DiSC, it defines the number of dimension, the number of pixels in each direction, the number of images, the coordinates in meters of the lower left corner of the image, the length at x and y dimension of each pixel the rotation period of the antenna, the units of the 3 dimensions and the name of the image sequence.

1	comment // Benutzerkommentar
2	3 // Dimension
3	288 // n1
4	288 // n2
5	256 // n3
6	3459944.4792 // o1
7	6101014.6577 // o2
8	0 // o3
9	6.8182 // s1
10	6.8182 // s2
11	1.70000000000 // s3
12	m // unit1
13	m // unit2
14	s // unit3
15	07120200_small.carth // filename

Appendix IV

Table IV-1: List of efforts of Processing data for Bathymetric Parameters during the tidal cycle of July 12, 2001.

Hour	Efforts	w-min	w-max	Power	Bin	Power	Confidence	Block
1207000	1	49	76	216	130	116	0.985	130
1207000	2	49	76	220	130	116	0.985	130
1207000	3	48	76	218	130	118	0.985	130
1207000	4	41	76	218	130	116	0.985	130
1207000	5	43	76	221	130	114	0.985	130
1207000	6	43	76	221	130	110	0.985	130
1207000	7	42	76	220	130	110	0.985	130
1207000	8	42	76	221	130	115	0.985	130
Hour	**Efforts**	**w-min**	**w-max**	**Power**	**Bin**	**Power**	**Confidence**	**Block**
1207100	1	38	84	216	130	115	0.985	130
1207100	2	40	76	216	130	115	0.985	130
1207100	3	40	76	220	130	115	0.985	130
1207100	4	40	76	220	130	118	0.985	130
1207100	5	42	76	219	130	110	0.985	130
1207100	6	40	76	220	130	112	0.985	130
1207100	7	41	80	220	130	118	0.985	130
1207100	8	41	80	220	130	120	0.985	130
Hour	**Efforts**	**w-min**	**w-max**	**Power**	**Bin**	**Power**	**Confidence**	**Block**
1207200	1	37	80	218	130	120	0.985	130
1207200	2	39	76	218	130	122	0.985	130
1207200	3	40	76	220	130	110	0.985	130
1207200	4	40	76	220	130	114	0.985	130
1207200	5	40	76	220	130	118	0.985	130
1207200	6	40	76	220	130	122	0.985	130
1207200	7	37	76	220	130	112	0.985	130
1207200	8	40	76	218	130	115	0.985	130
1207200	9	40	70	220	130	112	0.985	130
1207200	10	40	72	220	130	110	0.985	130
Hour	**Efforts**	**w-min**	**w-max**	**Power**	**Bin**	**Power**	**Confidence**	**Block**
1207300	1	40	76	217	130	122	0.985	130
1207300	2	42	70	217	130	120	0.985	130
1207300	3	37	79	220	130	110	0.985	130
1207300	4	38	79	220	130	114	0.985	130
1207300	5	38	79	222	130	114	0.985	130
1207300	6	38	77	222	130	118	0.985	130
1207300	7	39	77	220	130	116	0.985	130
1207300	8	39	76	219	130	114	0.985	130
1207300	9	39	77	219	130	110	0.985	130
1207300	10	39	77	217	130	112	0.985	130

table continued…

Hour	Efforts	w-min	w-max	Power	Bin	Power	Confidence	Block
1207400	1	35	86	218	130	115	0.985	130
1207400	2	38	83	218	130	120	0.985	130
1207400	3	38	78	218	130	112	0.985	130
1207400	4	38	75	216	130	120	0.985	130
1207400	5	38	75	218	130	116	0.985	130
1207400	6	38	75	220	130	114	0.985	130
1207400	7	38	73	220	130	118	0.985	130
1207400	8	38	73	220	130	116	0.985	130
1207400	9	36	73	219	130	114	0.985	130
1207400	10	36	73	218	130			
Hour	**Efforts**	**w-min**	**w-max**	**Power**	**Bin**	**Power**	**Confidence**	**Block**
1207500	1	35	84	215	130	112	0.985	130
1207500	2	37	76	218	130	115	0.985	130
1207500	3	37	76	220	130	115	0.985	130
1207500	4	37	76	220	130	112	0.985	130
1207500	5	37	76	220	130	118	0.985	130
1207500	6	37	76	222	130	110	0.985	130
1207500	7	37	76	222	130	114	0.985	130
1207500	8	37	76	222	130	112	0.985	130
1207500	9	36	75	220	130	110	0.985	130
1207500	10	37	75	219	130	110	0.985	130
Hour	**Efforts**	**w-min**	**w-max**	**Power**	**Bin**	**Power**	**Confidence**	**Block**
1207600	1	44	78	217	130	118	0.985	130
1207600	2	44	76	217	130	120	0.985	130
1207600	3	36	81	219	130	114	0.985	130
1207600	4	38	77	219	130	110	0.985	130
1207600	5	38	78	220	130	112	0.985	130
1207600	6	38	76	220	130	110	0.985	130
1207600	7	38	76	220	130	114	0.985	130
1207600	8	38	76	220	130	118	0.985	130
1207600	9							
1207600	10							
Hour	**Efforts**	**w-min**	**w-max**	**Power**	**Bin**	**Power**	**Confidence**	**Block**
1207700	1	40	80	215	130	115	0.985	130
1207700	2	40	80	218	130	119	0.985	130
1207700	3	40	80	218	130	123	0.985	130
1207700	4	36	76	216	130	110	0.985	130
1207700	5	38	76	218	130	110	0.985	130
1207700	6	38	76	218	130	114	0.985	130
1207700	7	38	76	218	130	118	0.985	130
1207700	8	38	76	218	130	122	0.985	130
1207700	9	38	76	218	130	126	0.985	130
1207700	10							

table continued…

Hour	Efforts	w-min	w-max	Power	Bin	Power	Confidence	Block
1207800	1	38	81	215	130	115	0.985	130
1207800	2	37	81	218	130	110	0.985	130
1207800	3	37	81	218	130	112	0.985	130
1207800	4	37	80	220	130	110	0.985	130
1207800	5	37	78	220	130	114	0.985	130
1207800	6	36	78	222	130	110	0.985	130
1207800	7	37	78	222	130	114	0.985	130
1207800	8	37	76	219	130	112	0.985	130
1207800	9							
1207800	10							
Hour	**Efforts**	**w-min**	**w-max**	**Power**	**Bin**	**Power**	**Confidence**	**Block**
1207900	1	44	72	215	130	110	0.985	130
1207900	2	47	74	215	130	115	0.985	130
1207900	3	47	74	218	130	115	0.985	130
1207900	4	40	75	218	130	114	0.985	130
1207900	5	40	75	216	130	110	0.985	130
1207900	6	40	75	216	130	114	0.985	130
1207900	7	40	75	218	130	110	0.985	130
1207900	8	42	76	220	130	110	0.985	130
1207900	9	42	76	220	130	112	0.985	130
1207900	10	42	76	218	130	112	0.985	130
Hour	**Efforts**	**w-min**	**w-max**	**Power**	**Bin**	**Power**	**Confidence**	**Block**
1207_10	1	40	77	218	130	110	0.985	130
1207_10	2	39	80	218	130	115	0.985	130
1207_10	3	39	77	215	130	108	0.985	130
1207_10	4	39	77	220	130			
1207_10	5	49	80	214	130	109	0.985	130
1207_10	6	40	80	220	130	110	0.985	130
1207_10	7	40	80	222	130	110	0.985	130
1207_10	8	42	80	220	130	112	0.985	130
1207_10	9	41	80	218	130	112	0.985	130
1207_10	10	40	78	216	130	114	0.985	130
Hour	**Efforts**	**w-min**	**w-max**	**Power**	**Bin**	**Power**	**Confidence**	**Block**
1207_11	1	42	76	215	130	112	0.985	130
1207_11	2	40	76	219	130	118	0.985	130
1207_11	3	40	80	220	130	114	0.985	130
1207_11	4	40	80	220	130	110	0.985	130
1207_11	5	40	80	220	130	108	0.985	130
1207_11	6	40	80	220	130	112	0.985	130
1207_11	7	40	78	220	130	110	0.985	130
1207_11	8	40	78	218	130	114	0.985	130
1207_11	9	40	78	216	130	112	0.985	130
1207_11	10	40	80	218	130	110	0.985	130

Appendix V

Table V-1: List of efforts of processing data for Current feature during the tidal cycle of July 12, 2001, using DiSC Bathymetry.

Hour	Efforts	w-min	w-max	Power	Bin	Power	Confidence	Block	Gauge
1207000	1	58	99	216	130	112	0.985	130	-0.9
1207000	2	60	96	220	130	114	0.985	130	-0.9
1207000	3	58	95	218	130	110	0.985	130	-0.9
1207000	4	58	95	219	130	110	0.985	130	-0.9
1207000	5	58	95	220	130	108	0.985	130	-0.9
Hour	**Efforts**	**w-min**	**w-max**	**Power**	**Bin**	**Power**	**Confidence**	**Block**	**Gauge**
1207100	1	60	100	218	130	110	0.985	130	0
	2	60	100	220	130	110	0.985	130	0
	3	55	95	218	130	115	0.985	130	1
S	4	58	98	218	130	115	0.985	130	0
E	5	58	98	220	130	110	0.985	130	0
N	6	58	98	221	130	110	0.985	130	0
S	7	58	90	221	130	110	0.9	130	0
I	8	58	90	221	130	110	0.85	130	0
T	9	58	90	221	130	110	0.8	130	0
I	10	58	90	221	130	110	0.99	130	0
V	11	58	90	221	130	110	0.75	130	0
I	12	58	90	221	130	110	0.75	130	0
T	13	58	90	221	120	110	0.985	130	-1
Y	14	58	90	221	140	110	0.985	130	0
	15	58	90	221	120	110	0.985	130	0
	16	58	90	221	110	110	0.985	130	0
T	17	58	90	221	150	110	0.985	130	0
R	18	58	90	221	160	110	0.985	130	0
A	19	58	90	221	130	110	0.985	130	-0.5
I	20	58	90	221	130	110	0.985	130	-1
L	21	58	90	221	130	110	0.985	130	-1.5
S	22	58	90	221	130	110	0.985	130	-2
	23	58	90	221	130	110	0.985	130	0.5
	24	58	90	221	130	110	0.985	130	1
	25	58	90	221	130	110	0.985	130	1.5
	26	58	90	221	130	110	0.985	130	2
	27	58	90	221	130	114	0.985	130	0
	28	40	80	220	130	112	0.985	130	0
	29	45	85	220	130	112	0.985	130	0
	30	50	90	220	130	112	0.985	130	0
	31	55	95	220	130	112	0.985	130	0
	32	60	100	220	130	112	0.985	130	0
Hour	**Efforts**	**w-min**	**w-max**	**Power**	**Bin**	**Power**	**Confidence**	**Block**	**Gauge**
1207100	1	55	98	216	130	115	0.985	130	-0.6
1207100	2	55	95	216	130	115	0.985	130	-0.6
1207100	3	56	96	220	130	115	0.985	130	-0.6
1207100	4	57	96	220	130	118	0.985	130	-0.6
1207100	5	57	96	220	130	110	0.985	130	-0.6

table continued...

Hour	Efforts	w-min	w-max	Power	Bin	Power	Confidence	Block	Gauge
1207200	1	55	85	220	130	112	0.985	130	-0.2
1207200	2	56	90	220	130	110	0.985	130	-0.2
1207200	3	57	95	222	130				
1207200	4	57	95	218	130	112	0.985	130	-0.2
1207200	5	57	95	220	130	110	0.985	130	-0.2
1207200	6	57	95	218	130	110	0.985	130	-0.2
Hour	**Efforts**	**w-min**	**w-max**	**Power**	**Bin**	**Power**	**Confidence**	**Block**	**Gauge**
1207300	1	58	88	217	130	122	0.985	130	0.2
1207300	2	60	90	217	130	120	0.985	130	0.2
1207300	3	60	92	220	130	110	0.985	130	0.2
1207300	4	62	95	220	130	114	0.985	130	0.2
1207300	5	62	95	222	130	114	0.985	130	0.2
1207300	6	58	95	222	130	118	0.985	130	0.2
Hour	**Efforts**	**w-min**	**w-max**	**Power**	**Bin**	**Power**	**Confidence**	**Block**	**Gauge**
1207400	1	55	98	218	130	112	0.985	130	0.8
1207400	2	57	98	216	130	110	0.985	130	0.8
1207400	3	60	99	218	130	110	0.985	130	0.8
1207400	4	60	98	220	130	110	0.985	130	0.8
1207400	5	60	97	218	130	110	0.985	130	0.8
Hour	**Efforts**	**w-min**	**w-max**	**Power**	**Bin**	**Power**	**Confidence**	**Block**	**Gauge**
1207500	1	56	96	215	130	112	0.985	130	1.1
1207500	2	58	97	218	130	114	0.985	130	1.1
1207500	3	60	99	220	130	114	0.985	130	1.1
1207500	4	60	99	218	130	112	0.985	130	1.1
1207500	5	60	99	218	130	110	0.985	130	1.1
1207500	6								
Hour	**Efforts**	**w-min**	**w-max**	**Power**	**Bin**	**Power**	**Confidence**	**Block**	**Gauge**
1207600	1	56	95	217	130	112	0.985	130	0.95
1207600	2	58	96	217	130	110	0.985	130	0.95
1207600	3	60	98	219	130	114	0.985	130	0.95
1207600	4	60	98	219	130	116	0.985	130	0.95
1207600	5	60	98	220	130	116	0.985	130	0.95
Hour	**Efforts**	**w-min**	**w-max**	**Power**	**Bin**	**Power**	**Confidence**	**Block**	**Gauge**
1207700	1	58	95	215	130	112	0.985	130	0.65
1207700	2	60	97	218	130	110	0.985	130	0.65
1207700	3	60	95	218	130	112	0.985	130	0.65
1207700	4	62	95	216	130	110	0.985	130	0.65
1207700	5	62	95	218	130	110	0.985	130	0.65
Hour	**Efforts**	**w-min**	**w-max**	**Power**	**Bin**	**Power**	**Confidence**	**Block**	**Gauge**
1207800	1	58	95	215	130	115	0.985	130	0.2
1207800	2	60	94	218	130	110	0.985	130	0.2
1207800	3	60	93	218	130	112	0.985	130	0.2
1207800	4	63	93	220	130	110	0.985	130	0.2
1207800	5	63	93	218	130	110	0.985	130	0.2

table continued…

Hour	Efforts	w-min	w-max	Power	Bin	Power	Confidence	Block	Gauge
1207900	1	56	90	215	130	110	0.985	130	-0.35
1207900	2	58	90	215	130	115	0.985	130	-0.35
1207900	3	60	88	220	130	112	0.985	130	-0.35
1207900	4	60	87	218	130	112	0.985	130	-0.35
1207900	5	60	87	218	130	110	0.985	130	-0.35
Hour	**Efforts**	**w-min**	**w-max**	**Power**	**Bin**	**Power**	**Confidence**	**Block**	**Gauge**
1207_10	1	55	90	218	130	110	0.985	130	-0.8
1207_10	2	51	88	218	130	112	0.985	130	-0.8
1207_10	3	60	85	220	130	108	0.985	130	-0.8
1207_10	4	61	85	218	130	110	0.985	130	-0.8
1207_10	5	61	85	218	130	110	0.985	130	-0.8
Hour	**Efforts**	**w-min**	**w-max**	**Power**	**Bin**	**Power**	**Confidence**	**Block**	**Gauge**
1207_11	1	55	90	215	130	112	0.985	130	-0.6
1207_11	2	58	92	219	130	110	0.985	130	-0.6
1207_11	3	59	90	220	130	114	0.985	130	-0.6
1207_11	4	59	90	218	130	112	0.985	130	-0.6
1207_11	5	59	90	216	130	112	0.985	130	-0.6

Table V-2: List of efforts of processing data for Current feature during the tidal cycle of July 12, 2001, using sounding Bathymetry.

Hour	Efforts	w-min	w-max	Power	Bin	Power	Confidence	Block	Gauge
1207000	1	57	95	220	130	110	0.985	130	-0.9
1207100	1	58	95	219	130	108	0.985	130	-0.6
1207200	1	57	96	220	130	108	0.985	130	-0.2
1207300	1	57	95	219	130	110	0.985	130	0.2
1207400	1	60	98	218	130	110	0.985	130	0.8
1207500	1	60	99	218	130	112	0.985	130	1.1
1207600	1	60	98	217	130	114	0.985	130	0.95
1207700	1	62	95	218	130	110	0.985	130	0.65
1207800	1	63	93	218	130	110	0.985	130	0.2
1207900	1	60	87	218	130	110	0.985	130	-0.35
1207_10	1	61	85	218	130	110	0.985	130	-0.8
1207_11	1	59	90	217	130	112	0.985	130	-0.6

Appendix VI

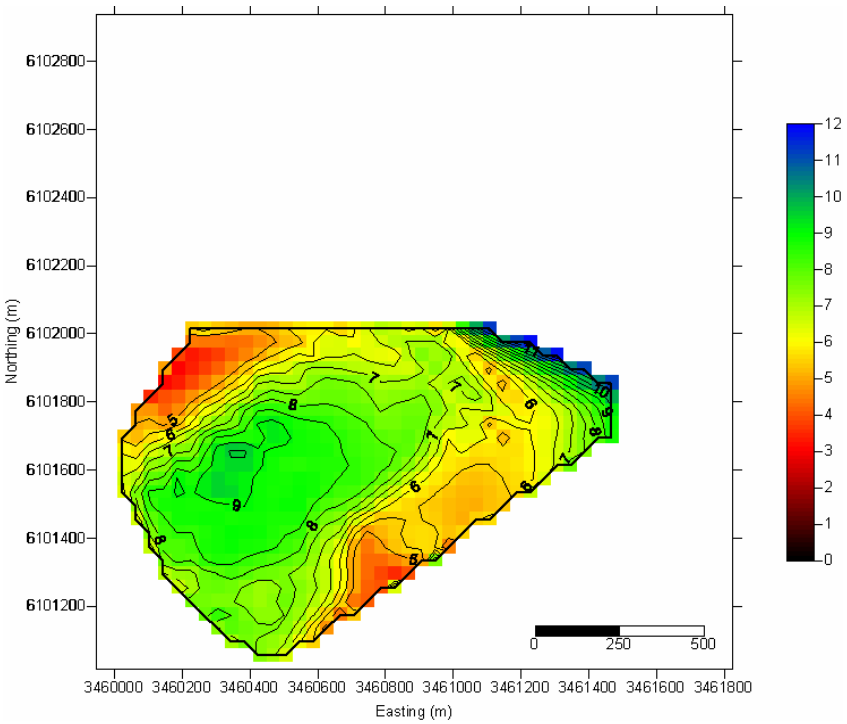

Figure VI-1: The echo-sounding bathymetry of the investigation area on 17-28/09/2001. (Source: GKSS/KOK)

Appendix VII

```
;*********************************************************************
; PV WAVE Header
;---------------------------------------------------------------------
; File name         :   echos
; Residency         :
; Programe name     :   Soundings_processing
; Module name       :   Bathymetry
; Version nr              :       1.1
; Date              :   05.12.2006
; Place             :   GKSS / Geesthacht
; Author            :   M. Zahedur Rahman Chowdhury
; Email             :   Mohammad.Chowdhury@gkss.de
;---------------------------------------------------------------------
; Description       :   Initializing the compiling of all routines
;---------------------------------------------------------------------
;
;*********************************************************************

RETALL
.LOCALS
DELVAR, /ALL
CLOSE, /ALL
DEVICE, /CLOSE



set_plot,'win32'
@stat_startup
@math_startup
@sigpro_startup
@ip_startup

.run readfile.pro
.run main_result.pro
.run filter.pro
.run read_radar.pro
.run averaging.pro
.run output.pro
main_result
```

```
;*********************************************************************
;
;---------------------------------------------------------------------
; Description       :   The main of the Soundings_processing
;---------------------------------------------------------------------
;
;*********************************************************************
;first step with pv-wave
PRO main_result

PRINT,'** main_result.pro is active **'

readfile, x_coordinate_dblarr,y_coordinate_dblarr, depth_dblarr

filter, x_coordinate_dblarr,y_coordinate_dblarr, depth_dblarr, $
      x_coordinate_dblarr_new,y_coordinate_dblarr_new, depth_dblarr_new

read_radar, x_coor_dblarr,y_coor_dblarr


averaging, x_coordinate_dblarr_new,y_coordinate_dblarr_new, depth_dblarr_new,
      x_coor_dblarr,y_coor_dblarr,z_depth_dblarr

output, x_coordinate_dblarr_new,y_coordinate_dblarr_new, depth_dblarr_new,
      x_coor_dblarr,y_coor_dblarr,z_depth_dblarr

STOP

PRINT,'** main_result.pro is finished **'


END
```

```
;*********************************************************************
;
;---------------------------------------------------------------------
; Description:   The Subroutine 'readfile' is reading the soudings
;---------------------------------------------------------------------
;
;*********************************************************************

PRO readfile,x_coordinate_dblarr,y_coordinate_dblarr, depth_dblarr

PRINT,'** readfile.pro is active **'

; definition of variables
line_strarr=STRARR(1)

file='D:\Wind\ssyltnord_1.txt'

;the file will be opened to count lines

line_counter=0l

OPENR, 1, file

      WHILE (NOT EOF(1)) DO BEGIN
            READF, 1,line_strarr

                  ;PRINT,'Number of lines=', line_counter,line_strarr

                        line_counter=line_counter+1

      ENDWHILE

CLOSE, 1


x_coordinate_dblarr = DBLARR (line_counter)
y_coordinate_dblarr = DBLARR (line_counter)
depth_dblarr = DBLARR (line_counter)

line_counter2=0l


OPENR, 1, file
      PRINT,'** file',file,'  has been opend **'

      WHILE (NOT EOF(1)) DO BEGIN
            READF, 1,line_strarr

                  ;PRINT,line_counter2,line_strarr

            ;reading the x_coordinates
            pos_point1 = STRPOS(line_strarr, '.')
                  ;PRINT,'pos_point1=', pos_point1

            x_coordinate= STRMID(line_strarr,pos_point1(0)-7,10)
                  ;PRINT, 'x_coordinate=', x_coordinate

            x_coordinates_dbl= DOUBLE(x_coordinate)
                  ;PRINT, 'x_coordinates_dbl=', x_coordinates_dbl
```

```
            x_coordinate_dblarr(line_counter2) = x_coordinates_dbl
                  ;PRINT, 'x_coordinate_dblarr=', x_coordinate_dblarr



            ;reading the y_coordinates
            pos_point2 = STRPOS(line_strarr, '.',pos_point1(0)+1)
                  ;PRINT,'pos_point2=', pos_point2

            y_coordinate= STRMID(line_strarr,pos_point2(0)-7,10)
                  ;PRINT, 'y_coordinate=', y_coordinate

            y_coordinates_dbl= DOUBLE(y_coordinate)
                  ;PRINT, 'y_coordinates_dbl=', y_coordinates_dbl


            y_coordinate_dblarr(line_counter2) = y_coordinates_dbl


            ;reading death from the file
            pos_point3 = STRPOS(line_strarr, '.',pos_point2(0)+1)
            ;PRINT,'pos_point3=', pos_point3

            depth= STRMID(line_strarr,pos_point3(0)-2,9)
                  ;PRINT, 'depth=', depth

            depth_dbl= DOUBLE(depth)
                  ;PRINT, 'depth_dbl=', depth_dbl

                  depth_dblarr(line_counter2) = depth_dbl

                                    line_counter2=line_counter2+1


      ENDWHILE

CLOSE, 1


PRINT,'**  has been closed **'

;PRINT, 'x_coordinate_dblarr=', x_coordinate_dblarr
;PRINT, 'y_coordinate_dblarr=', y_coordinate_dblarr
;PRINT, 'depth_dblarr=', depth_dblarr

PRINT,'** readfile.pro is finished **'

END
```

```
;*********************************************************************
;
;---------------------------------------------------------------------
; Description       :   Finding the study area in the Soudings result
;---------------------------------------------------------------------
;
;*********************************************************************
PRO filter, x_coordinate_dblarr,y_coordinate_dblarr, depth_dblarr, $
            x_coordinate_dblarr_new,y_coordinate_dblarr_new, depth_dblarr_new

PRINT,'** filter.pro is active **'

;for the qualification

index_xyd = WHERE (((x_coordinate_dblarr GE 3460535) AND $
      (x_coordinate_dblarr LE 3462400))AND ((y_coordinate_dblarr GE $ 6102800)
      AND (y_coordinate_dblarr LE 6103800)))

            x_coordinate_dblarr_new=x_coordinate_dblarr(index_xyd)
            y_coordinate_dblarr_new=y_coordinate_dblarr(index_xyd)
            depth_dblarr_new=depth_dblarr(index_xyd)

;,y_coordinate_dblarr, depth_dblarr


; Get the subscripts of the area defined


; Put the selected values into result.
;PRINT, 'x_coordinate_dblarr_new=', x_coordinate_dblarr_new
;PRINT, 'y_coordinate_dblarr_new=', y_coordinate_dblarr_new
;PRINT, 'depth_dblarr_new=', depth_dblarr_new

PRINT,'** filter.pro is finished **'


END
```

```
;*******************************************************************
;
;-------------------------------------------------------------------
; Description:   Reading radar coordinates for maching the area
;-------------------------------------------------------------------
;
;*******************************************************************
PRO read_radar, x_coor_dblarr, y_coor_dblarr

PRINT,'** read_radar.pro is active **'

; definition of variables
line_strarr=STRARR(1)

file='D:\Wind\disc_coor.txt'
;the file will be opened to count lines
line_counter=0l

OPENR, 1, file
      WHILE (NOT EOF(1)) DO BEGIN
            READF, 1,line_strarr
                  ;PRINT,'Number of lines=', line_counter,line_strarr
            line_counter=line_counter+1
      ENDWHILE
CLOSE, 1

x_coor_dblarr = DBLARR (line_counter)
y_coor_dblarr = DBLARR (line_counter)
line_counter2=0l

OPENR, 1, file
      PRINT,'** file',file,'  has been opend **'
      WHILE (NOT EOF(1)) DO BEGIN
            READF, 1,line_strarr
                  ;PRINT,line_counter2,line_strarr

      ;reading the x_coordinates
      pos_point1 = STRPOS(line_strarr, '.')
            ;PRINT,'pos_point1=', pos_point1

            x_coor= STRMID(line_strarr,pos_point1(0)-7,13)+'D'
                  ;PRINT, 'x_coor=', x_coor

                  x_coor_dbl= DOUBLE(x_coor)
                        ;PRINT, 'x_coor_dbl=', x_coor_dbl

                        x_coor_dblarr(line_counter2) = x_coor_dbl
```

```
;reading the y_coordinates
      pos_point2 = STRPOS(line_strarr, '.',pos_point1(0)+1)
            ;PRINT,'pos_point2=', pos_point2

            y_coor= STRMID(line_strarr,pos_point2(0)-7,13)+'D'
                  ;PRINT, 'y_coor=', y_coor

                  y_coor_dbl= DOUBLE(y_coor)
                        ;PRINT, 'y_coor_dbl=', y_coor_dbl

                        y_coor_dblarr(line_counter2) = y_coor_dbl

                        line_counter2=line_counter2+1


      ENDWHILE
CLOSE, 1
PRINT,'**  has been closed **'
;PRINT, 'x_coor_dblarr=', x_coor_dblarr
;PRINT, 'y_coor_dblarr=', y_coor_dblarr

PRINT,'** readfile.pro is finished **'


END
```

```
;*********************************************************************
;---------------------------------------------------------------------
; Description:   Averaging the sounding results according to radar cell
;---------------------------------------------------------------------
;*********************************************************************
PRO averaging, x_coordinate_dblarr_new,y_coordinate_dblarr_new, $
      depth_dblarr_new, x_coor_dblarr,y_coor_dblarr,z_depth_dblarr

Print, '-------------------------------------
Print, 'The averaging is running'
Print, '-------------------------------------

;z_depth_dblarr=DBLARR(N_ELEMENTS(x_coor_dblarr))
z_depth_dblarr=REPLICATE((-999.9d),N_ELEMENTS(x_coor_dblarr))

;index
FOR i=0L, N_ELEMENTS(x_coor_dblarr)-1 DO BEGIN

;print,'i=',i

x_index= WHERE((x_coordinate_dblarr_new LE x_coor_dblarr(i) + 20.0) $
            AND (x_coordinate_dblarr_new GE x_coor_dblarr(i) - 20.0))
                  ;PRINT, 'x_index=',x_index

IF (x_index(0) NE -1) THEN BEGIN

      FOR j=0L, N_ELEMENTS(x_index)-1 DO BEGIN

      y_coordinate_dblarr_new_temp=y_coordinate_dblarr_new(x_index)
      y_index=WHERE((y_coordinate_dblarr_new_temp LE y_coor_dblarr(i) + 20.0)
      AND (y_coordinate_dblarr_new_temp GE y_coor_dblarr(i) - 20.0))
            ;PRINT, 'y_index=',y_index

            IF (y_index(0) NE -1) THEN BEGIN
                  ;Print, 'a match is found'

                  all_index = x_index(y_index)
                  ;PRINT, all_index

            z=AVG(depth_dblarr_new(all_index))
                  ;PRINT, z
                  z_depth_dblarr(i)= z
                  ;PRINT, 'z_depth_dblarr=', z_depth_dblarr

            ENDIF

      ENDFOR            ;j=0l

ENDIF       ;(x_index(0) NE -1)

ENDFOR      ;i=0L

;print,'z_depth_dblarr',z_depth_dblarr
;print,'x_coordinate_dblarr_new(x_index)',x_coordinate_dblarr_new(x_index)
END
```

```
;*********************************************************************
;
;---------------------------------------------------------------------
; Description:   Creation of output file with radar coordinates
;---------------------------------------------------------------------
;
;*********************************************************************
PRO output, x_coordinate_dblarr_new,y_coordinate_dblarr_new, $
      depth_dblarr_new, x_coor_dblarr,y_coor_dblarr,z_depth_dblarr

Print, '-------------------------------------
Print,            'The output is running'
Print, '-------------------------------------


;creation of the full data array with coordinates and depth values

OPENW, 2, 'D:\Wind\syltarea_file.txt'

      FOR i=0L, N_ELEMENTS(x_coor_dblarr)-1 DO BEGIN

              printf,2, x_coordinate_dblarr_new(i),
                   y_coordinate_dblarr_new(i), z_depth_dblarr(i)

             ;y_coor_dblarr,z_depth_dblarr x_coordinate_dblarr_new(i), ,
             ;depth_dblarr_new(i), y_coordinate_dblarr_new(i),

      ENDFOR

CLOSE,2

END
```

Appendix VIII

```
;*********************************************************************
; PV WAVE Header
;---------------------------------------------------------------------
; File name         :   Results
; Residency         :
; Programe name     :   After_DiSC
; Module name       :   Bathymetry
; Version nr        :   1.1
; Date              :   03.11.2006
; Place             :   GKSS / Geesthacht
; Author            :   M. Zahedur Rahman Chowdhury
; Email             :   Mohammad.Chowdhury@gkss.de
;---------------------------------------------------------------------
; Description       :   Initializing the compiling of all routines
;---------------------------------------------------------------------
;
;*********************************************************************

RETALL
.LOCALS
DELVAR, /ALL
CLOSE, /ALL
DEVICE, /CLOSE



set_plot,'win32'
@stat_startup
@math_startup
@sigpro_startup
@ip_startup

.run readfile.pro
.run main_result.pro
.run filter.pro
.run coordinates.pro
.run comparison.pro
.run output.pro
main_result
```

```
;*********************************************************************
;
;---------------------------------------------------------------------
; Description:   The main of the After_DiSC
;---------------------------------------------------------------------
;
;*********************************************************************
;first step with pv-wave

PRO main_result

PRINT,'** main_result.pro is active **'

readfile, x_coordinate_dblarr,y_coordinate_dblarr, reg_point_intarr,$
      depth_dblarr

filter, x_coordinate_dblarr,y_coordinate_dblarr, reg_point_intarr, $
      depth_dblarr, x_coordinate_dblarr_new, y_coordinate_dblarr_new, $
      reg_point_intarr_new,depth_dblarr_new

coordinates, x_coord_exact,y_coord_exact

comparison, x_coord_exact,y_coord_exact,x_coordinate_dblarr_new,$
            y_coordinate_dblarr_new,depth_dblarr_new,z_depth_dblarr

output, x_coord_exact,y_coord_exact,z_depth_dblarr

STOP

PRINT,'** main_result.pro is finished **'


END
```

```
;*********************************************************************
;
;---------------------------------------------------------------------
; Description:   The Subroutine 'readfile' is reading the DiSC result
;---------------------------------------------------------------------
;
;*********************************************************************
PRO readfile, x_coordinate_dblarr,y_coordinate_dblarr,$ reg_point_intarr,
      depth_dblarr

PRINT,'** readfile.pro is active **'

; definition of variables
line_strarr=STRARR(1)

file='C:\surfer\Carry\Files\Hour000\Effort9\EE1_result_6x6.txt'
;the file will be opened to count lines

line_counter=0

OPENR, 1, file
      WHILE (NOT EOF(1)) DO BEGIN
            READF, 1,line_strarr
                  ;PRINT,'Number of lines=', line_counter,line_strarr
            line_counter=line_counter+1

      ENDWHILE

CLOSE, 1

x_coordinate_dblarr = DBLARR (line_counter)
y_coordinate_dblarr = DBLARR (line_counter)
reg_point_intarr = INTARR (line_counter)
depth_dblarr = DBLARR (line_counter)

line_counter2=0

OPENR, 1, file
      PRINT,'** file',file,'  has been opend **'

      WHILE (NOT EOF(1)) DO BEGIN
            READF, 1,line_strarr

            ;PRINT,line_counter2,line_strarr

            ;reading the x_coordinates
            pos_point1 = STRPOS(line_strarr, '.')
                  ;PRINT,'pos_point1=', pos_point1

                  x_coordinate= STRMID(line_strarr,pos_point1(0)-7,13)
                  ;PRINT, 'x_coordinate=', x_coordinate

                  x_coordinates_dbl= DOUBLE(x_coordinate)
                  ;PRINT, 'x_coordinates_dbl=', x_coordinates_dbl

            x_coordinate_dblarr(line_counter2) = x_coordinates_dbl
```

```
            ;reading the y_coordinates
                  pos_point2 = STRPOS(line_strarr, '.',pos_point1(0)+1)
                  ;PRINT,'pos_point2=', pos_point2

                  y_coordinate= STRMID(line_strarr,pos_point2(0)-7,13)
                  ;PRINT, 'y_coordinate=', y_coordinate

                  y_coordinates_dbl= DOUBLE(y_coordinate)
                  ;PRINT, 'y_coordinates_dbl=', y_coordinates_dbl

            y_coordinate_dblarr(line_counter2) = y_coordinates_dbl


            ;reading the regretion points
                  reg_point= STRMID(line_strarr,pos_point2(0)+10,3)
                  ;PRINT, 'reg_point=', reg_point

                  reg_point_int= FIX(reg_point)
                  ;PRINT, 'reg_point_int=', reg_point_int

            reg_point_intarr(line_counter2) = reg_point_int


            ;reading death from the file
                  pos_point3 = STRPOS(line_strarr, '.',pos_point2(0)+1)
                  ;PRINT,'pos_point3=', pos_point3

                  depth= STRMID(line_strarr,pos_point3(0)-2,6)
                  ;PRINT, 'depth=', depth

                  depth_dbl= DOUBLE(depth)
                  ;PRINT, 'depth_dbl=', depth_dbl

                  depth_dblarr(line_counter2) = depth_dbl

                        line_counter2=line_counter2+1


      ENDWHILE

CLOSE, 1
PRINT,'**  has been closed **'
;PRINT, 'x_coordinate_dblarr=', x_coordinate_dblarr
;PRINT, 'y_coordinate_dblarr=', y_coordinate_dblarr
;PRINT, 'reg_point_intarr=', reg_point_intarr
;PRINT, 'depth_dblarr=', depth_dblarr

PRINT,'** readfile.pro is finished **'


END
```

```
;*********************************************************************
;
;---------------------------------------------------------------------
; Description:   Filtering the result according to Reg. Coordinate
;---------------------------------------------------------------------
;
;*********************************************************************
PRO filter, x_coordinate_dblarr,y_coordinate_dblarr, reg_point_intarr,$
      depth_dblarr, x_coordinate_dblarr_new, y_coordinate_dblarr_new, $
      reg_point_intarr_new, depth_dblarr_new

PRINT,'** filter.pro is active **'

;for the qualification

      index_regp_in = WHERE ((reg_point_intarr GT 40) AND $ (reg_point_intarr
      LT 110))

            x_coordinate_dblarr_new=x_coordinate_dblarr(index_regp_in)
            y_coordinate_dblarr_new=y_coordinate_dblarr(index_regp_in)
            reg_point_intarr_new=reg_point_intarr(index_regp_in)
            depth_dblarr_new=depth_dblarr(index_regp_in)

;,y_coordinate_dblarr, reg_point_intarr, depth_dblarr


; Get the subscripts of those elements greater than 35 and less
; than 110.

; Put the selected values into result.
;PRINT, 'x_coordinate_dblarr_new=', x_coordinate_dblarr_new
;PRINT, 'y_coordinate_dblarr_new=', y_coordinate_dblarr_new
;PRINT, 'reg_point_intarr_new=', reg_point_intarr_new
;PRINT, 'depth_dblarr_new=', depth_dblarr_new


PRINT,'** filter.pro is finished **'


END
```

```
;*********************************************************************
;
;---------------------------------------------------------------------
; Description:   Creating Coordinates for the whole area
;---------------------------------------------------------------------
;
;*********************************************************************
PRO coordinates, x_coord_exact,y_coord_exact

Print, '--------------------------------------
Print, 'The coordinates is running'
Print, '--------------------------------------

x_coord_vecdbl= DBLARR(1)
y_coord_vecdbl= DBLARR(1)

FOR x_coord1= (3459944.47920D), (3461867.21160D), (40.9092D) DO BEGIN
            x_coord = STRING(x_coord1,format="(D12.4)")
            ;PRINT, x_coord

      FOR y_coord1=(6101014.65770D),(6102947.39010D),(40.9092D)DO BEGIN
            y_coord = STRING(y_coord1,format="(D12.4)")
            ;PRINT, y_coord

      x_coord_vecdbl=STRING([x_coord_vecdbl,x_coord],format="(D12.4)")

      y_coord_vecdbl=STRING([y_coord_vecdbl,y_coord],format="(D12.4)")

      ENDFOR ;y_coord

ENDFOR ;x_coord

;PRINT,'x_coord_vecdbl',x_coord_vecdbl
;PRINT,'y_coord_vecdbl',y_coord_vecdbl

;elemination of the first false value in the vecdbl of x and y coordinates
;n_elemennts function is used

            x_coord_elem=N_ELEMENTS(x_coord_vecdbl)

                        x_coord_exact=x_coord_vecdbl(1:x_coord_elem-1)

            y_coord_elem=N_ELEMENTS(y_coord_vecdbl)

                        y_coord_exact=y_coord_vecdbl(1:y_coord_elem-1)

            ;PRINT,'x_coord_exact=',x_coord_exact
            ;PRINT,'y_coord_exact=',y_coord_exact


END
```

```
;*********************************************************************
;
;---------------------------------------------------------------------
; Description:   Comparing the created coordinates with result coor.
;---------------------------------------------------------------------
;
;*********************************************************************PRO
comparison, x_coord_exact,y_coord_exact,x_coordinate_dblarr_new,$
      y_coordinate_dblarr_new,depth_dblarr_new,z_depth_dblarr

Print, '-------------------------------------
Print, 'The comparison is running'
Print, '-------------------------------------

z_depth_dblarr=DBLARR(N_ELEMENTS(x_coord_exact))

;index
FOR i=0L, N_ELEMENTS(x_coord_exact)-1 DO BEGIN

            x_index= WHERE(LONG(x_coordinate_dblarr_new) EQ $
            LONG(x_coord_exact(i)))
                  ;PRINT, 'x_index=',x_index

                  IF (x_index(0) NE -1) THEN BEGIN

      y_index=WHERE(LONG(y_coordinate_dblarr_new(x_index)) $
            EQ LONG(y_coord_exact(i)))
                  ;PRINT, 'y_index=',y_index

                        IF (y_index(0) NE -1) THEN BEGIN
                              ;Print, 'a match is found'

                              index_match=x_index(y_index)
                              ;PRINT, 'index_match=', index_match


                  z=depth_dblarr_new(index_match)
                        z_depth_dblarr(i)=z
                              ;PRINT, 'z=',z_depth_dblarr(i)
                              ;PRINT, 'i=', i

                        ENDIF

                  ENDIF

ENDFOR
;print,'x_coord_exact(i)',x_coord_exact(i)
;print,'x_coordinate_dblarr_new(x_index)'

END
```

```
;*********************************************************************
;
;---------------------------------------------------------------------
; Description:   Creation of output file with qualified results
;---------------------------------------------------------------------
;
;*********************************************************************PRO
output, x_coord_exact,y_coord_exact,z_depth_dblarr

Print, '-------------------------------------
Print,      'The output is running'
Print, '-------------------------------------


;creation of the full data array with coordinates and depth values

      OPENW, 2, 'C:\surfer\Carry\Files\Hour000\Effort9\Processed_z.txt'

            FOR i=0L, N_ELEMENTS(x_coord_exact)-1 DO BEGIN

      printf,2, x_coord_exact(i), ' ', y_coord_exact(i), $  z_depth_dblarr(i)

            LONG(y_coord_exact(i)),,,y_coord_exact(i)

            ENDFOR


      CLOSE,2
      END
```

Appendix IX

```
;*********************************************************************
; PV WAVE Header
;---------------------------------------------------------------------
; File name         :   Current
; Residency         :
; Programe name     :   current_vectors
; Module name       :   Current feature
; Version nr        :   1.1
; Date              :   15.12.2006
; Place             :   GKSS / Geesthacht
; Author            :   M. Zahedur Rahman Chowdhury
; Email             :   Mohammad.Chowdhury@gkss.de
;---------------------------------------------------------------------
; Description       :   Initializing the compiling of all routines
;---------------------------------------------------------------------
;
;*********************************************************************

RETALL
.LOCALS
DELVAR, /ALL
CLOSE, /ALL
DEVICE, /CLOSE



set_plot,'win32'
@stat_startup
@math_startup
@sigpro_startup
@ip_startup

.run readfile.pro
.run current.pro
.run main_result.pro
.run filter.pro
.run coordinates.pro
.run comparison.pro
.run output.pro
main_result
```

```
;*******************************************************************
;
;-------------------------------------------------------------------
; Description       :   The main of the current_vectors
;-------------------------------------------------------------------
;
;*******************************************************************
PRO main_result

PRINT,'** main_result.pro is active **'

readfile, x_coordinate_dblarr,y_coordinate_dblarr, reg_point_intarr, $
     depth_dblarr, vecx_dblarr, vecy_dblarr,

current, vecx_dblarr, vecy_dblarr, curdir_dblarr, curmgn_dblarr

filter, x_coordinate_dblarr,y_coordinate_dblarr, reg_point_intarr, $
     depth_dblarr, x_coordinate_dblarr_new, y_coordinate_dblarr_new, $
     reg_point_intarr_new, depth_dblarr_new, vecx_dblarr, vecy_dblarr,$
     vecx_dblarr_new, vecy_dblarr_new,x_vector_dblarr, y_vector_dblarr,$
     curmgn_dblarr, curmgn_dblarr_new, curdir_dblarr, curdir_dblarr_new

coordinates, x_coord_exact,y_coord_exact

comparison, x_coord_exact,y_coord_exact,x_coordinate_dblarr_new,$
      y_coordinate_dblarr_new,depth_dblarr_new,vecx_dblarr_new,$
      vecy_dblarr_new, z_depth_dblarr, x_vector_dblarr,y_vector_dblarr, $
      curmgn_dblarr, curmgn_dblarr_new,curdir_dblarr, curdir_dblarr_new,$
      cur_mag_dblarr, cur_dir_dblarr

output, x_coord_exact, y_coord_exact, z_depth_dblarr, x_vector_dblarr,$
     y_vector_dblarr, cur_mag_dblarr,cur_dir_dblarr

STOP

PRINT,'** main_result.pro is finished **'


END
```

```
;*********************************************************************
;
;---------------------------------------------------------------------
; Description:   Reading the DiSC result for Current components
;---------------------------------------------------------------------
;
;*********************************************************************

PRO readfile,x_coordinate_dblarr,y_coordinate_dblarr, reg_point_intarr,
      depth_dblarr, vecx_dblarr, vecy_dblarr,


PRINT,'** readfile.pro is active **'

      ; definition of variables
      line_strarr=STRARR(1)

      file='D:\Current\EFFORTS\Effort4\A000_result_6x6.txt'

      ;the file will be opened to count lines

      line_counter=0

      OPENR, 1, file

            WHILE (NOT EOF(1)) DO BEGIN
                  READF, 1,line_strarr

                  ;PRINT,'Number of lines=', line_counter,line_strarr
                        line_counter=line_counter+1

            ENDWHILE
      CLOSE, 1

x_coordinate_dblarr = DBLARR (line_counter)
y_coordinate_dblarr = DBLARR (line_counter)
reg_point_intarr = INTARR (line_counter)
depth_dblarr = DBLARR (line_counter)
vecx_dblarr = DBLARR (line_counter)
vecy_dblarr = DBLARR (line_counter)
curmgn_dblarr= DBLARR (line_counter)

line_counter2=0

      OPENR, 1, file
            PRINT,'** file',file,'  has been opend **'

            WHILE (NOT EOF(1)) DO BEGIN
                  READF, 1,line_strarr

                  ;PRINT,line_counter2,line_strarr

                  ;reading the x_coordinates

                        pos_point1 = STRPOS(line_strarr, '.')
                        ;PRINT,'pos_point1=', pos_point1

                  x_coordinate= STRMID(line_strarr,pos_point1(0)-7,13)
                        ;PRINT, 'x_coordinate=', x_coordinate
```

```
      x_coordinates_dbl= DOUBLE(x_coordinate)
            ;PRINT, 'x_coordinates_dbl=', x_coordinates_dbl

x_coordinate_dblarr(line_counter2) = x_coordinates_dbl


      ;reading the y_coordinates

      pos_point2 = STRPOS(line_strarr, '.',pos_point1(0)+1)
            ;PRINT,'pos_point2=', pos_point2

      y_coordinate= STRMID(line_strarr,pos_point2(0)-7,13)
            ;PRINT, 'y_coordinate=', y_coordinate

                  y_coordinates_dbl= DOUBLE(y_coordinate)
            ;PRINT, 'y_coordinates_dbl=', y_coordinates_dbl


y_coordinate_dblarr(line_counter2) = y_coordinates_dbl


      ;reading the regretion points

      reg_point=STRMID(line_strarr,pos_point2(0)+10,3)
            ;PRINT, 'reg_point=', reg_point

            reg_point_int= FIX(reg_point)
            ;PRINT, 'reg_point_int=', reg_point_int

reg_point_intarr(line_counter2) = reg_point_int


      ;reading death from the file

pos_point3=STRPOS(line_strarr,'.',pos_point2(0)+1)
            ;PRINT,'pos_point3=', pos_point3

            depth= STRMID(line_strarr,pos_point3(0)-2,6)
            ;PRINT, 'depth=', depth

                  depth_dbl= DOUBLE(depth)
                  ;PRINT, 'depth_dbl=', depth_dbl

      depth_dblarr(line_counter2) = depth_dbl


      ;reading x vector from the file

      pos_point4 = STRPOS(line_strarr, '.',pos_point3(0)+1)
            ;PRINT,'pos_point4=', pos_point4

            vectorx= STRMID(line_strarr,pos_point4(0)-2,6)
            ;PRINT, 'vectorx=', vectorx

                  vecx_dbl= DOUBLE(vectorx)
                  ;PRINT, 'vecx_dbl=', vecx_dbl

      vecx_dblarr(line_counter2) = vecx_dbl
```

```
                  ;reading y vector from the file

                  pos_point5 = STRPOS(line_strarr, '.',pos_point4(0)+1)
                        ;PRINT,'pos_point5=', pos_point5

                        vectory= STRMID(line_strarr,pos_point5(0)-2,6)
                        ;PRINT, 'vectory=', vectory

                              vecy_dbl= DOUBLE(vectory)
                              ;PRINT, 'vecy_dbl=', vecy_dbl

                  vecy_dblarr(line_counter2) = vecy_dbl


                        line_counter2=line_counter2+1

      ENDWHILE
CLOSE, 1

PRINT,'**  has been closed **'

;PRINT, 'x_coordinate_dblarr=', x_coordinate_dblarr
;PRINT, 'y_coordinate_dblarr=', y_coordinate_dblarr
;PRINT, 'reg_point_intarr=', reg_point_intarr
;PRINT, 'depth_dblarr=', depth_dblarr
;PRINT, 'vecx_dblarr=', vecx_dblarr
;PRINT, 'vecy_dblarr=', vecy_dblarr

PRINT,'** readfile.pro is finished **'


END
```

```
;*********************************************************************
;
;---------------------------------------------------------------------
; Description:   Calculating Current magnitude & direction
;---------------------------------------------------------------------
;
;*********************************************************************PRO
current, vecx_dblarr, vecy_dblarr, curmgn_dblarr, curdir_dblarr

Print, '-------------------------------------
Print,      'The current is running'
Print, '-------------------------------------

PRINT,'** current.pro is active **'

      curdir_dblarr=DBLARR(N_ELEMENTS(vecx_dblarr))

            ;index
            FOR i=0L, N_ELEMENTS(vecx_dblarr)-1 DO BEGIN

      ;creating magnitude of current from vector x and y

                  curmgn = SQRT(vectorx^2+vectory^2)
                  ;PRINT, 'curmgn=',curmgn

                        curmgn_dbl= DOUBLE(curmgn)
                        ;PRINT, 'curmgn_dbl=', curmgn_dbl

                  curmgn_dblarr(line_counter2) = curmgn_dbl

      ;creating direction of current from vector x and y with ATAN

            east= vecx_dblarr(i)
            north= vecy_dblarr(i)

      IF ((east GT 0.0) AND (north GT 0.0)) THEN curdir = ATAN $
(east/north)*180.0/!Pi
      IF ((east GT 0.0) AND (north LT 0.0)) THEN curdir = 180.0 + ATAN$
(east/north)*180.0/!Pi
      IF ((east LT 0.0) AND (north LT 0.0)) THEN curdir = 180.0 + ATAN$
(east/north)*180.0/!Pi
      IF ((east LT 0.0) AND (north GT 0.0)) THEN curdir = 360.0 + ATAN$
(east/north)*180.0/!Pi
                  ;PRINT, 'curdir=',curdir

                        curdir_dbl= DOUBLE(curdir)
                        ;PRINT, 'curdir_dbl=', curdir_dbl

                  curdir_dblarr(i) = curdir_dbl

ENDFOR

;PRINT, 'curdir_dblarr=',curdir_dblarr
;PRINT, 'curmag_dblarr=',curmag_dblarr
END
```

```
;*********************************************************************
;
;---------------------------------------------------------------------
; Description:   Qualifying the results
;---------------------------------------------------------------------
;
;*********************************************************************
PRO filter, x_coordinate_dblarr,y_coordinate_dblarr, reg_point_intarr,$
      depth_dblarr,x_coordinate_dblarr_new, y_coordinate_dblarr_new,$
      reg_point_intarr_new, depth_dblarr_new,vecx_dblarr, vecy_dblarr,$
      vecx_dblarr_new, vecy_dblarr_new, x_vector_dblarr, $ y_vector_dblarr,
      curmgn_dblarr, curmgn_dblarr_new, $ curdir_dblarr, curdir_dblarr_new

PRINT,'** filter.pro is active **'

;for the qualification

      index_regp_in = WHERE ((reg_point_intarr GT 10) AND (reg_point_intarr $
      LT 100))

            x_coordinate_dblarr_new=x_coordinate_dblarr(index_regp_in)
            y_coordinate_dblarr_new=y_coordinate_dblarr(index_regp_in)
            reg_point_intarr_new=reg_point_intarr(index_regp_in)
            depth_dblarr_new=depth_dblarr(index_regp_in)
            vecx_dblarr_new=vecx_dblarr(index_regp_in)
            vecy_dblarr_new=vecy_dblarr(index_regp_in)
            curmgn_dblarr_new=curmgn_dblarr(index_regp_in)
            curdir_dblarr_new=curdir_dblarr(index_regp_in)

;,y_coordinate_dblarr, reg_point_intarr, depth_dblarr


; Get the subscripts of those elements greater than 10 and less
; than 100.

; Put the selected values into result.
;PRINT, 'x_coordinate_dblarr_new=', x_coordinate_dblarr_new
;PRINT, 'y_coordinate_dblarr_new=', y_coordinate_dblarr_new
;PRINT, 'reg_point_intarr_new=', reg_point_intarr_new
;PRINT, 'depth_dblarr_new=', depth_dblarr_new


PRINT,'** filter.pro is finished **'


END
```

```
;*********************************************************************
;
;---------------------------------------------------------------------
; Description:   Creating coordinates of the whole area
;---------------------------------------------------------------------
;
;*********************************************************************
PRO coordinates, x_coord_exact,y_coord_exact

Print, '-------------------------------------
Print, 'The coordinates is running'
Print, '-------------------------------------

x_coord_vecdbl= DBLARR(1)
y_coord_vecdbl= DBLARR(1)

FOR x_coord1= (3459944.47920D), (3461867.21160D), (40.9092D) DO BEGIN
      DOUBLE(40.9092) DO BEGIN
            x_coord = STRING(x_coord1,format="(D12.4)")
            ;PRINT, x_coord

      FOR y_coord1=(6101014.65770D),(6102947.39010D),(40.9092D)DO BEGIN
            DOUBLE(6102947.39010), DOUBLE(40.9092) DO BEGIN
                  y_coord = STRING(y_coord1,format="(D12.4)")
                  ;PRINT, y_coord

      x_coord_vecdbl=STRING([x_coord_vecdbl,x_coord],format="(D12.4)")

      y_coord_vecdbl=STRING([y_coord_vecdbl,y_coord],format="(D12.4)")

      ENDFOR ;y_coord

ENDFOR ;x_coord

;PRINT,'x_coord_vecdbl',x_coord_vecdbl
;PRINT,'y_coord_vecdbl',y_coord_vecdbl

;elemination of the first false value in the vecdbl of x and y ;coordinates
;n_elemennts function is used

      x_coord_elem=N_ELEMENTS(x_coord_vecdbl)
            x_coord_exact=x_coord_vecdbl(1:x_coord_elem-1)

      y_coord_elem=N_ELEMENTS(y_coord_vecdbl)
            y_coord_exact=y_coord_vecdbl(1:y_coord_elem-1)

            ;PRINT,'x_coord_exact=',x_coord_exact
            ;PRINT,'y_coord_exact=',y_coord_exact


END
```

```
;*******************************************************************
;-------------------------------------------------------------------
; Description:   Matching the coordinate with results
;-------------------------------------------------------------------
;*******************************************************************
PRO comparison, x_coord_exact,y_coord_exact,x_coordinate_dblarr_new,$
                y_coordinate_dblarr_new,depth_dblarr_new,vecx_dblarr_new,$
                vecy_dblarr_new,    z_depth_dblarr, x_vector_dblarr,$
                y_vector_dblarr, curmgn_dblarr, curmgn_dblarr_new,$
      curdir_dblarr, curdir_dblarr_new, cur_mag_dblarr, cur_dir_dblarr

Print, '-------------------------------------
Print, 'The comparison is running'
Print, '-------------------------------------
z_depth_dblarr=DBLARR(N_ELEMENTS(x_coord_exact))
x_vector_dblarr=DBLARR(N_ELEMENTS(x_coord_exact))
y_vector_dblarr=DBLARR(N_ELEMENTS(x_coord_exact))
cur_mag_dblarr=DBLARR(N_ELEMENTS(x_coord_exact))
cur_dir_dblarr=DBLARR(N_ELEMENTS(x_coord_exact))

;index
FOR i=0L, N_ELEMENTS(x_coord_exact)-1 DO BEGIN

      x_index= WHERE(LONG(x_coordinate_dblarr_new) EQ LONG(x_coord_exact(i)))
            ;PRINT, 'x_index=',x_index

      IF (x_index(0) NE -1) THEN BEGIN
            y_index=WHERE(LONG(y_coordinate_dblarr_new(x_index)) EQ $
            LONG(y_coord_exact(i)))

            IF (y_index(0) NE -1) THEN BEGIN

                  index_match=x_index(y_index)

                  z=depth_dblarr_new(index_match)
                  z_depth_dblarr(i)=z

                        vecx=vecx_dblarr_new(index_match)
                        x_vector_dblarr(i)=vecx

                        vecy=vecy_dblarr_new(index_match)
                        y_vector_dblarr(i)=vecy

                  magcur=curmgn_dblarr_new(index_match)
                  cur_mag_dblarr(i)=magcur

                  dircur=curdir_dblarr_new(index_match)
                  cur_dir_dblarr(i)=dircur
                        ;PRINT, 'vecx=',x_vector_dblarr(i)
                        ;PRINT, 'i=', i
            ENDIF

      ENDIF
ENDFOR
END
```

```
;*********************************************************************
;
;---------------------------------------------------------------------
; Description:   Creation of output file with current results
;---------------------------------------------------------------------
;
;*********************************************************************
      PRO output, x_coord_exact, y_coord_exact, z_depth_dblarr, $
                  x_vector_dblarr, y_vector_dblarr, cur_mag_dblarr,
                  cur_dir_dblarr

Print, '-------------------------------------
Print,      'The output is running'
Print, '-------------------------------------


;creation of the full data array with coordinates and depth values

      OPENW, 2, 'D:\Editing\Processed_data.txt'

            FOR i=0L, N_ELEMENTS(x_coord_exact)-1 DO BEGIN

            printf,2, LONG(x_coord_exact(i)), LONG(y_coord_exact(i)),$
                  cur_mag_dblarr(i), cur_dir_dblarr(i)


            ENDFOR

CLOSE,2

END
```

Appendix X

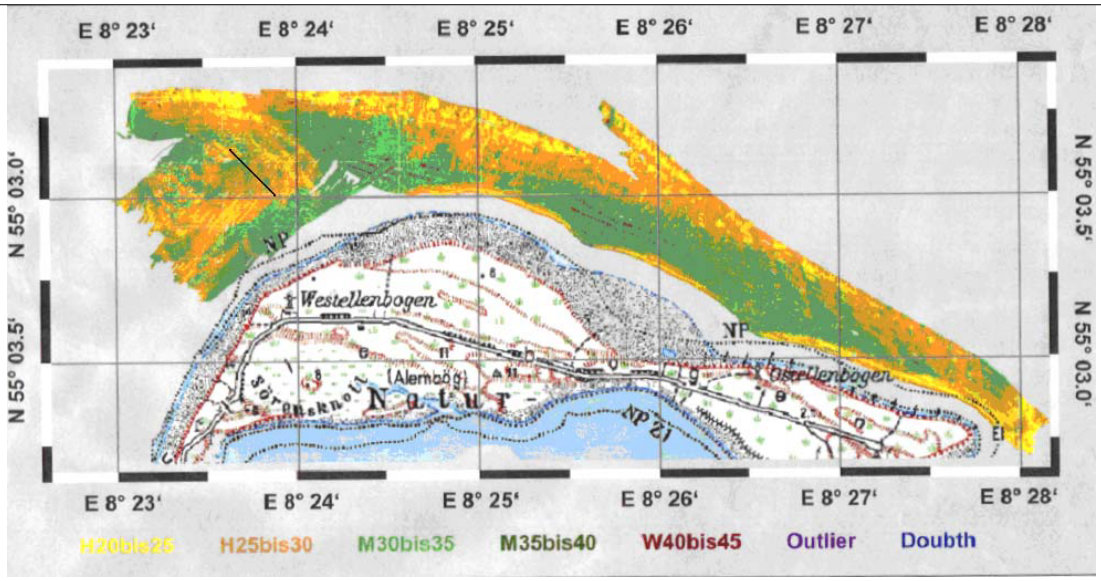

Figure X-1: Grain Size Distribution along the North of Sylt. Black line indicates the cross-section on the List Landtief (Source: KOK, GKSS)

Stations	1	2	3	4	5	6	7	8	9	10	11	12	13	14	15
Dist. (m)	0.00	39.80	79.59	119.39	159.19	198.99	238.78	278.58	318.38	358.18	397.97	437.77	477.57	517.37	557.16
d_{50} **(mm)**	3.6	4.8	2.4	2.4	2.4	2.4	2.4	2.4	2.4	3.6	3.6	4.8	4.8	4.8	36
U_{cr} **(m/s)**	1.60	1.72	1.62	1.57	1.54	1.54	1.52	1.54	1.54	1,60	1.63	1.65	1.82	1.90	2.24

Appendix XI

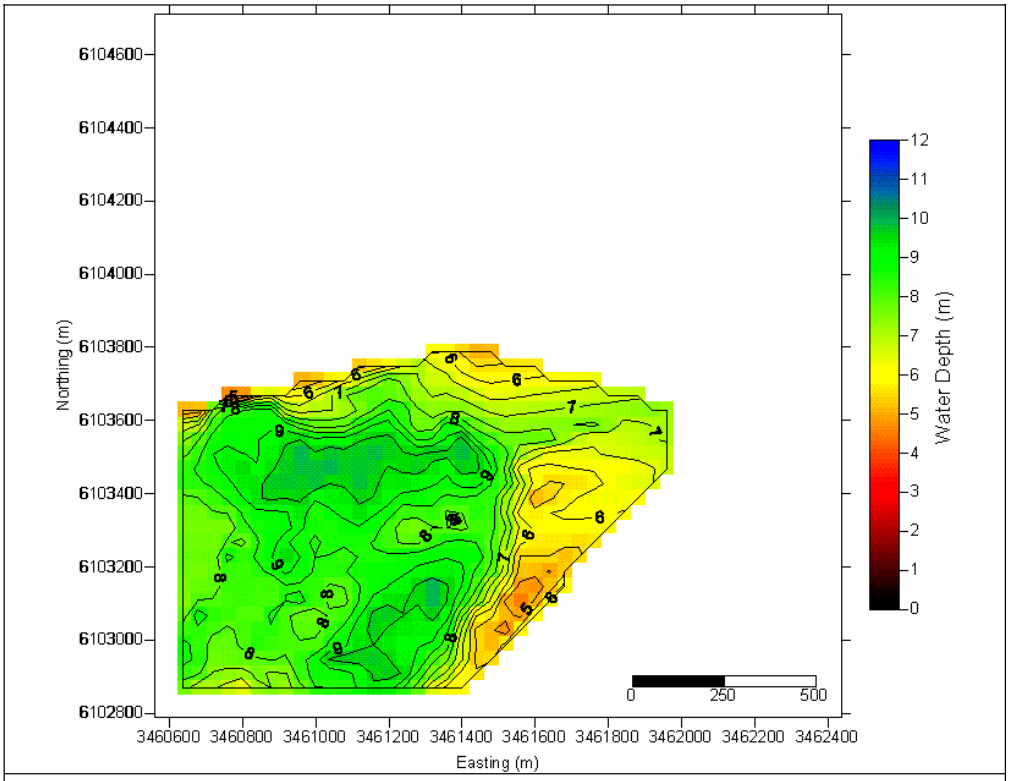

Bathymetry H00:00

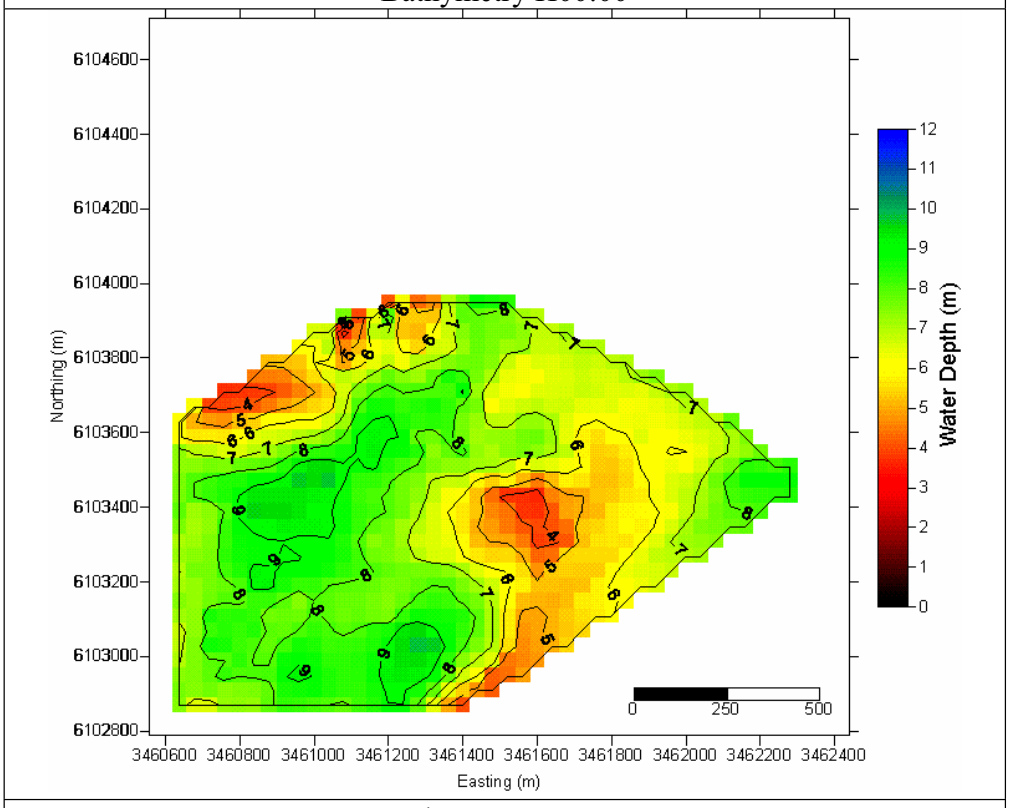

Bathymetry H01:00

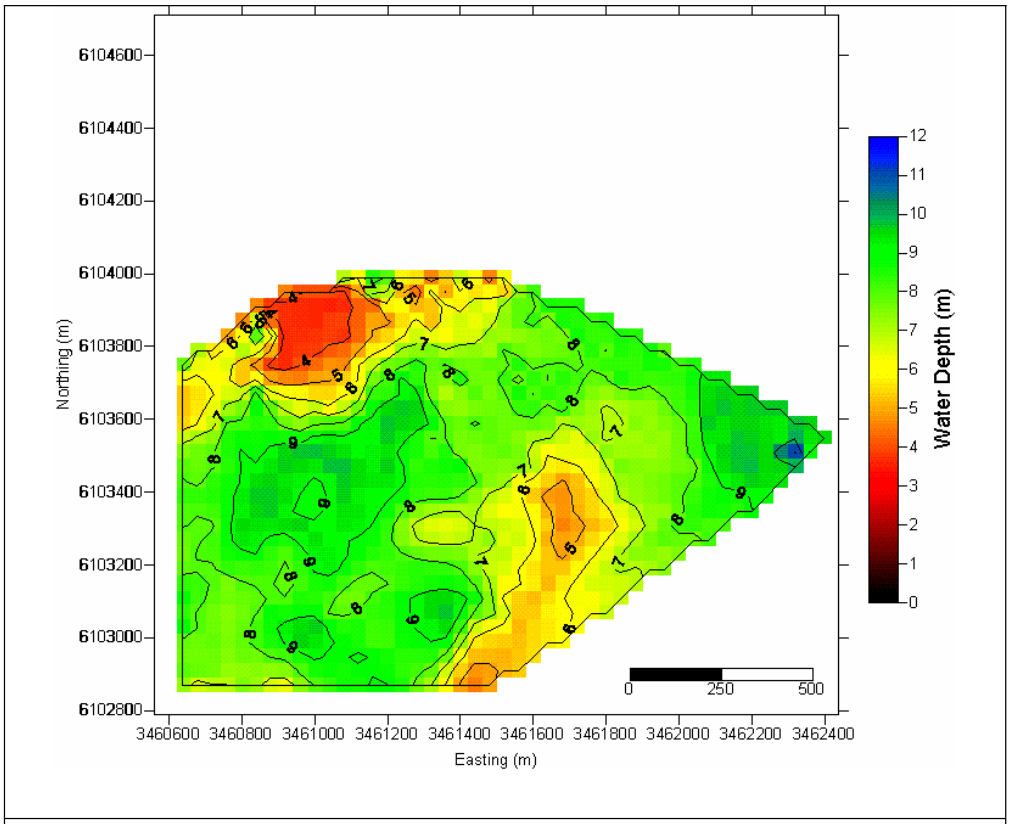

Bathymetry H02:00

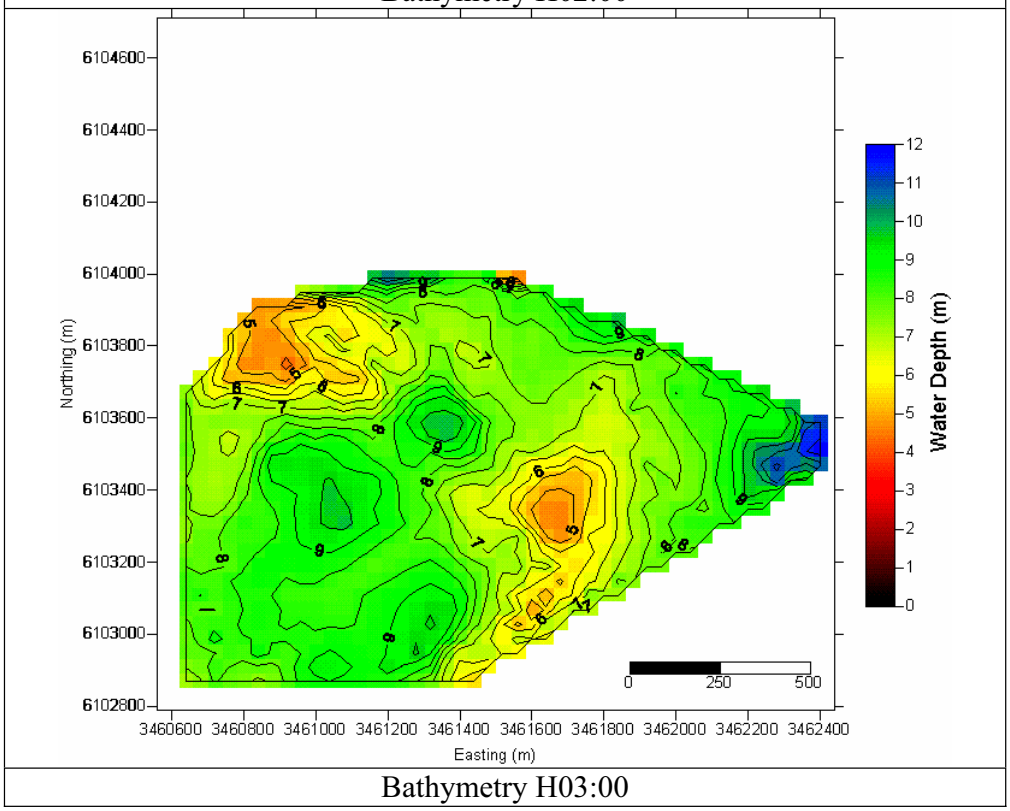

Bathymetry H03:00

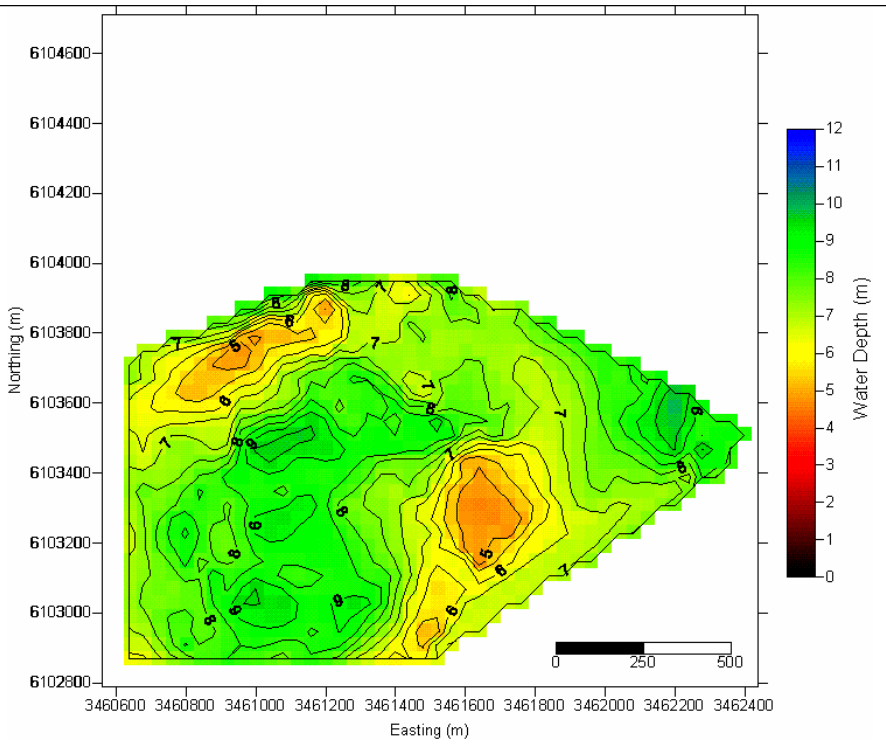

Bathymetry H04:00

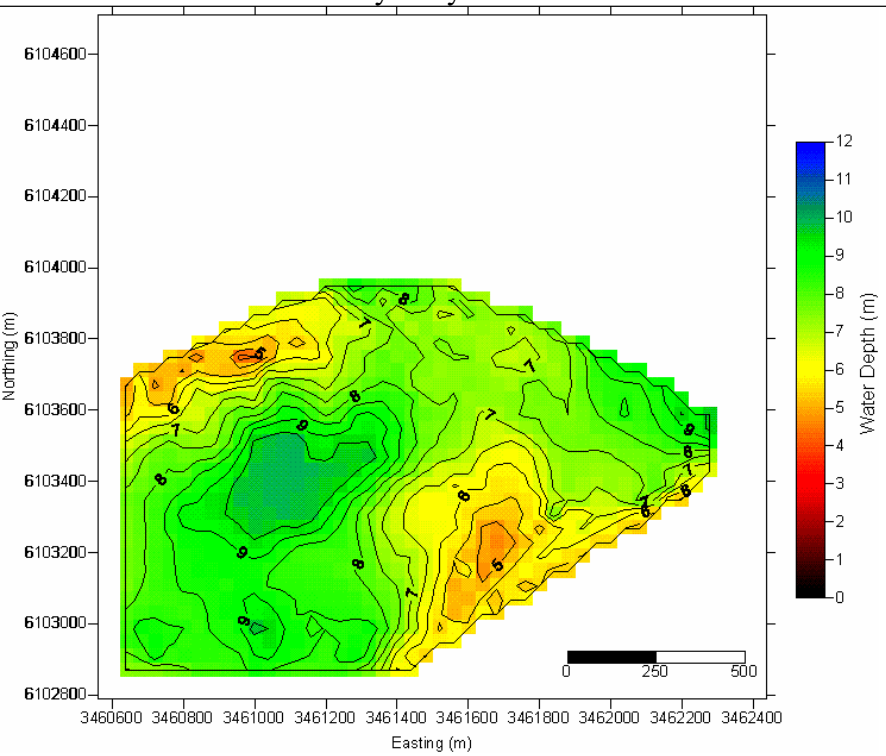

Bathymetry H05:00

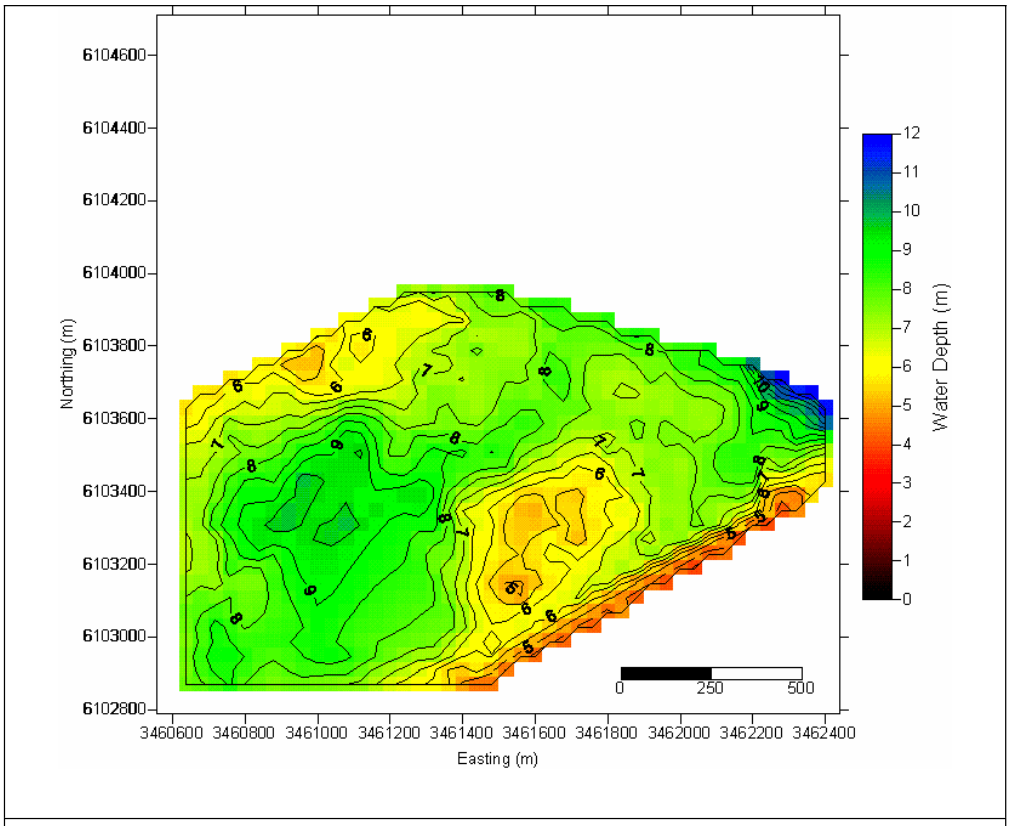

Bathymetry H06:00

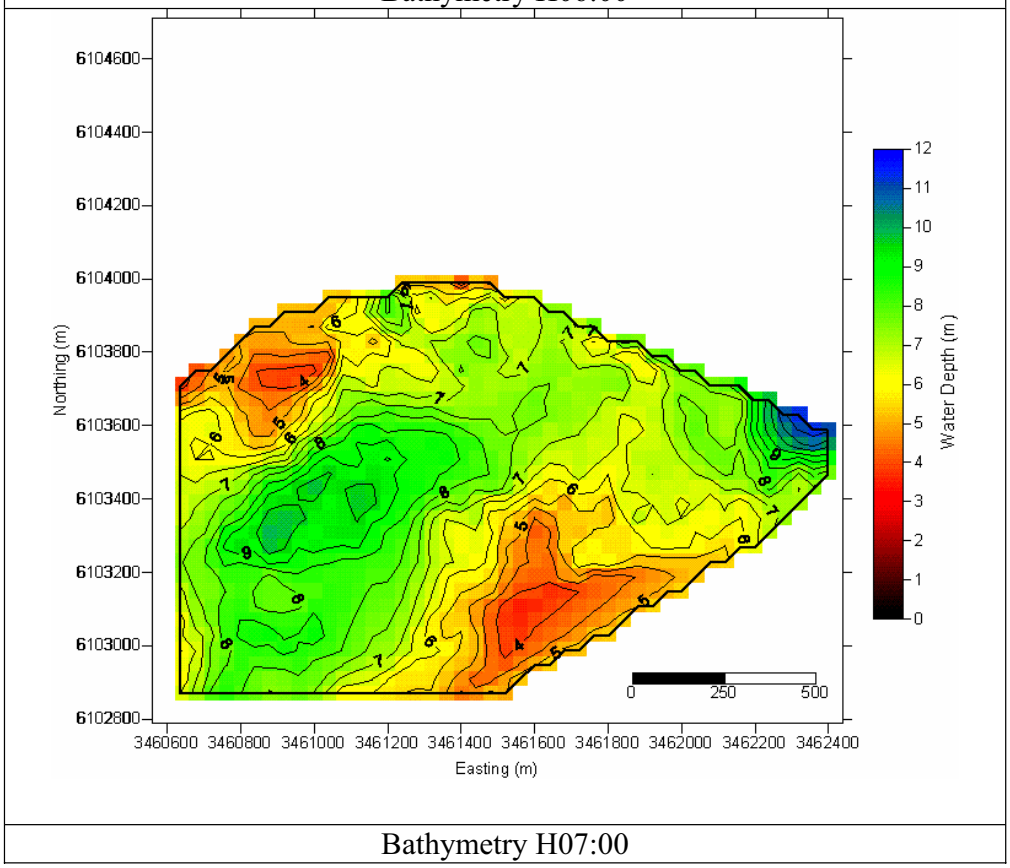

Bathymetry H07:00

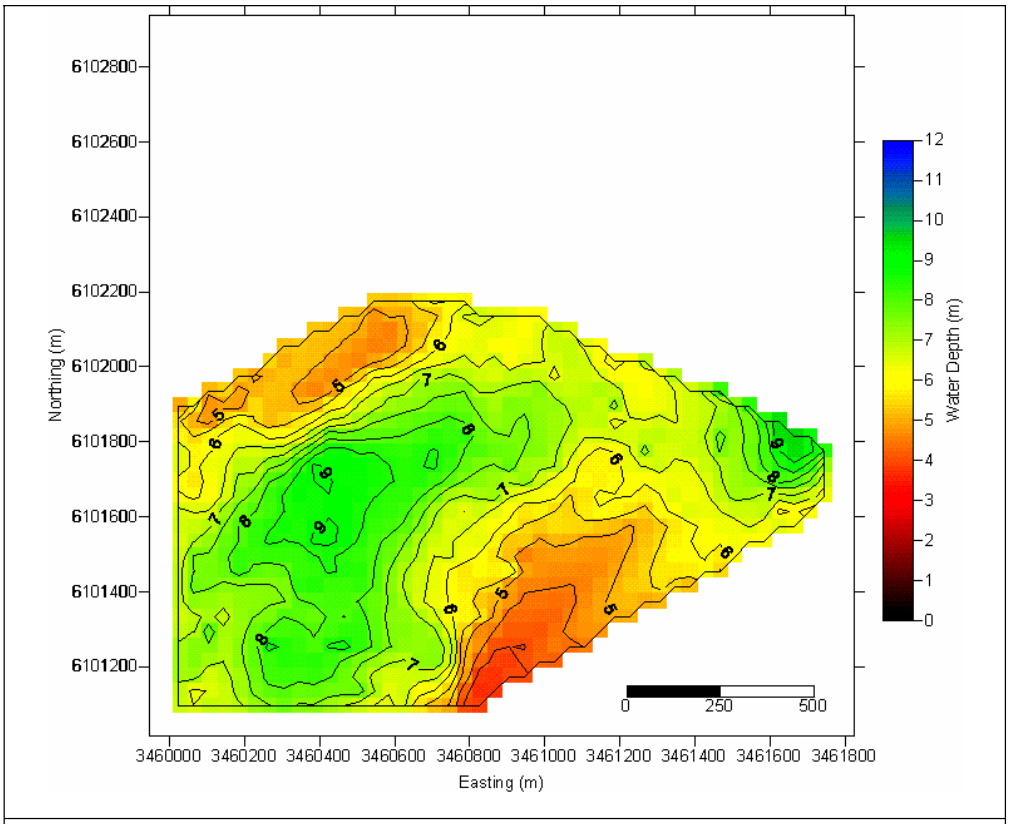

Bathymetry H08:00

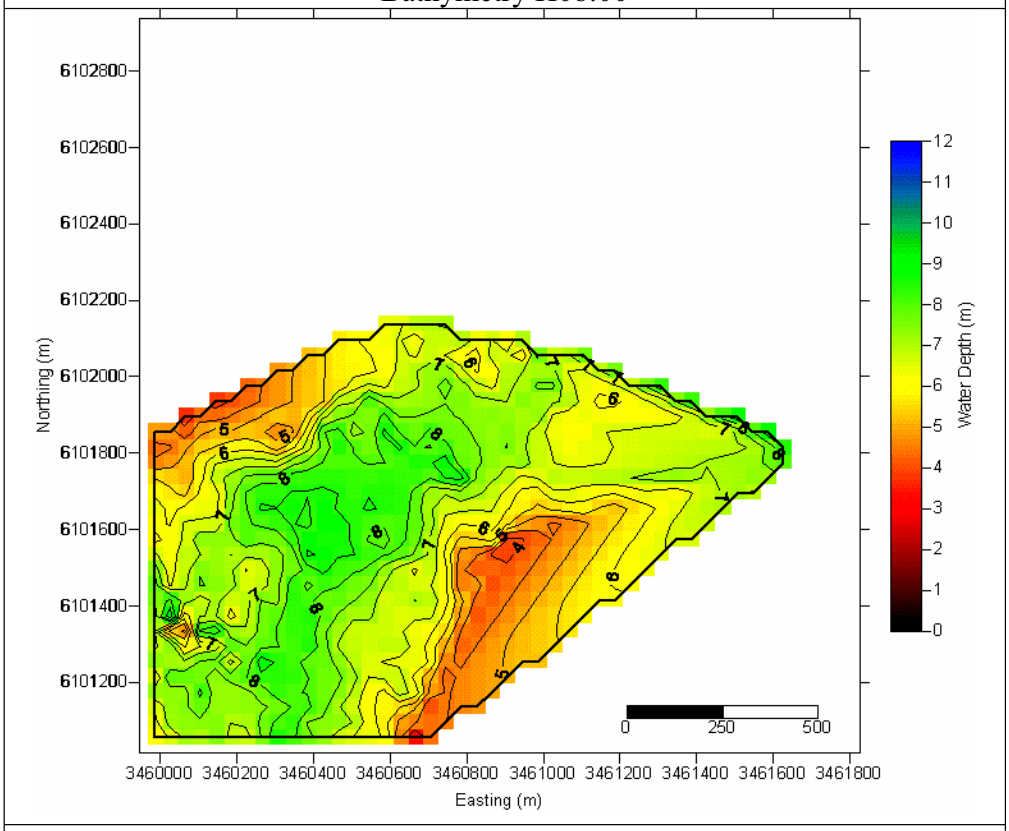

Bathymetry H09:00

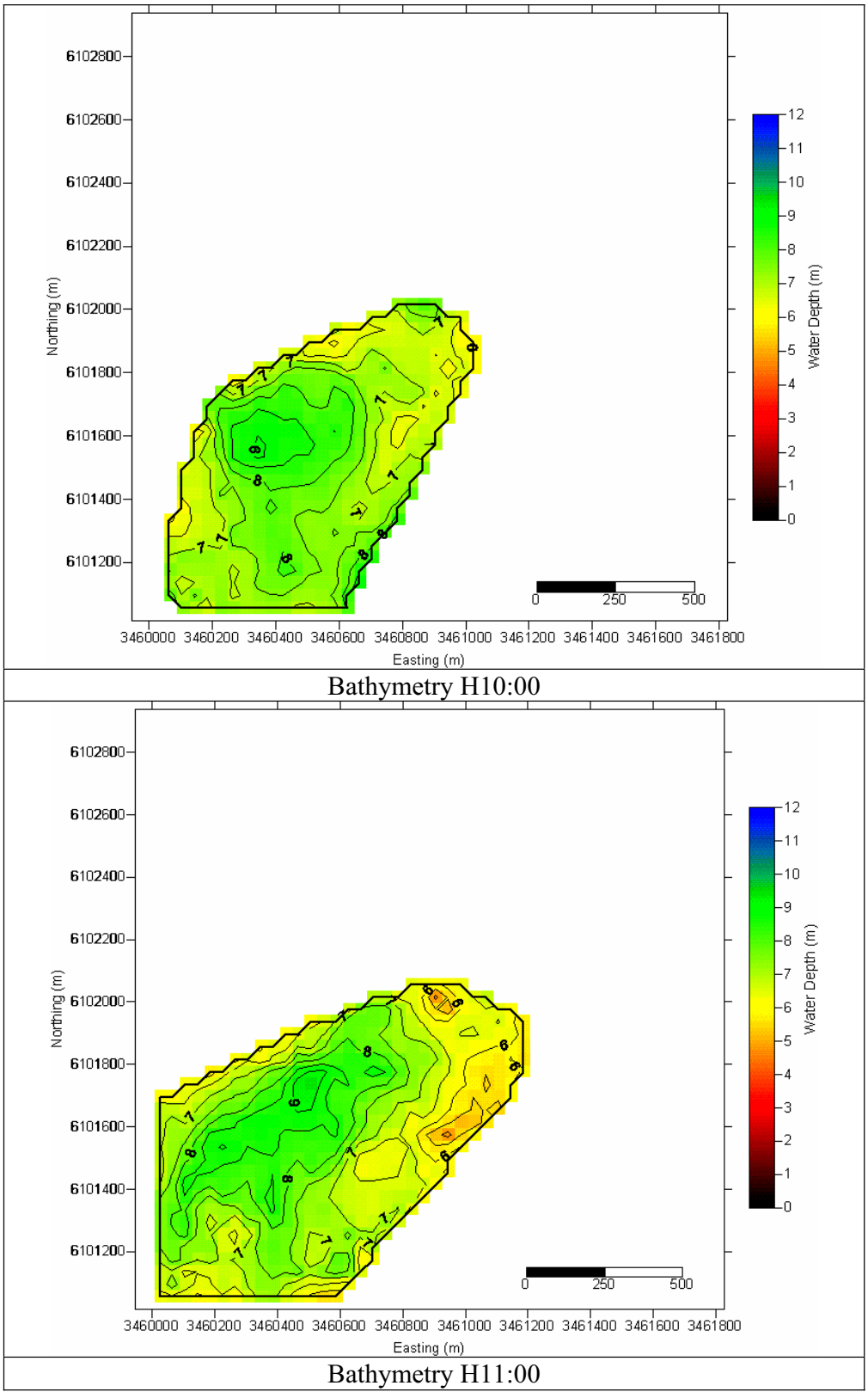

Figure XI-1: Visualization of hourly bathymetries of the whole tidal cycle, during July 12, 2001 (0:00 to 11:00h UTC).

Appendix XII

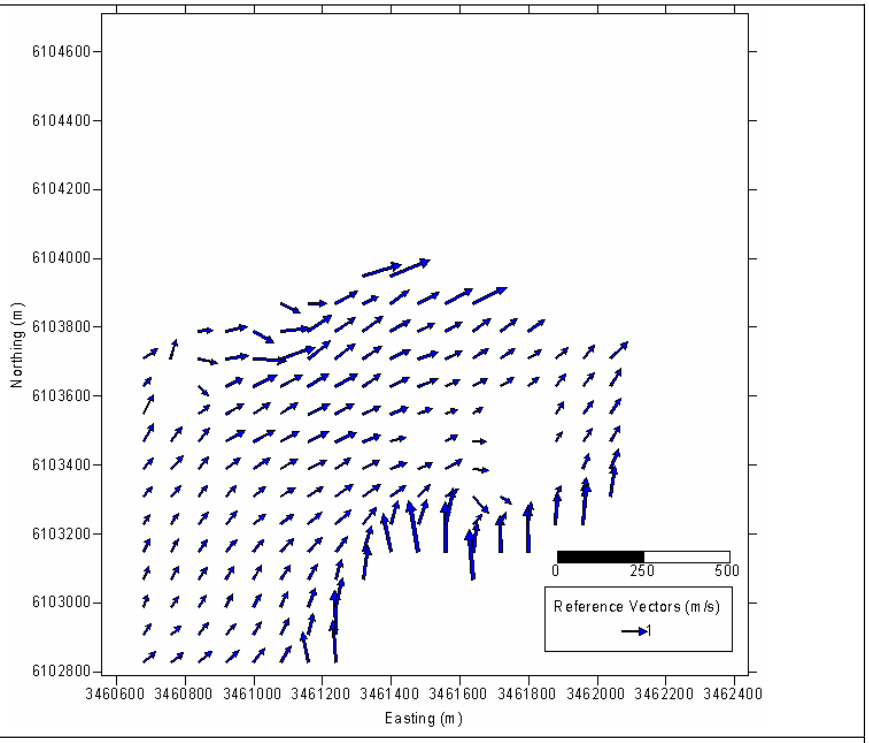

Vector map H00:00

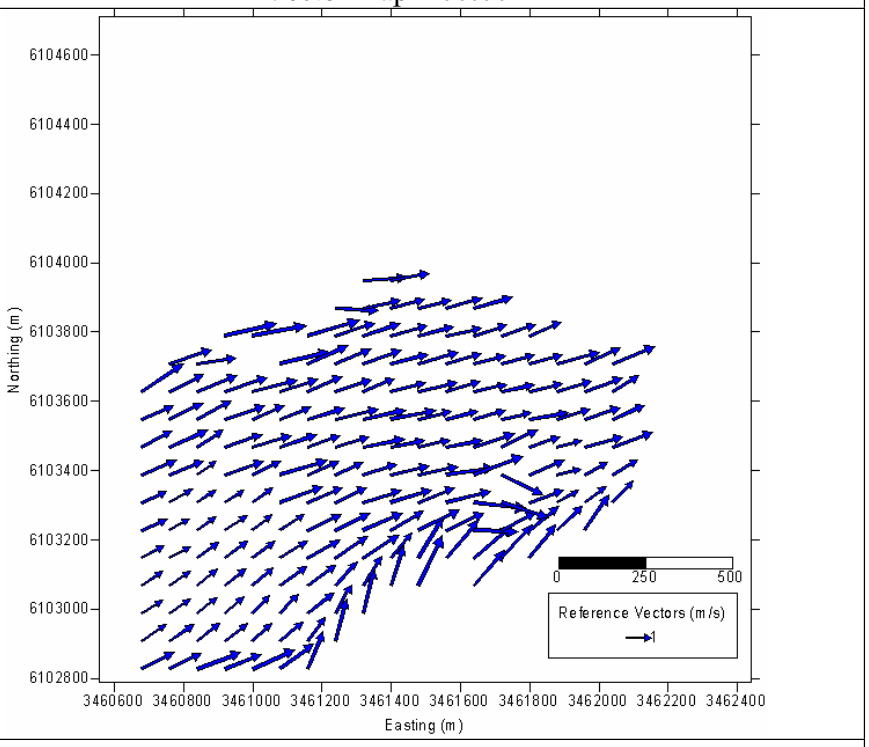

Vector map H01:00

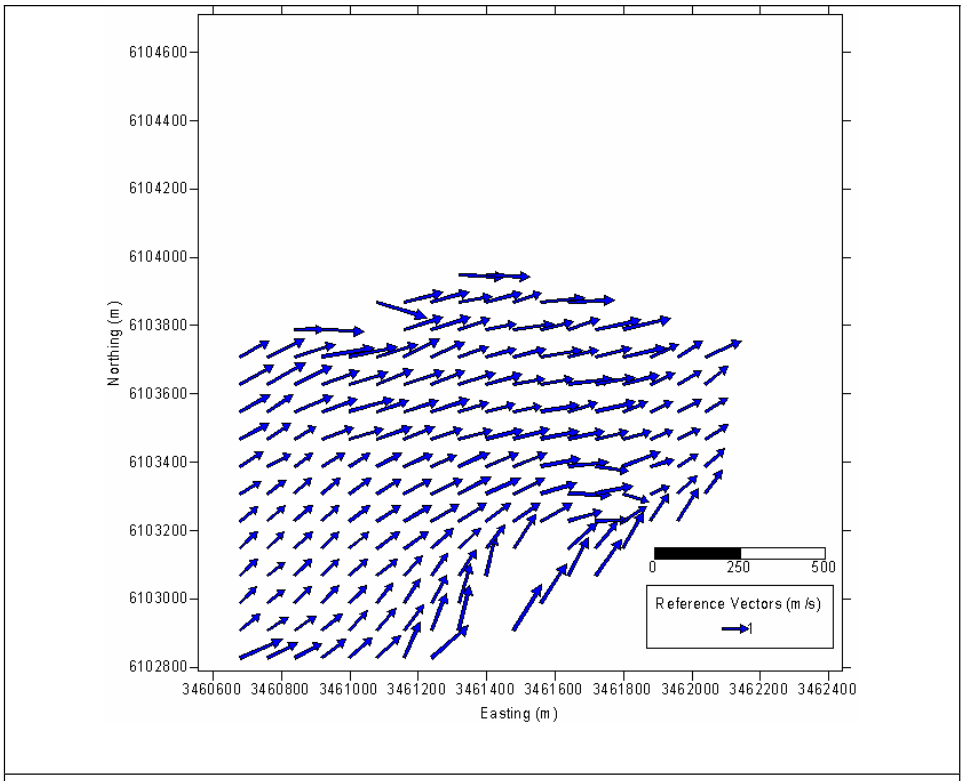

Vector map H02:00

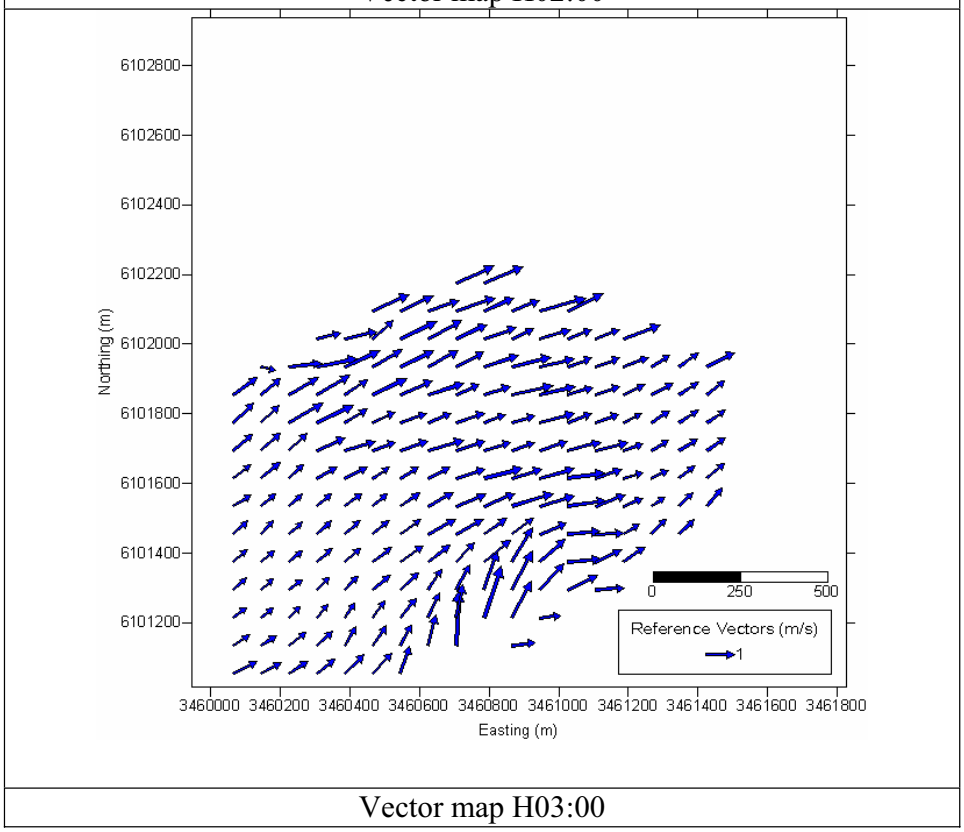

Vector map H03:00

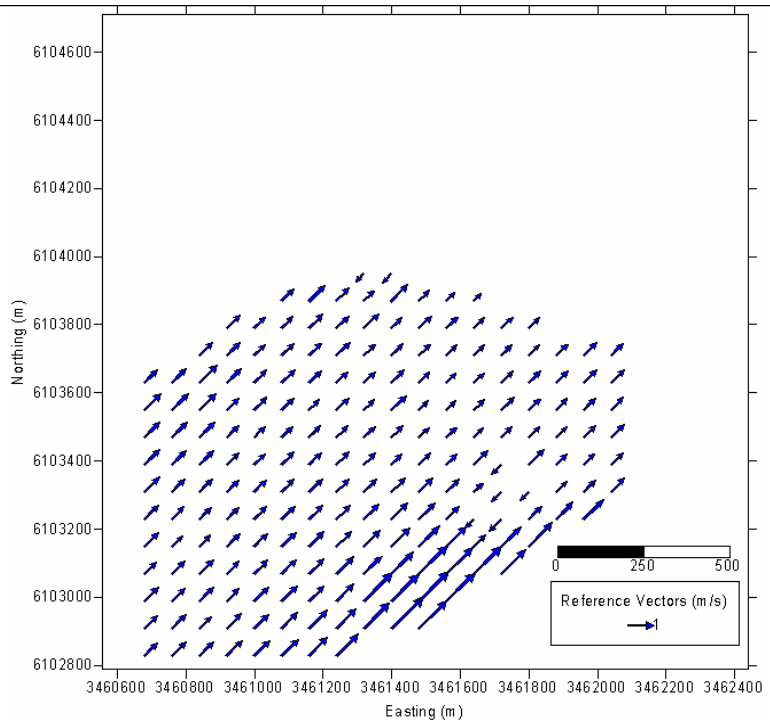

Vector map H04:00

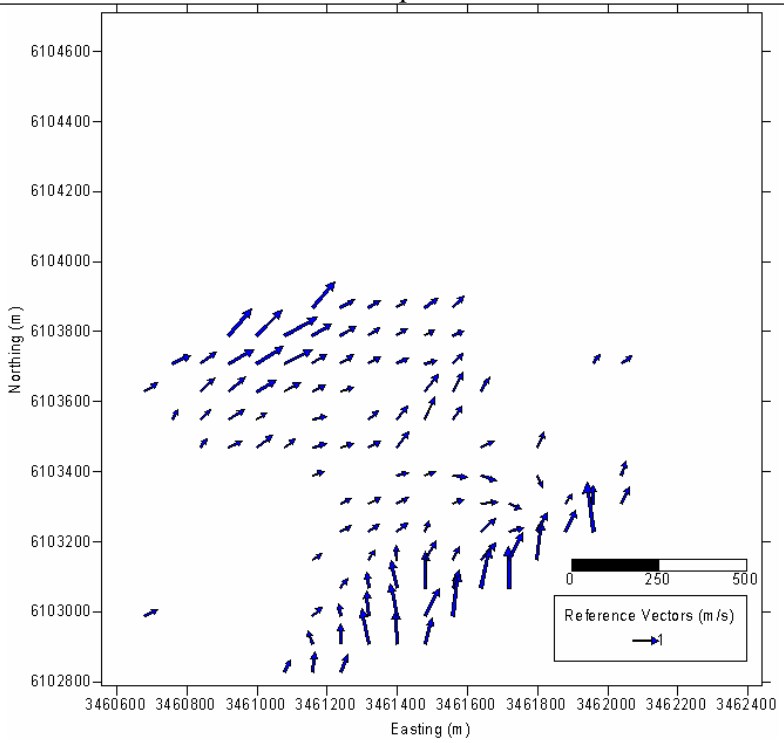

Vector map H05:00

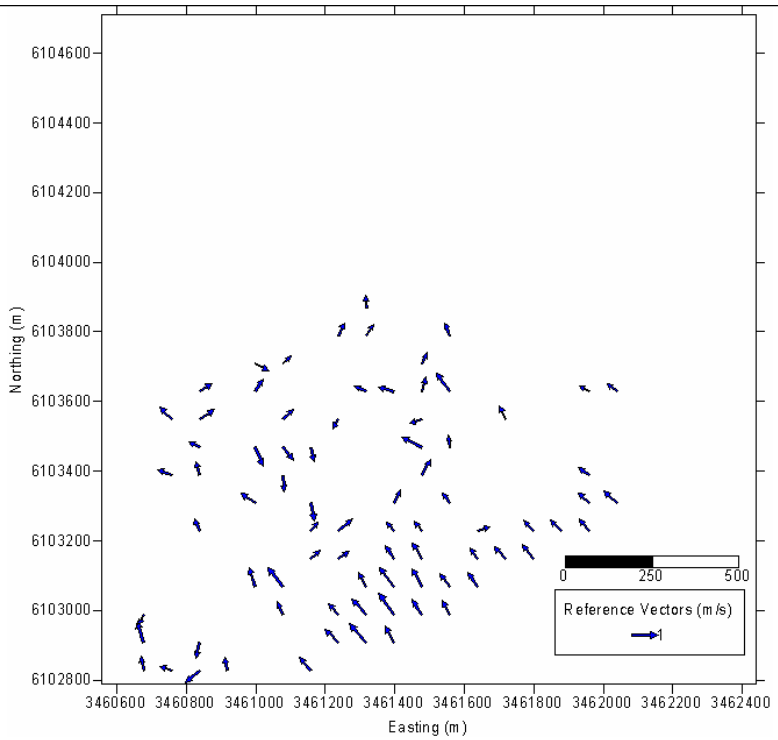

Vector map H06:00

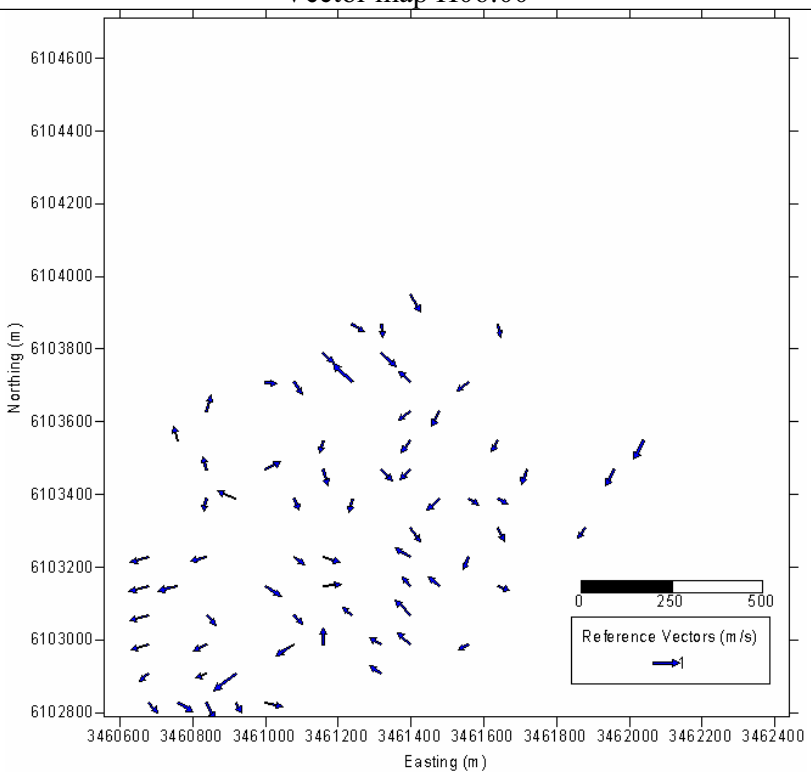

Vector map H07:00

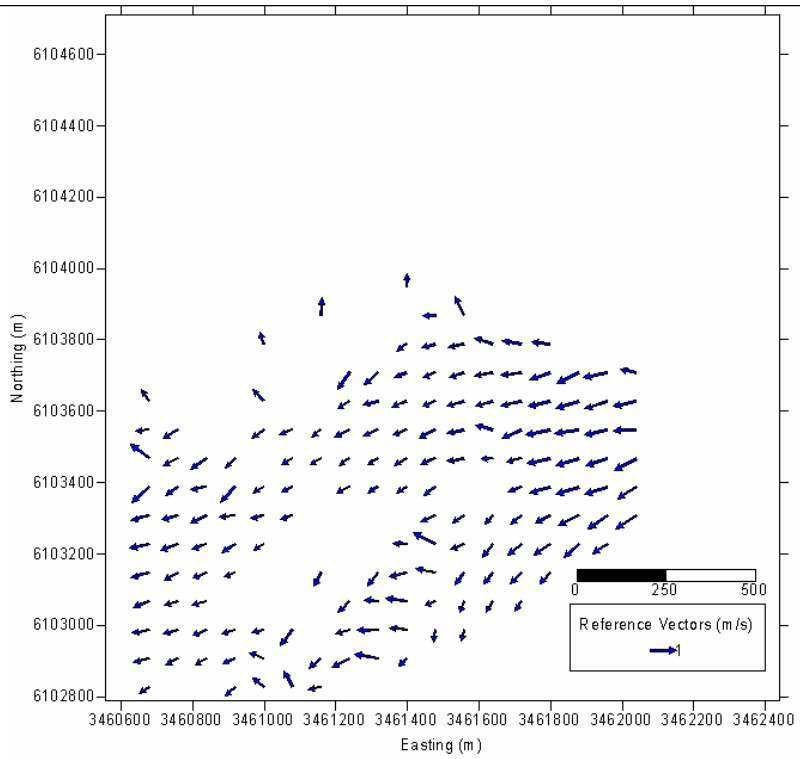

Vector map H08:00

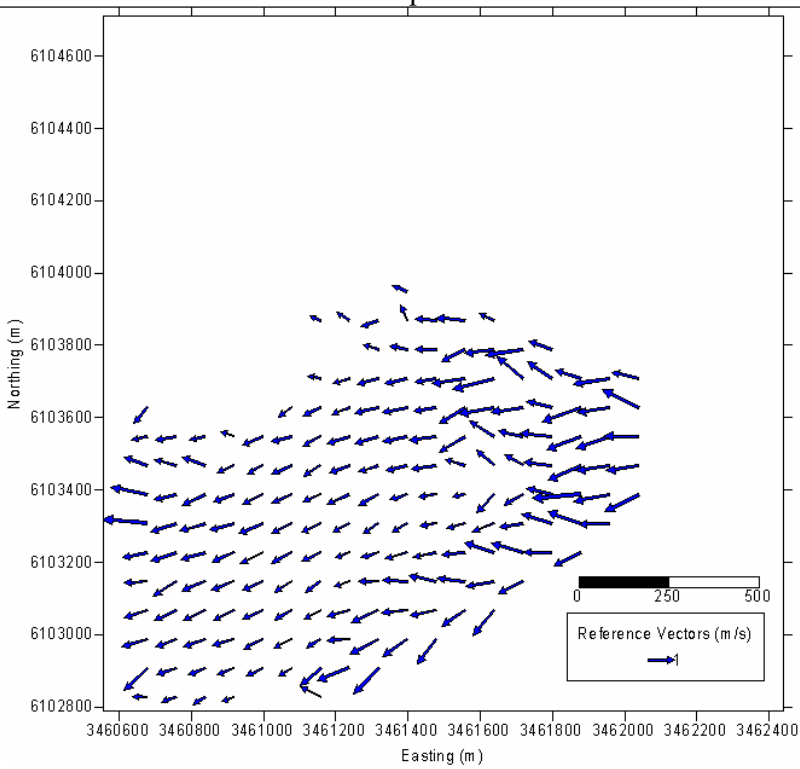

Vector map H09:00

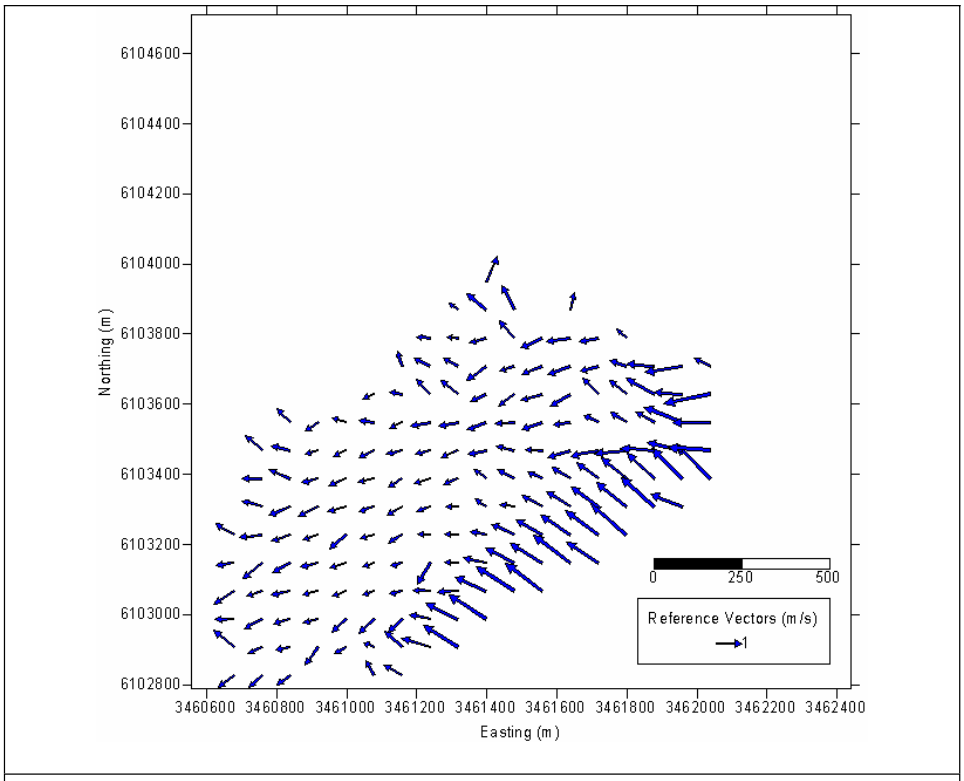

Vector map H10:00

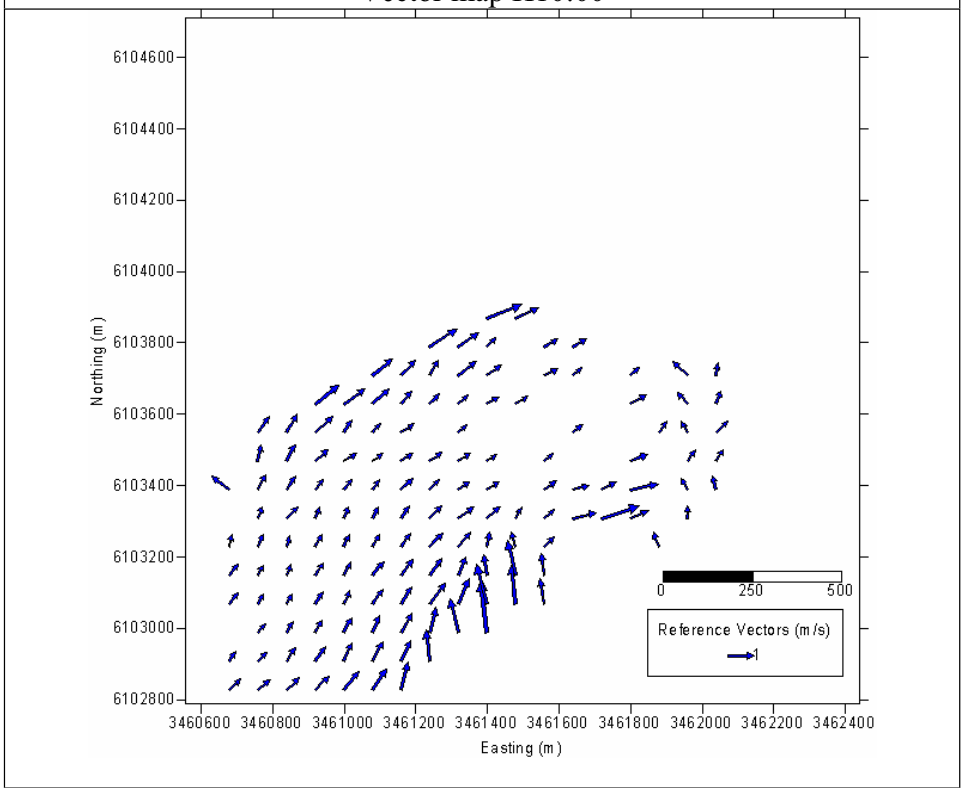

Vector map H11:00

Figure XII-1: Visualization of current maps of the tidal cycle during July 12, 2001 (0.00-11.00H).

Appendix XIII

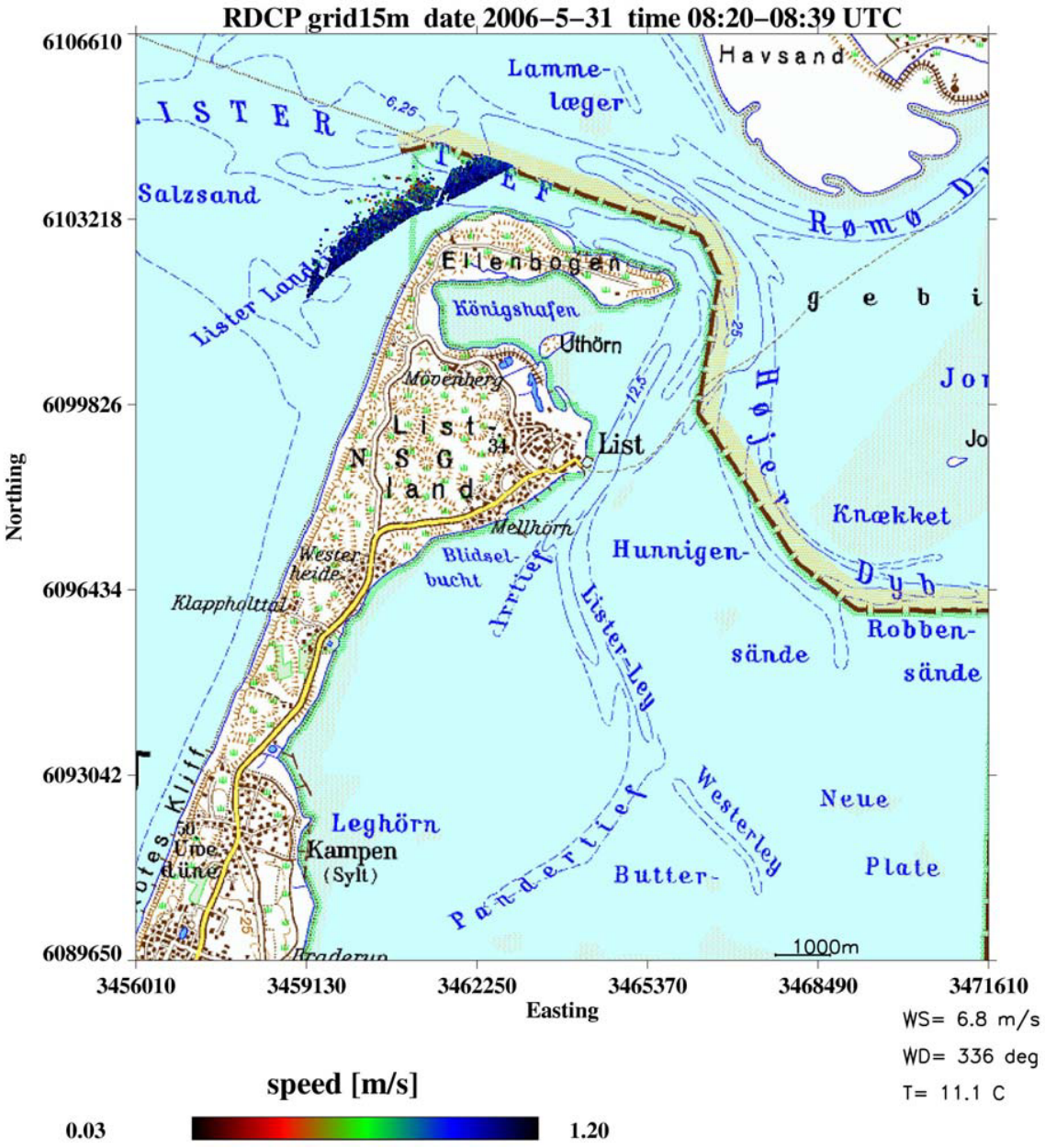

Figure XIII-1: ADCP measurements of the study area during a survey campaign in May 31, 2006 (Source: Radar Hydrography Department , GKSS).